



PROCUREMENT EXECUTIVE, MINISTRY OF DEFENCE
AERONAUTICAL RESEARCH COUNCIL
REPORTS AND MEMORANDA

Compressible Turbulent Boundary Layers with Discontinuous Air Transpiration: An Experimental and Theoretical Investigation

By P. G. MARRIOTT

Cambridge University Engineering Department

LONDON: HER MAJESTY'S STATIONERY OFFICE

1977

£8 net

Compressible Turbulent Boundary Layers with Discontinuous Air Transpiration: An Experimental and Theoretical Investigation

By P. G. MARRIOTT

Cambridge University Engineering Department†

*Reports and Memoranda No. 3780**
June, 1974

Summary

Experimental data are presented for the development of compressible turbulent boundary layers moving from a solid onto a transpired surface, and *vice versa*. The data were obtained at free stream Mach numbers of 1.8 and 3.6 (Reynolds numbers per metre of 2.45×10^7 and 5.45×10^7 respectively) and transpiration rates ($\rho_w V_w / \rho_1 U_1$) up to 0.0044, for nominally zero heat-transfer conditions.

The results are compared with theoretical predictions obtained from a method based on the eddy-viscosity concept.

The work described in this report is based on experimental investigations conducted by the author while at Cambridge University Engineering Department, and presented in a Ph.D. dissertation (Marriott¹).

* Replaces A.R.C. 35 398

† Now at Hunting Engineering Ltd., (STG), Reddings Wood, Ampthill, Bedford.

LIST OF CONTENTS

1. Introduction
2. Experimental Details
 - 2.1. Apparatus
 - 2.2. Data Measurement
 - 2.3. Data Reduction
 - 2.4. Two-Dimensionality
 - 2.5. Test Conditions
3. Discussion of Results
 - 3.1. Free-Stream Mach Number Distribution
 - 3.2. Velocity Profile Developments
 - 3.3. Temperature Profile Developments
 - 3.4. Integral Parameters
 - 3.5. Skin-Friction Variations
 - 3.6. Inner-Law Profile Representation
 - 3.7. Shear-Stress Profile Calculations
 - 3.8. Mixing-Length Distributions
 - 3.9. Eddy-Viscosity Distributions
4. Conclusions
5. Tables of Experimental Results
 - 5.1. Wall Temperature
 - 5.2. Free-Stream Velocity and Temperature
 - 5.3. Displacement and Momentum Thicknesses
 - 5.4. Tabulated Velocity and Temperature Profiles

Acknowledgements

List of Symbols

References

Appendix: Eddy Viscosity Formulation

Tables 1 to 7

Illustrations: Figs. 1 to 49

Detachable Abstract Cards

1. Introduction

Papers by Jeromin² and Squire³ have reported experiments concerning the development of compressible turbulent boundary layers on surfaces with uniform transpiration. A logical extension of this work is the investigation of the situation where transpiration rates are non-uniform. The simplest case of non-uniform transpiration, namely a plane discontinuity, where a solid surface boundary layer encounters, and develops on, a transpired surface, is the subject of the present investigation.

Apart from the work of Kays and others at Stanford (summarised by Kays⁴), and that of McQuaid⁵, studies of non-uniform transpiration are generally insubstantial.

The purpose of the present investigation was to obtain basic experimental data for a compressible turbulent boundary layer developing over a straight discontinuity in surface transpiration rate, for which tabulated profile data are presented in this report. A theoretical eddy viscosity method, due to Verma⁶, was used for predictions of the flow developments, and these are also presented in comparison with the experimental results.

The eddy-viscosity formulation is given in Appendix A and the parameters used in the method are given in Table 1.

2. Experimental Details

2.1. Apparatus

All the experimental work in the present study has been carried out in an intermittent blow-down supersonic tunnel at the Cambridge University Engineering Department. A description of the tunnel and associated transpiration apparatus has been given by Jeromin⁷ and Squire³. A photograph of the tunnel can be seen in Fig. 1, and a sketch of the working section in Fig. 2.

At the two Mach numbers investigated, Mach 1.8 and 3.6, the stagnation chamber pressures were respectively 82.7 kN/m² and 887 kN/m² gauge. There was no provision to control the stagnation temperature, which was found to vary by about ± 2 K during a run, having a nominal value of 293 K ± 4 K. The temperature of the transpired air was close to stagnation temperature or slightly below.

The working section of the tunnel, as described in Jeromin⁷, allows for boundary-layer measurements to be made over a surface approximately 200 mm long by 100 mm wide. This surface forms part of a plate, measuring approximately 400 mm \times 100 mm, which can be easily interchanged, allowing for a variety of surface configurations to be tested.

The porous surface in the present investigation was constructed from rolled sintered bronze, butt-jointed to the solid portion of the plate, as shown in Figs. 3 and 4. Copper-constantan type thermocouples were inserted in the plate for the measurement of wall temperature. For the porous to solid measurements, the plate was simply reversed. The zero transpiration data were obtained on a completely solid surface.

2.2. Data Measurement

Boundary-layer total-pressure measurements were obtained using a flattened pitot probe, as shown in Figs. 5 and 6, which was attached to a pressure transducer and mounted on a traversing mechanism. A sliding potentiometer on the traverse mechanism provided an electrical signal which was fed into one channel of an X-Y recorder, the other channel being connected to the pressure transducer, thus enabling a complete profile record to be obtained during a single tunnel run.

Temperature profiles were obtained in a similar manner using a copper-constantan thermocouple embedded in a 10 degree included-angle steel cone, itself mounted on ceramic tube to reduce heat-transfer effects, and connected directly to the X-Y recorder. Dimensions can be found in Fig. 6.

2.3. Data Reduction

All the X-Y recorder plots were analysed by reading off a series of points, each corresponding to a measured pressure (or temperature) and its associated distance from the surface, together with the relevant scale lengths. These results were fed into a computer program which calculated the velocity and static temperature profiles from the normal Rayleigh pitot formulae, using static pressure from static probe measurements. About 50 points were found adequate to cover the complete profile, and these were spaced according to the rate of change of pressure (or temperature), more being taken in the region near the wall, where the rate of change was normally largest.

From these basic results, boundary-layer parameters, such as displacement thickness and momentum thickness, were calculated. Shear-stress profiles were also obtained, using the momentum equation and the measured velocity and temperature profiles.

2.4. Two-Dimensionality

Jeromin², who used essentially the same equipment as used in the present tests, measured velocity profiles 25 mm either side of the centre line, and reported variations of θ and δ^* of about 2 per cent, from which he assumed that three-dimensional effects were negligible. However, in a further publication, Jeromin⁷ concluded there may well be three-dimensional effects present at Mach 3·6, since he found that skin-friction coefficients evaluated from the momentum-integral equation were about 8 per cent too high when compared to the results of other investigators. His skin-friction results evaluated at Mach 1·8 and 2·5 agreed well with published values, suggesting that in these cases, three-dimensional effects, if any, were minimal.

In the present investigation, spanwise pressures were measured simultaneously using a number of pitot probes and typical results are shown in Fig. 7. Compared with the results at Mach 1·8, those at Mach 3·6 show significant total pressure variations across the span. As will be shown later, the experimental Mach 3·6 data are in good agreement with theory, and it is therefore considered that the error introduced by three-dimensional effects is not large.

2.5. Test Conditions

	Solid-Porous		Porous-Solid
Nominal Mach number	1·8	3·6	3·6
Stagnation pressure	82·7 kN/m ² gauge	887 kN/m ² gauge	887 kN/m ² gauge
Stagnation temperature	293 K	293 K	293 K
Reynolds number per metre	$2\cdot45 \times 10^7$	$5\cdot45 \times 10^7$	$5\cdot45 \times 10^7$
Transpiration rate $\frac{\rho_w V_w}{\rho_1 U_1}$	0 0·00174 0·00311 0·00446	0 0·00164 0·00294 0·00421	0·00294

With the discontinuity as the datum the traverse positions were:

$$\begin{aligned} -25\cdot4 \text{ mm}, & \quad 0 \text{ mm}, \quad 3\cdot2 \text{ mm}, \quad 6\cdot3 \text{ mm}, \quad 9\cdot5 \text{ mm}, \\ 12\cdot7 \text{ mm}, & \quad 19\cdot0 \text{ mm}, \quad 25\cdot4 \text{ mm}, \quad 38\cdot1 \text{ mm}, \quad 50\cdot8 \text{ mm}, \\ 63\cdot5 \text{ mm}, & \quad 88\cdot9 \text{ mm}, \quad 114\cdot3 \text{ mm}, \quad 139\cdot7 \text{ mm}, \quad 171\cdot4 \text{ mm}. \end{aligned}$$

3. Discussion of Results

3.1. Free-Stream Mach Number Distribution

Although the experimental results were obtained in a nominally zero pressure gradient, some localised pressure gradients were present, as is apparent from the free-stream Mach-number distributions shown in Figs. 8 and 9. These were caused by the shock fields in the working section, which can be seen in the schlieren photographs in Fig. 5 and also by the presence of three-dimensional effects described previously. The most serious flow disturbance was generated by the discontinuity itself, in that the sudden change in boundary-layer displacement thickness downstream of the discontinuity gives rise to an expansion wave (porous to solid change), or a compression wave (solid to porous). This can be clearly seen in the schlieren photographs, and is apparent in the results by a sudden change in free-stream Mach number. The fall in free-stream Mach number for the Mach 1·8 flows, at about 125 mm downstream of the discontinuity, is due to a reflected shock starting from the leading edge of the plate, and visible in the schlieren pictures.

Due to the decrease in shock angle with increasing Mach number, the effects of the discontinuity-induced shock wave are felt further downstream for the flows at Mach 3·6 than those at Mach 1·8. On average, the affected regions extend to about 12 mm and 25 mm for the Mach 1·8 and 3·6 flows respectively.

3.2. Velocity-Profile Developments

Figs. 10 to 20 show typical profile developments, together with theoretical predictions obtained using an eddy-viscosity method due to Verma⁶. The experimental velocity and temperature profiles at $x = -25\cdot4$ mm are used in the method to provide starting conditions for the theoretical developments. Experimentally measured free-stream temperature and Mach-number distributions are used in the method for the free-stream boundary conditions. It can be seen that the experimental and theoretical results agree very well, particularly at the lower transpiration rates. The major differences to be found between the experimental and theoretical profiles occur at the rear of the plate, most noticeably at the higher transpiration rates. This is apparent in Fig. 18, where for the Mach 3·6, $F = 0\cdot00421$ development, the measured velocity profile exhibits an inflexion typical of that in a boundary layer near to separation. Indeed, it was found that separation, or 'blow-off', conditions did exist at the last measuring station (at $x = 171\cdot4$ mm), the results for which are not shown, for both the $F = 0\cdot00421$ and $F = 0\cdot00294$ flows at Mach 3·6.

Some individual experimental profiles are also seen to be in slight disagreement with the theoretical predictions. This is possibly a result of localised shock-wave interference at the outer edge of the boundary layer, introducing errors in the determination of the free-stream conditions, and hence producing unrealistic profile shapes.

It will also be observed that the generally good agreement between experiment and theory for the Mach 3·6 developments suggests that the three-dimensional effects mentioned earlier are minimal.

3.3. Temperature-Profile Developments

Figs. 11 to 21 also show typical temperature profile developments, together with theoretical predictions (using the method due to Verma⁶). Good agreement is obtained between the predicted and experimental profiles, but deteriorating towards the rear of the plate, particularly at the higher blowing rates. Again, as was discussed in the previous section, impending 'blow-off' is probably responsible for the inflexion in the profile shapes. It is interesting to observe, however, that the inflexion is also apparent in the predicted profiles.

Figs. 22 and 23 show typical distributions of T/T_1 plotted against u/U_1 , together with the Crocco relation, in which the recovery temperature, T_r , was assumed equal to the wall temperature T_w . Thus it can be written:

$$\frac{T}{T_1} = \frac{T_w}{T_1} + \left(\frac{T_1 - T_w}{T_1} \right) \left(\frac{u}{U_1} \right)^2. \quad (1)$$

While the agreement between the results and the Crocco relation is quite good at Mach 1·8, at Mach 3·6 it is less satisfactory. It should be noticed, however, that these comparisons are somewhat biased, in that the temperature profiles in the region $0 < u/U_1 < 0\cdot7$ approximately, have been deduced from a simple linear extrapolation of the recorded probe temperature nearest the wall, to that of the wall itself.

3.4. Integral Parameters

In general, the predicted developments of θ compare well with the experimental results, as can be seen in Figs. 24 to 26. It might be expected that some disagreement would exist just downstream of the discontinuity where there are marked changes in the values of θ , and which can be attributed to the interference effects on the boundary-layer of the shock wave produced at the start of the transpired region. The shock-wave boundary-layer interaction may also account for the slight differences noticeable between the experimental and predicted developments, since modifications to the initial structure of the boundary-layer will obviously affect the remainder of its growth.

The results for the porous-to-solid situation show most disagreement with theory, as do the velocity and temperature profile predictions for this particular case. It can be seen that the positions of shock-wave interferences on the boundary layer, shown in the Schlieren photographs, correspond closely to those where there are marked changes in the developments of θ . It therefore appears probable that, as before, shock-wave boundary-layer interactions are responsible.

Figs. 27 and 28 show composite plots of shape factor variations against R_θ for the various Mach number and transpiration rates, together with some equilibrium boundary-layer results of Squire³. (For clarity,

individual experimental points have been omitted and replaced by mean curves.) The results are consistent with those of Squire, except for the solid surface Mach 3·6 development, which show slightly different trends. This might possibly be due to three-dimensional effects, or to the slightly different flow conditions for the two sets of experiments. (In the present investigation, the duralumin liner forming the nozzle in the tunnel was moved 152 mm further upstream, relative to its position in Squire's experiments, allowing a longer flow development. It is possible, therefore, that there existed small differences in the flow conditions for the two configurations.)

The data suggest that, in the present experiment, equilibrium conditions have not been reached, in the sense that H has not become a unique function of R_θ and F , even at the last measuring station, since the curves do not attain the levels inferred from Squire's results. This conclusion is supported by the development of the y/θ vs. u/U_1 profiles, shown in Figs. 29 to 31, in which it can be seen that the experimental profiles do not reach a common shape at the end of the development. However, it would appear that the flow is in a near-equilibrium condition, since the profiles show a reasonable degree of collapse at the rear of the plate for the solid-to-porous flows, and the one comparison available of an equilibrium profile from Squire's results confirms this.

Anomalously, the y/θ vs. u/U_1 curves for the porous-to-solid configuration tend to suggest that an equilibrium layer is established in a relatively short distance downstream of the discontinuity, even though the 'equilibrium' profile shape does not agree with either the solid-surface equilibrium profile of Squire, or the solid-surface results from the present investigation. This may be due to errors in the experimental θ variations over the rear of the plate, which appear to be too high compared to the theory. Certainly, for this case, the H vs. R_θ curves suggest that equilibrium conditions have yet to be reached.

3.5. Skin Friction Variations

Figs. 32 and 34 show the predicted skin friction developments, while Figs. 33 and 35 show the variation in dynamic pressure measured by positioning the total-pressure probe onto the surface as a Stanton tube. It is interesting to note that the variations in both predicted skin friction, and measured dynamic pressure near the surface, correspond remarkably well, and indicate that most of their variations occur within the first 25 mm downstream of the discontinuity (about 4 to 5 boundary-layer thicknesses). The exception is the porous-to-solid development, which appears to vary rather more slowly, but again, the trend predicted by the theory, and that shown by the dynamic-pressure variation, are in good agreement.

3.6. Inner-Law Profile Representation

Using the inner law proposed by Squire⁸, of the form

$$G(u^x) = \frac{1}{k} \log_e \left(\frac{y U_\tau}{\nu_w} \right) + B \quad (2)$$

where

$$G(u^x) = \int_0^{u^x} \frac{\sqrt{\rho^x}}{\sqrt{[F u^x + (C_f/2)]}} du^x,$$

$$u^x = \frac{u}{U_1},$$

$$\rho^x = \frac{\rho}{\rho_1}$$

and the skin-friction variation given by theory, inner-law plots were obtained, as shown in Figs. 36 to 41. It can be seen that the profiles (with the exception of the porous-to-solid and the $M = 3\cdot6$, $F = 0\cdot00421$ cases) show an extremely good collapse, bearing in mind the uncertainty in value of C_f . Dunbar⁹ reported that a variation of 10 per cent in the value of C_f can give rise to an overall change in the levels of $G(u^x)$ of about 5 per cent, and thus errors in C_f could well account for the small variations between profiles, particularly just downstream of

the discontinuity where rapid changes occur. The poor result at $M = 3.6$, $F = 0.00421$ could also be due to large errors in C_f , which for this case is small (approaching zero at the separation point).

Similar arguments could also explain the lack of collapse for the porous-to-solid profiles. In this case it will be noticed that the maximum levels of $G(u^x)$ for the profiles in the region of the discontinuity are far higher than those obtained at the rear of the solid-to-porous configuration with the same transpiration rate.

With the exception of the porous-to-solid configuration, the results for the solid-to-porous cases show that the inner part of the boundary layer responds very quickly to the change in surface conditions.

3.7. Shear-Stress Profile Calculations

A numerical technique was used for calculating the shear-stress distributions from the measured velocity and temperature profiles, using the momentum equation. The momentum equation, usually written

$$\tau(y) - \tau_w - y \frac{dp}{dx} = \int_0^y \frac{\partial}{\partial x} (\rho u^2) dy' - u(y) \int_0^y \frac{\partial}{\partial x} (\rho u) dy' + \rho_w V_w u(y), \quad (3)$$

is rewritten in the form

$$\tau(y) - \tau_w - y \frac{dp}{dx} = \frac{\partial}{\partial x} \left[\int_0^y (\rho u^2) dy' - u(y) \int_0^y (\rho u) dy' + \int_0^{u(y)} \left\{ \int_0^{y(u')} (\rho u) dy' \right\} du' \right] + \rho_w V_w u(y). \quad (4)$$

Whilst the two equations are essentially the same, the computational advantage in the second lies in the single numerical differentiation.

Using equation (4), the shear-stress profiles were calculated, and typical cases are shown in Figs. 42 to 44. It can be seen that the experimental results agree reasonably well with the overall predictions, considering the limitations of the calculation technique. Shock-wave boundary-layer interactions producing profile distortions obviously introduce errors, and is particularly relevant just downstream of the discontinuity. In addition, errors in the skin-friction value used are reflected directly in the shear-stress profiles.

Analytical errors are introduced primarily in obtaining the x -derivatives in the calculation procedure. To reduce these errors, the derivatives were found by fitting a curve to the function inside the square brackets in equation (4). However, the errors may become dominant towards the edge of the layer, where small errors in the shape of the profiles give rise to finite shear-stress values. A non-zero shear stress at the outer edge of the boundary layer was assumed, for the purposes of the numerical procedure, to be a result of a localised pressure gradient, which was then applied proportionately throughout the layer. In this manner, the shear-stress profiles were forced to zero at $y = \delta(u/U_1 = 1)$.

Predicted and experimental shear-stress profiles for the porous-solid situation, although exhibiting similar shape, are not in good agreement at the start of the development. However, the agreement improves towards the end of the plate where it is, in fact, extremely good. This behaviour might be expected following the rather poor results shown in the logarithmic inner-law plots, with the associated uncertainty over the magnitude of the skin friction.

3.8. Mixing-Length Distributions

Using the shear-stress profiles calculated as described in the previous section, the mixing length distributions were obtained, from

$$l = \left(\frac{\tau}{\rho} \right)^{\frac{1}{2}} / \frac{du}{dy} \quad (5)$$

and shown in Figs. 45 to 49. In general, the results show a reasonable collapse onto a straight line in the wall region, with a slope of about 0.4. However, at the higher transpiration rates, and particularly for the mixing length distributions calculated from profiles in the region just downstream of the discontinuity, some scatter in the results is evident. This is to be expected, since the shear-stress profiles in this region showed some disagreement with the theoretical predictions, particularly near the wall.

The porous-to-solid results do not show a good collapse, which is to be expected considering the dissimilarity between the theoretical and calculated shear-stress profiles.

In the outer region, the mixing-length distributions do not show any consistent trends. The scatter can be attributed to errors in both the shear-stress profile and the slope of the velocity profile (du/dy) in the outer region (particularly just downstream of the discontinuity where shock-wave interaction effects are dominant), both parameters tending to zero at the outer edge of the layer. However, results suggest that the adoption of a constant value for l/δ if between 0·07 and 0·08 is not unreasonable.

The outer region mixing-length distributions for the porous-to-solid case appear to be somewhat lower than those of the solid-to-porous developments. However this might be expected, considering the experimental shear-stress profiles for this case which also appear low.

3.9. Eddy-Viscosity Distributions

These were obtained from the relation

$$\nu_e = \frac{\tau}{\rho} \frac{du}{dy} \quad (6)$$

and shown in Figs. 45 to 49. The profiles exhibit a fair collapse in the outer region, except for the first few profiles immediately downstream of the discontinuity. Apart from these, a value of about 0·015 would appear to be a reasonable estimate of the maximum value of the eddy viscosity. The exceptions are the results for the porous-to-solid development, which appear to be extremely low, having a maximum of about 0·08. This particular case reflects the experimental shear-stress profiles, which can be seen to be much lower than those given by prediction. From these findings, it would seem probable that there are deficiencies in the outer region eddy-viscosity model as used to predict the porous-to-solid development.

4. Conclusions

4.1. The boundary layer was not found to reach an equilibrium state even at the end of the measuring region (equivalent to about 35 boundary-layer thickness). However, from the experimental results for the Mach 1·8 flows at the lower transpiration rates, it would appear that a near equilibrium condition is attained, as indicated by the near-collapse of the u/U_1 vs. y/θ curves.

4.2. Except for the porous-to-solid situation, the inner part of the boundary layer appears to respond rapidly to the change in surface conditions, as is shown by the generally good collapse of the logarithmic law in this region. Lack of collapse for the porous-to-solid development is not necessarily indicative of a slow response of the inner region. Errors in the magnitude of the skin friction may be responsible for this.

4.3. Uncertainties in the experimental results, particularly for the value of skin friction, makes quantitative analysis of the mixing-length and eddy-viscosity results difficult. However, it would appear that the adoption of a mixing-length relation of the form $l = \text{const.} \times y$ in the inner region is not unreasonable. In addition, while the eddy-viscosity results do not show a good collapse in the outer part of the flow, there would appear to be no justification in adopting a complex model in this region.

4.4. In general, the experimental results agree reasonably well with the eddy viscosity theoretical predictions. Most noticeable differences occur in the regions of shock wave boundary interactions, and towards the end of the measuring region where the boundary layer was tending towards separation, particularly at the higher transpiration rates.

4.5. Three-dimensional effects may be present in the Mach 3·6 flows, although their influence on the data is considered minimal.

5. Tables of Experimental Results

5.1. Wall Temperature

The three thermocouples in the porous surface each gave approximately the same reading, being nominally 2 K below stagnation temperature for the Mach 1·8 flows, and 6 K below at Mach 3·6.

5.2. Free-Stream Velocity and Temperature

Tables 2 and 3 show the measured free-stream velocities and temperatures. Identification of the flow situation is given at the head of each column, in the form

$$A - B - C$$

where A is the nominal free-stream Mach number

B is the flow situation, set equal to

0 for the solid surface

1 for the solid-to-porous surface

2 for the porous-to-solid surface

C is the transpiration rate, $F (= \rho_w V_w / \rho_1 U_1)$

5.3. Displacement and Momentum Thicknesses

Tables 4 and 5 give the displacement and momentum thicknesses respectively, calculated from the velocity and temperature profiles.

5.4. Tabulated Velocity and Temperature Profiles

The remaining tables list the values of u/U_1 and T/T_1 which have been interpolated onto a fixed y -grid from the experimental results. Each set of results is again identified in the manner described in the previous section.

It should be noted that the data points shown in the figures are those from experimental and not the interpolated values given in the tables.

Acknowledgements

The author would like to express his appreciation for the advice and direction given by Dr. L. C. Squire (CUED) and for the provision of financial assistance from the Ministry of Technology.

LIST OF SYMBOLS

A_0	Damping-function constant
B	Log-law constant
C_f	Skin friction ($= \tau_w / \rho_1 U_1^2$)
F	Transpiration parameter ($= \rho_w V_w / \rho_1 U_1$)
H	Shape factor
k_1, k_2	Constants in eddy-viscosity model
l	Mixing length
M	Mach number
p	Static pressure
Pr	Laminar Prandtl number
Pr_t	Turbulent Prandtl number
T	Static temperature
T_r	Recovery temperature
u, U	Streamwise velocity
U_τ	Friction velocity ($= \sqrt{\tau_w / \rho_w}$)
V	Velocity normal to surface
x	Streamwise coordinate
y	Normal coordinate
δ	Boundary-layer thickness (at $u/U_1 = 0.995$)
δ^*	Displacement thickness ($= \int_0^\infty \left(1 - \frac{\rho U}{\rho_1 U_1}\right) dy$)
δ_k^*	Incompressible-displacement thickness ($= \int_0^\infty \left(1 - \frac{u}{U_1}\right) dy$)
θ	Momentum thickness ($= \int_0^\infty \frac{\rho u}{\rho_1 U_1} \left(1 - \frac{u}{U_1}\right) dy$)
ν	Kinematic viscosity
ν_e	'Effective' kinematic viscosity ($= -u'v' / \frac{\partial u}{\partial y} + \nu$)
τ	Shear stress
ρ	Density
ε	$uv / \frac{\partial u}{\partial y}$
<i>Subscripts</i>	
w	Value at wall
1	Value at free stream
a	Atmospheric conditions

REFERENCES

<i>No.</i>	<i>Author(s)</i>	<i>Title, etc.</i>
1	P. G. Marriott	Compressible turbulent boundary layers with discontinuous injection. Ph.D. Dissertation, Cambridge University (1973).
2	L. O. F. Jeromin	Compressible turbulent boundary layers with fluid injection. Ph.D. Dissertation, Cambridge University (1966).
3	L. C. Squire	Further experimental investigations of compressible turbulent boundary layers with air injection. A.R.C. R. & M. 3627 (1968).
4	W. M. Kays	Heat transfer to the transpired turbulent boundary layer. Report HMT-14. Thermosciences Div., Dept. of Mech. Eng., Stanford University (1971).
5	J. McQuaid	Incompressible turbulent boundary layers with distributed injection. Ph.D. Dissertation, Cambridge Univ. (1966).
6	V. K. Verma	A method of calculation for two-dimensional and axisymmetric boundary layers. CUED/A-Aero/TR3 Cambridge University (1971).
7	L. O. F. Jeromin	An experimental investigation of the compressible turbulent boundary layer with air injection. A.R.C. R. & M. 3526 (1968).
8	L. C. Squire	A law of the wall for compressible turbulent boundary layers with injection. <i>J. Fluid. Mech.</i> 37 , 449–456 (1969).
9	D. I. A. Dunbar	Turbulent boundary layers with foreign gas injection. Ph.D. Dissertation, Cambridge University (1968).

APPENDIX A

Eddy Viscosity Formulation

The eddy-viscosity formulation adopted by Verma⁶ in the prediction method is as follows
Inner region:

$$\nu_e = \nu + k_1 y^2 \{1 - e^{(-y^+/A^+)}\}^2 \frac{\partial u}{\partial y}$$

where

$$y^+ = \frac{U_\tau y}{\nu},$$

$$A^+ = A_0 \left\{ e^{(11 \cdot 8 V_w^+)} - \frac{p^+}{V_w^+} (e^{(11 \cdot 8 V_w^+)} - 1) \right\}^{-\frac{1}{2}},$$

$$p^+ = - \left(\frac{dp}{dx} \right) \frac{\nu}{\rho_w U_\tau}$$

and

$$V_w^+ = \frac{V_w}{U_\tau}.$$

Outer region:

$$\nu_e = \nu + k_2 \delta_k^* U_1 \left(1 + 5 \cdot 5 \left(\frac{y}{\delta} \right)^6 \right)^{-\frac{1}{2}}.$$

TABLE 1
Parameters Used in the Eddy-Viscosity Method

$A_0 = 26$ (constant in Van Driest damping function)
 $k_1 = 0.4$ (inner-region constant)
 $k_2 = 0.016$ (outer-region constant)
 $Pr = 0.7$ (laminar Prandtl number)
 $Pr_t = 0.89$ (turbulent Prandtl number)

TABLE 2
Tables of U_1 (m/s) at Experimental Stations

Case x mm	1·8-0- 0·0000	1·8-1- 0·00174	1·8-1- 0·00311	1·8-1- 0·00446	3·6-0- 0·0000	3·6-1- 0·00164	3·6-1- 0·00294	3·6-1- 0·00421	3·6-2- 0·00294
-25·4	481·22	482·06	481·06	480·09	659·05	655·68	659·82	655·71	657·70
0		482·56	482·56	484·96		656·76	656·59	652·99	658·52
3·2		484·02	480·12	480·60		655·74	652·63	653·85	658·65
6·3		486·47	484·48	482·07		655·35	654·34	655·74	659·66
9·5		482·31	482·87	476·69		651·25	653·68	657·96	651·74
12·7	481·25	476·50	476·85	474·70	655·65	656·23	656·92	657·93	653·56
19·0		482·31	479·23	477·56		659·30	654·47	659·30	656·62
25·4		475·86	476·20	474·52		652·12	654·63	647·00	657·96
38·1		480·74	481·22	482·59		655·06	652·65	651·46	660·91
50·8		483·15	484·11	480·66		653·77	653·57	652·85	659·35
63·5	489·08	484·94	483·92	483·92	656·89	657·53	648·64	651·38	662·76
88·9		489·33	478·80	483·51		655·62	654·68	651·76	655·53
114·3	475·58	487·42	483·24	482·70	658·23	654·18	655·17	651·14	658·02
139·7		480·15	481·65	479·91		654·86	653·97	650·29	661·80
171·4	478·15	474·57	465·82	467·47	659·76	656·46			661·32

TABLE 3
Tables of T_1 (Kelvin) at Experimental Stations

Case x mm \	1·8-0- 0·0000	1·8-1- 0·00174	1·8-1- 0·00311	1·8-1- 0·00446	3·6-0- 0·0000	3·6-1- 0·00164	3·6-1- 0·00294	3·6-1- 0·00421	3·6-2- 0·00294
-25·4	176·6	176·8	177·2	176·5	83·0	82·1	83·7	82·7	84·3
0		176·1	176·1	178·9		83·2	83·3	82·5	83·8
3·2		177·1	174·3	175·7		83·2	82·1	82·6	83·8
6·3		176·7	178·6	175·7		82·8	82·8	83·2	83·8
9·5		179·5	177·6	181·2		81·8	82·7	83·6	81·5
12·7	175·4	175·2	178·9	179·8	82·7	83·4	83·6	83·6	83·3
19·0		179·5	180·0	182·1		84·0	82·2	84·0	84·3
25·4		177·1	178·6	181·0		84·6	87·1	86·9	84·2
38·1		177·3	177·7	178·8		84·1	85·4	87·2	81·9
50·8		174·7	177·6	177·4		84·8	86·6	88·1	81·2
63·5	175·6	177·3	178·8	178·8	83·7	86·1	85·4	87·8	82·1
88·9		178·2	170·9	175·2		84·3	85·4	86·5	80·6
114·3	180·6	177·9	176·3	178·2	83·4	83·5	85·7	87·4	81·9
139·7		179·8	179·7	182·1		83·7	85·3	88·9	83·1
171·4	180·1	179·3	183·9	187·7	83·7	83·9			83·9

TABLE 4
Tables of δ^* (mm) at Experimental Stations

Case x mm \	1·8-0- 0·0000	1·8-1- 0·00174	1·8-1- 0·00311	1·8-1- 0·00446	3·6-1- 0·0000	3·6-1- 0·00164	3·6-1- 0·00294	3·6-1- 0·00421	3·6-2- 0·00294
-25·4	1·209	1·219	1·255	1·232	2·736	2·720	2·705	2·703	2·361
0		1·288	1·303	1·295		2·797	2·797	2·786	2·607
3·2		1·293	1·318	1·321		2·858	2·858	2·827	2·587
6·3		1·290	1·341	1·351		2·819	2·835	2·835	2·638
9·5		1·377	1·384	1·488		2·812	2·807	2·817	2·597
12·7	1·308	1·415	1·488	1·565	2·883	2·819	2·822	2·868	2·899
19·0		1·478	1·575	1·643		2·908	3·025	3·061	2·940
25·4		1·534	1·638	1·775		3·096	3·299	3·553	2·922
38·1		1·641	1·753	1·877		3·287	3·612	3·993	2·297
50·8		1·694	1·877	2·106		3·498	3·957	4·417	2·224
63·5	1·400	1·791	2·045	2·294	3·099	3·658	4·282	4·874	2·219
88·9		1·971	2·342	2·715		3·978	4·793	5·677	2·448
114·3	1·737	2·195	2·611	3·124	3·261	4·397	5·380	6·751	2·470
139·7		2·410	2·934	3·635		4·722	6·043	7·943	2·777
171·4	1·750	2·784	3·813	5·674	3·490	5·593			2·803

TABLE 5

Tables of θ (mm) at Experimental Stations

Case x mm \	18-0- 0-0000	1·8-1- 0-00174	1·8-1- 0-00311	1·8-1- 0-00446	3·6-1- 0-0000	3·6-1- 0-00164	3·6-1- 0-00294	3·6-1- 0-00421	3·6-2- 0-00294
-25·4	0·424	0·427	0·439	0·427	0·401	0·381	0·396	0·389	0·869
0		0·450	0·455	0·465		0·404	0·404	0·401	0·947
3·2		0·460	0·452	0·455		0·411	0·396	0·399	0·953
6·3		0·452	0·470	0·455		0·394	0·378	0·389	0·975
9·5		0·493	0·480	0·521		0·396	0·394	0·384	0·963
12·7	0·460	0·485	0·523	0·536	0·422	0·399	0·394	0·386	1·021
19·0		0·523	0·539	0·561		0·411	0·404	0·419	1·069
25·4		0·526	0·554	0·592		0·445	0·472	0·493	1·069
38·1		0·564	0·594	0·627		0·470	0·505	0·551	0·975
50·8		0·574	0·638	0·681		0·500	0·551	0·605	0·950
63·5	0·500	0·597	0·671	0·726	0·462	0·523	0·582	0·653	0·958
88·9		0·668	0·742	0·836		0·554	0·643	0·719	0·970
114·3	0·645	0·732	0·836	0·960	0·448	0·607	0·726	0·836	1·049
139·7		0·815	0·953	1·113		0·650	0·795	0·975	1·090
171·4	0·653	0·914	1·143	1·580	0·533	0·732			1·110

TABLE 6
Tables of u/U_1 at Traverse Positions

Y (mm)	X (mm)=	1·8-0-0-00000					3·6-0-0-00000				
		-25·4	12·7	63·5	14·3	171·4	-25·4	12·7	63·5	114·3	171·4
0·081		0·494	0·494	0·496	0·422	0·477	0·428	0·432	0·436	0·448	0·453
0·090		0·505	0·506	0·505	0·431	0·485	0·438	0·456	0·450	0·459	0·461
0·100		0·518	0·519	0·514	0·441	0·494	0·451	0·480	0·466	0·472	0·471
0·110		0·530	0·532	0·524	0·452	0·503	0·462	0·500	0·481	0·484	0·480
0·120		0·541	0·453	0·533	0·462	0·511	0·473	0·515	0·494	0·495	0·490
0·130		0·551	0·554	0·541	0·472	0·519	0·483	0·526	0·507	0·506	0·500
0·140		0·561	0·564	0·549	0·481	0·526	0·493	0·533	0·518	0·515	0·509
0·150		0·569	0·573	0·556	0·491	0·533	0·502	0·536	0·528	0·524	0·519
0·160		0·576	0·581	0·563	0·500	0·540	0·511	0·535	0·537	0·532	0·529
0·180		0·588	0·594	0·575	0·513	0·551	0·526	0·540	0·552	0·546	0·545
0·200		0·596	0·603	0·587	0·525	0·559	0·543	0·555	0·562	0·557	0·558
0·250		0·616	0·624	0·613	0·557	0·584	0·575	0·585	0·589	0·586	0·586
0·300		0·637	0·642	0·633	0·581	0·614	0·597	0·605	0·610	0·609	0·608
0·350		0·653	0·656	0·650	0·598	0·627	0·614	0·624	0·627	0·627	0·628
0·400		0·669	0·667	0·665	0·616	0·641	0·628	0·635	0·643	0·643	0·646
0·450		0·678	0·676	0·677	0·629	0·647	0·640	0·645	0·653	0·657	0·659
0·500		0·687	0·687	0·688	0·641	0·657	0·650	0·656	0·661	0·667	0·670
0·600		0·705	0·705	0·705	0·662	0·676	0·664	0·671	0·676	0·682	0·687
0·700		0·718	0·719	0·715	0·678	0·688	0·677	0·683	0·688	0·694	0·697
0·800		0·732	0·733	0·730	0·691	0·701	0·687	0·692	0·696	0·702	0·704
0·900		0·744	0·743	0·744	0·703	0·711	0·695	0·701	0·702	0·706	0·710
1·000		0·756	0·751	0·754	0·713	0·722	0·702	0·709	0·708	0·714	0·718
1·100		0·767	0·764	0·762	0·725	0·732	0·711	0·714	0·715	0·721	0·725
1·200		0·778	0·774	0·771	0·735	0·739	0·719	0·720	0·722	0·726	0·730
1·300		0·788	0·782	0·779	0·743	0·748	0·726	0·727	0·727	0·732	0·735
1·400		0·797	0·790	0·787	0·752	0·756	0·734	0·735	0·733	0·739	0·740
1·600		0·815	0·805	0·802	0·766	0·768	0·749	0·748	0·747	0·752	0·751
1·800		0·832	0·822	0·817	0·780	0·780	0·765	0·763	0·760	0·763	0·762
2·000		0·848	0·837	0·831	0·794	0·792	0·779	0·775	0·772	0·775	0·773
2·500		0·886	0·872	0·861	0·823	0·823	0·814	0·810	0·801	0·800	0·799
3·000		0·921	0·905	0·890	0·852	0·849	0·849	0·842	0·829	0·827	0·825
3·500		0·952	0·935	0·917	0·877	0·875	0·880	0·872	0·857	0·852	0·844
4·000		0·974	0·959	0·943	0·903	0·899	0·909	0·899	0·883	0·887	0·866
4·500		0·989	0·980	0·964	0·925	0·920	0·936	0·925	0·908	0·898	0·887
5·000		0·997	0·990	0·981	0·944	0·938	0·961	0·950	0·930	0·919	0·903

TABLE 6 (continued)
Tables of u/U_1 at Traverse Positions

Y (mm)	X (mm)=	1·8-0-0-00000					3·6-0-0-00000				
		-25·4	12·7	63·5	14·3	171·4	-25·4	12·7	63·5	14·3	171·4
6·000		1·000	0·998	0·996	0·970	0·972	0·993	0·985	0·968	0·955	0·939
7·000		1·000	1·000	1·000	0·992	0·990	1·000	0·997	0·992	0·983	0·968
8·000		1·000	1·000	1·000	1·000	0·997	1·000	1·000	1·000	0·996	0·987
9·000		1·000	1·000	1·000	1·000	1·000	1·000	1·000	1·000	1·000	0·996
10·000		1·000	1·000	1·000	1·000	1·000	1·000	1·000	1·000	1·000	0·998
11·000		1·000	1·000	1·000	1·000	1·000	1·000	1·000	1·000	1·000	1·000
12·000		1·000	1·000	1·000	1·000	1·000	1·000	1·000	1·000	1·000	1·000
13·000		1·000	1·000	1·000	1·000	1·000	1·000	1·000	1·000	1·000	1·000
14·000		1·000	1·000	1·000	1·000	1·000	1·000	1·000	1·000	1·000	1·000
15·000		1·000	1·000	1·000	1·000	1·000	1·000	1·000	1·000	1·000	1·000

TABLE 6 (continued)
Tables of u/U_1 at Traverse Positions

1·8-1-0-00174

Y (mm)	X (mm)=	-25·4	0·0	3·2	6·3	9·5	12·7	19·0	25·4	38·1	50·8	63·5	88·9	114·3	139·7	171·4
0·081		0·492	0·497	0·476	0·472	0·432	0·428	0·411	0·394	0·388	0·393	0·379	0·364	0·373	0·329	0·281
0·090		0·500	0·502	0·485	0·479	0·439	0·435	0·417	0·402	0·393	0·397	0·388	0·370	0·377	0·337	0·286
0·100		0·509	0·509	0·496	0·488	0·447	0·443	0·425	0·411	0·400	0·403	0·399	0·378	0·381	0·347	0·291
0·110		0·518	0·517	0·506	0·497	0·455	0·451	0·433	0·419	0·407	0·409	0·408	0·385	0·486	0·356	0·297
0·120		0·527	0·525	0·516	0·506	0·462	0·458	0·440	0·427	0·414	0·415	0·418	0·393	0·391	0·366	0·303
0·130		0·535	0·533	0·525	0·514	0·470	0·466	0·447	0·435	0·422	0·422	0·427	0·400	0·396	0·375	0·309
0·140		0·543	0·542	0·533	0·523	0·478	0·474	0·454	0·442	0·430	0·429	0·435	0·406	0·401	0·383	0·315
0·150		0·550	0·552	0·541	0·531	0·485	0·481	0·460	0·448	0·438	0·436	0·443	0·413	0·406	0·391	0·321
0·160		0·557	0·562	0·548	0·538	0·492	0·488	0·468	0·454	0·446	0·444	0·450	0·420	0·411	0·400	0·327
0·180		0·570	0·582	0·560	0·550	0·506	0·502	0·484	0·468	0·462	0·456	0·462	0·433	0·421	0·415	0·338
0·200		0·582	0·592	0·571	0·561	0·521	0·515	0·498	0·481	0·476	0·469	0·473	0·446	0·432	0·428	0·351
0·250		0·606	0·614	0·598	0·589	0·552	0·545	0·525	0·513	0·503	0·503	0·497	0·475	0·456	0·455	0·380
0·300		0·624	0·635	0·624	0·611	0·574	0·573	0·545	0·538	0·521	0·527	0·518	0·498	0·473	0·471	0·400
0·350		0·642	0·651	0·639	0·629	0·595	0·591	0·567	0·558	0·540	0·545	0·536	0·517	0·491	0·490	0·413
0·400		0·657	0·663	0·659	0·644	0·615	0·612	0·586	0·576	0·554	0·565	0·547	0·533	0·508	0·505	0·430
0·450		0·667	0·673	0·671	0·659	0·630	0·626	0·603	0·594	0·568	0·584	0·565	0·540	0·521	0·516	0·447
0·500		0·679	0·685	0·683	0·674	0·646	0·644	0·619	0·608	0·590	0·599	0·580	0·555	0·533	0·527	0·462
0·600		0·696	0·702	0·704	0·692	0·671	0·666	0·645	0·632	0·613	0·622	0·601	0·577	0·554	0·546	0·486
0·700		0·712	0·716	0·717	0·709	0·687	0·687	0·664	0·654	0·635	0·641	0·620	0·597	0·572	0·561	0·505
0·800		0·724	0·728	0·729	0·722	0·702	0·705	0·682	0·672	0·654	0·657	0·638	0·616	0·588	0·571	0·523
0·900		0·738	0·740	0·738	0·733	0·715	0·718	0·698	0·688	0·669	0·673	0·654	0·629	0·604	0·583	0·543
1·000		0·751	0·752	0·749	0·747	0·727	0·729	0·714	0·702	0·683	0·687	0·668	0·641	0·618	0·596	0·558
1·100		0·762	0·764	0·761	0·758	0·739	0·741	0·727	0·715	0·697	0·700	0·682	0·654	0·629	0·609	0·572
1·200		0·773	0·772	0·770	0·769	0·749	0·751	0·739	0·728	0·711	0·712	0·694	0·667	0·640	0·619	0·584
1·300		0·784	0·783	0·780	0·778	0·762	0·762	0·749	0·741	0·724	0·725	0·706	0·681	0·652	0·627	0·596
1·400		0·794	0·792	0·789	0·788	0·772	0·772	0·758	0·752	0·736	0·735	0·717	0·691	0·662	0·635	0·607
1·600		0·812	0·807	0·807	0·805	0·788	0·788	0·778	0·771	0·757	0·758	0·739	0·711	0·682	0·655	0·627
1·800		0·829	0·823	0·823	0·821	0·805	0·807	0·794	0·791	0·776	0·778	0·759	0·730	0·702	0·670	0·647
2·000		0·846	0·840	0·840	0·838	0·824	0·824	0·810	0·807	0·795	0·793	0·779	0·750	0·723	0·688	0·665
2·500		0·888	0·875	0·873	0·876	0·859	0·862	0·849	0·846	0·835	0·831	0·821	0·794	0·766	0·732	0·702
3·000		0·923	0·908	0·906	0·910	0·894	0·898	0·884	0·880	0·870	0·864	0·856	0·831	0·806	0·771	0·740
3·500		0·952	0·939	0·934	0·938	0·928	0·928	0·916	0·911	0·901	0·894	0·887	0·865	0·840	0·811	0·776
4·000		0·975	0·964	0·961	0·964	0·955	0·954	0·943	0·941	0·929	0·923	0·914	0·893	0·871	0·844	0·809
4·500		0·990	0·982	0·978	0·983	0·975	0·974	0·966	0·965	0·953	0·946	0·940	0·921	0·899	0·876	0·841
5·000		0·997	0·993	0·990	0·994	0·988	0·988	0·984	0·984	0·973	0·966	0·961	0·943	0·925	0·902	0·866

TABLE 6 (continued)
Tables of u/U_1 at Traverse Positions

1.8-1-0-00174

Y (mm)	X (mm)=	-25.4	0.0	3.2	6.3	9.5	12.7	19.0	25.4	38.1	50.8	63.5	88.9	114.3	139.7	171.4
6.000		1.000	1.000	1.000	1.000	1.000	0.998	0.998	0.994	0.991	0.991	0.980	0.965	0.947	0.916	
7.000		1.000	1.000	1.000	1.000	1.000	1.000	1.000	0.998	1.000	1.000	0.996	0.989	0.979	0.959	
8.000		1.000	1.000	1.000	1.000	1.000	1.000	1.000	1.000	1.000	1.000	1.000	0.998	0.995	0.985	
9.000		1.000	1.000	1.000	1.000	1.000	1.000	1.000	1.000	1.000	1.000	1.000	1.000	1.000	0.996	
10.000		1.000	1.000	1.000	1.000	1.000	1.000	1.000	1.000	1.000	1.000	1.000	1.000	1.000	1.000	
11.000		1.000	1.000	1.000	1.000	1.000	1.000	1.000	1.000	1.000	1.000	1.000	1.000	1.000	1.000	
12.000		1.000	1.000	1.000	1.000	1.000	1.000	1.000	1.000	1.000	1.000	1.000	1.000	1.000	1.000	
13.000		1.000	1.000	1.000	1.000	1.000	1.000	1.000	1.000	1.000	1.000	1.000	1.000	1.000	1.000	
14.000		1.000	1.000	1.000	1.000	1.000	1.000	1.000	1.000	1.000	1.000	1.000	1.000	1.000	1.000	
15.000		1.000	1.000	1.000	1.000	1.000	1.000	1.000	1.000	1.000	1.000	1.000	1.000	1.000	1.000	

TABLE 6 (continued)
Tables of u/U_1 at Traverse Positions

1·8-1-0-00311

Y (mm)	X (mm)=	-25·4	0·0	3·2	6·3	9·5	12·7	19·0	25·4	38·1	50·8	63·5	88·9	114·3	139·7	171·4
0·181		0·488	0·500	0·467	0·425	0·416	0·373	0·364	0·338	0·354	0·317	0·294	0·371	0·347	0·264	0·122
0·090		0·495	0·504	0·475	0·433	0·423	0·379	0·368	0·346	0·361	0·321	0·301	0·374	0·353	0·270	0·130
0·100		0·503	0·509	0·483	0·443	0·431	0·386	0·373	0·356	0·369	0·327	0·309	0·378	0·359	0·277	0·140
0·110		0·511	0·515	0·492	0·452	0·438	0·393	0·379	0·364	0·376	0·333	0·317	0·382	0·366	0·285	0·149
0·120		0·520	0·522	0·499	0·461	0·446	0·401	0·385	0·373	0·384	0·339	0·325	0·386	0·372	0·292	0·157
0·130		0·528	0·529	0·505	0·471	0·454	0·409	0·391	0·380	0·392	0·346	0·333	0·390	0·377	0·299	0·164
0·140		0·536	0·536	0·511	0·480	0·461	0·417	0·397	0·388	0·399	0·353	0·341	0·393	0·382	0·306	0·171
0·150		0·544	0·544	0·517	0·489	0·468	0·426	0·404	0·394	0·406	0·360	0·348	0·397	0·387	0·312	0·177
0·160		0·551	0·552	0·525	0·498	0·475	0·434	0·411	0·400	0·413	0·367	0·356	0·401	0·392	0·319	0·183
0·180		0·560	0·569	0·540	0·514	0·489	0·452	0·426	0·414	0·427	0·382	0·369	0·408	0·400	0·332	0·191
0·200		0·569	0·588	0·554	0·524	0·502	0·462	0·441	0·427	0·440	0·396	0·381	0·415	0·407	0·344	0·198
0·250		0·594	0·616	0·580	0·550	0·532	0·489	0·467	0·457	0·463	0·423	0·410	0·431	0·420	0·369	0·214
0·300		0·616	0·632	0·608	0·576	0·557	0·518	0·494	0·485	0·487	0·453	0·435	0·446	0·433	0·388	0·230
0·350		0·634	0·646	0·629	0·599	0·581	0·545	0·517	0·505	0·503	0·477	0·454	0·462	0·446	0·407	0·241
0·400		0·648	0·659	0·646	0·626	0·605	0·569	0·538	0·522	0·517	0·498	0·472	0·474	0·458	0·426	0·254
0·450		0·662	0·671	0·663	0·640	0·621	0·586	0·558	0·541	0·533	0·517	0·489	0·484	0·468	0·440	0·266
0·500		0·673	0·682	0·677	0·653	0·639	0·603	0·576	0·553	0·549	0·534	0·503	0·496	0·477	0·451	0·280
0·600		0·689	0·698	0·696	0·678	0·666	0·627	0·603	0·579	0·575	0·557	0·526	0·513	0·494	0·472	0·305
0·700		0·704	0·711	0·712	0·693	0·684	0·654	0·630	0·611	0·593	0·584	0·547	0·533	0·512	0·491	0·325
0·800		0·720	0·724	0·726	0·707	0·702	0·674	0·654	0·634	0·615	0·603	0·571	0·547	0·524	0·503	0·345
0·900		0·732	0·736	0·736	0·702	0·714	0·692	0·675	0·653	0·633	0·623	0·592	0·563	0·535	0·516	0·367
1·000		0·746	0·749	0·747	0·735	0·727	0·707	0·690	0·671	0·651	0·636	0·608	0·577	0·549	0·530	0·388
1·100		0·759	0·759	0·759	0·747	0·743	0·720	0·706	0·689	0·667	0·652	0·623	0·590	0·563	0·542	0·407
1·200		0·767	0·768	0·768	0·756	0·754	0·732	0·719	0·703	0·680	0·665	0·636	0·602	0·573	0·551	0·424
1·300		0·778	0·779	0·776	0·764	0·762	0·744	0·731	0·715	0·695	0·680	0·650	0·615	0·586	0·560	0·438
1·400		0·786	0·787	0·786	0·774	0·772	0·753	0·743	0·728	0·709	0·692	0·662	0·628	0·600	0·570	0·450
1·600		0·810	0·806	0·804	0·794	0·790	0·773	0·763	0·750	0·733	0·716	0·689	0·651	0·620	0·588	0·471
1·800		0·826	0·822	0·821	0·813	0·809	0·791	0·783	0·770	0·755	0·737	0·712	0·674	0·641	0·603	0·494
2·000		0·844	0·837	0·838	0·830	0·825	0·808	0·802	0·791	0·777	0·755	0·734	0·695	0·660	0·620	0·521
2·500		0·882	0·875	0·876	0·867	0·861	0·846	0·842	0·834	0·821	0·803	0·783	0·742	0·708	0·660	0·572
3·000		0·915	0·910	0·909	0·903	0·898	0·883	0·878	0·870	0·859	0·841	0·823	0·789	0·752	0·703	0·613
3·500		0·947	0·938	0·937	0·934	0·930	0·915	0·908	0·902	0·891	0·875	0·862	0·830	0·793	0·746	0·659
4·000		0·973	0·963	0·963	0·960	0·958	0·944	0·937	0·933	0·918	0·906	0·895	0·867	0·831	0·785	0·702
4·500		0·987	0·981	0·982	0·983	0·980	0·969	0·963	0·959	0·945	0·932	0·924	0·897	0·864	0·821	0·741
5·000		0·995	0·991	0·993	0·993	0·993	0·986	0·980	0·980	0·967	0·957	0·948	0·924	0·892	0·854	0·775

TABLE 6 (continued)
Tables of u/U_1 at Traverse Positions

1·8-1-0-00311

Y (mm)	X (mm)=	-25·4	0·0	3·2	6·3	9·5	12·7	19·0	25·4	38·1	50·8	63·5	88·9	114·3	139·7	171·4
6·000		1·000	1·000	1·000	1·000	1·000	1·000	0·997	0·997	0·993	0·986	0·981	0·966	0·944	0·912	0·839
7·000		1·000	1·000	1·000	1·000	1·000	1·000	1·000	1·000	0·998	0·997	0·994	0·990	0·978	0·957	0·899
8·000		1·000	1·000	1·000	1·000	1·000	1·000	1·000	1·000	1·000	1·000	1·000	0·997	0·995	0·984	0·944
9·000		1·000	1·000	1·000	1·000	1·000	1·000	1·000	1·000	1·000	1·000	1·000	1·000	0·997	0·997	0·976
10·000		1·000	1·000	1·000	1·000	1·000	1·000	1·000	1·000	1·000	1·000	1·000	1·000	1·000	1·000	0·994
11·000		1·000	1·000	1·000	1·000	1·000	1·000	1·000	1·000	1·000	1·000	1·000	1·000	1·000	1·000	1·000
12·000		1·000	1·000	1·000	1·000	1·000	1·000	1·000	1·000	1·000	1·000	1·000	1·000	1·000	1·000	1·000
13·000		1·000	1·000	1·000	1·000	1·000	1·000	1·000	1·000	1·000	1·000	1·000	1·000	1·000	1·000	1·000
14·000		1·000	1·000	1·000	1·000	1·000	1·000	1·000	1·000	1·000	1·000	1·000	1·000	1·000	1·000	1·000
15·000		1·000	1·000	1·000	1·000	1·000	1·000	1·000	1·000	1·000	1·000	1·000	1·000	1·000	1·000	1·000

TABLE 6 (continued)
Tables of u/U_1 at Traverse Positions

1·8-1-0-00446

Y (mm)	X (mm)=	-25·4	0·0	3·2	6·3	9·5	12·7	19·0	25·4	38·1	50·8	63·5	88·9	114·3	139·7	171·4
0·081		0·494	0·503	0·444	0·426	0·351	0·327	0·307	0·281	0·317	0·252	0·247	0·231	0·303	0·222	0·245
0·090		0·502	0·509	0·450	0·430	0·358	0·337	0·314	0·290	0·323	0·263	0·255	0·235	0·307	0·225	0·245
0·100		0·511	0·517	0·458	0·435	0·367	0·348	0·323	0·300	0·331	0·276	0·264	0·241	0·311	0·230	0·246
0·110		0·520	0·524	0·446	0·441	0·376	0·358	0·332	0·310	0·338	0·287	0·273	0·246	0·316	0·234	0·247
0·120		0·529	0·531	0·474	0·446	0·385	0·367	0·340	0·318	0·345	0·296	0·281	0·252	0·320	0·238	0·248
0·130		0·537	0·538	0·483	0·453	0·393	0·375	0·348	0·326	0·352	0·305	0·289	0·257	0·324	0·242	0·249
0·140		0·546	0·545	0·491	0·459	0·402	0·382	0·356	0·332	0·359	0·312	0·297	0·263	0·328	0·247	0·249
0·150		0·554	0·551	0·499	0·466	0·410	0·388	0·363	0·338	0·366	0·318	0·304	0·269	0·331	0·251	0·250
0·160		0·562	0·557	0·506	0·473	0·418	0·394	0·370	0·343	0·373	0·323	0·311	0·275	0·334	0·255	0·251
0·180		0·577	0·569	0·517	0·488	0·434	0·406	0·384	0·353	0·385	0·333	0·325	0·288	0·340	0·262	0·253
0·200		0·591	0·583	0·529	0·502	0·449	0·418	0·396	0·368	0·397	0·346	0·336	0·300	0·346	0·270	0·254
0·250		0·611	0·609	0·563	0·531	0·478	0·447	0·423	0·398	0·422	0·374	0·358	0·322	0·361	0·284	0·259
0·300		0·634	0·628	0·593	0·557	0·510	0·480	0·449	0·422	0·443	0·397	0·379	0·340	0·375	0·298	0·260
0·350		0·649	0·646	0·617	0·577	0·533	0·502	0·474	0·443	0·460	0·420	0·402	0·358	0·384	0·316	0·262
0·400		0·661	0·656	0·637	0·607	0·556	0·526	0·499	0·459	0·476	0·445	0·420	0·375	0·392	0·330	0·265
0·450		0·672	0·669	0·652	0·627	0·577	0·550	0·516	0·475	0·493	0·463	0·436	0·390	0·402	0·341	0·267
0·500		0·682	0·680	0·667	0·647	0·589	0·568	0·532	0·490	0·508	0·475	0·451	0·403	0·412	0·351	0·269
0·600		0·697	0·694	0·688	0·671	0·629	0·602	0·568	0·525	0·533	0·504	0·476	0·426	0·427	0·372	0·276
0·700		0·715	0·710	0·704	0·690	0·654	0·631	0·591	0·554	0·556	0·524	0·498	0·449	0·443	0·388	0·280
0·800		0·727	0·723	0·717	0·706	0·675	0·650	0·615	0·585	0·574	0·549	0·517	0·468	0·455	0·406	0·283
0·900		0·739	0·734	0·732	0·722	0·692	0·673	0·641	0·606	0·595	0·569	0·533	0·485	0·468	0·422	0·287
1·000		0·751	0·746	0·743	0·735	0·705	0·690	0·662	0·629	0·614	0·586	0·550	0·503	0·481	0·435	0·291
1·100		0·759	0·755	0·754	0·747	0·721	0·707	0·680	0·650	0·632	0·604	0·568	0·519	0·491	0·448	0·295
1·200		0·772	0·765	0·763	0·759	0·733	0·720	0·694	0·665	0·646	0·621	0·581	0·532	0·502	0·459	0·299
1·300		0·784	0·776	0·774	0·777	0·742	0·732	0·709	0·681	0·661	0·636	0·598	0·545	0·513	0·470	0·303
1·400		0·794	0·785	0·782	0·784	0·751	0·744	0·723	0·697	0·677	0·650	0·614	0·557	0·522	0·482	0·308
1·600		0·814	0·803	0·802	0·797	0·772	0·764	0·748	0·723	0·705	0·675	0·643	0·564	0·545	0·502	0·318
1·800		0·831	0·818	0·819	0·816	0·789	0·783	0·769	0·750	0·728	0·698	0·667	0·607	0·564	0·520	0·329
2·000		0·848	0·835	0·836	0·833	0·805	0·801	0·789	0·770	0·752	0·720	0·689	0·629	0·584	0·537	0·340
2·500		0·885	0·872	0·874	0·871	0·847	0·839	0·832	0·815	0·802	0·774	0·745	0·681	0·630	0·573	0·368
3·000		0·919	0·906	0·909	0·905	0·883	0·877	0·869	0·853	0·844	0·820	0·793	0·734	0·678	0·617	0·404
3·500		0·950	0·936	0·940	0·936	0·917	0·910	0·902	0·887	0·875	0·857	0·836	0·780	0·723	0·655	0·446
4·000		0·974	0·960	0·965	0·964	0·946	0·939	0·934	0·921	0·908	0·888	0·873	0·822	0·766	0·700	0·483
4·500		0·988	0·979	0·984	0·987	0·971	0·964	0·959	0·950	0·936	0·917	0·903	0·863	0·809	0·741	0·529
5·000		0·997	0·991	0·992	0·997	0·987	0·983	0·979	0·974	0·962	0·942	0·932	0·893	0·848	0·780	0·570

TABLE 6 (continued)
Tables of u/U_1 at Traverse Positions

1·8-1-0-00446

Y (mm)	X (mm)=	-25·4	0·0	3·2	6·3	9·5	12·7	19·0	25·4	38·1	50·8	63·5	88·9	114·3	139·7	171·4	
6·000		1·000	0·998	0·997	1·000	1·000	0·998	0·996	0·997	0·991	0·981	0·970	0·946	0·910	0·855	0·650	
7·000		1·000	1·000	1·000	1·000	1·000	1·000	1·000	1·000	1·000	1·000	0·997	0·993	0·979	0·957	0·918	0·728
8·000		1·000	1·000	1·000	1·000	1·000	1·000	1·000	1·000	1·000	1·000	1·000	0·995	0·986	0·960	0·799	
9·000		1·000	1·000	1·000	1·000	1·000	1·000	1·000	1·000	1·000	1·000	1·000	1·000	0·996	0·988	0·864	
10·000		1·000	1·000	1·000	1·000	1·000	1·000	1·000	1·000	1·000	1·000	1·000	1·000	1·000	0·998	0·920	
11·000		1·000	1·000	1·000	1·000	1·000	1·000	1·000	1·000	1·000	1·000	1·000	1·000	1·000	1·000	0·959	
12·000		1·000	1·000	1·000	1·000	1·000	1·000	1·000	1·000	1·000	1·000	1·000	1·000	1·000	1·000	0·985	
13·000		1·000	1·000	1·000	1·000	1·000	1·000	1·000	1·000	1·000	1·000	1·000	1·000	1·000	1·000	0·995	
14·000		1·000	1·000	1·000	1·000	1·000	1·000	1·000	1·000	1·000	1·000	1·000	1·000	1·000	1·000	0·998	
15·000		1·000	1·000	1·000	1·000	1·000	1·000	1·000	1·000	1·000	1·000	1·000	1·000	1·000	1·000	1·000	

TABLE 6 (continued)
Tables of u/U_1 at Traverse Positions

3-6-1-0-00164

Y (mm)	X (mm) =	-25.4	0.0	3.2	6.3	9.5	12.7	19.0	25.4	38.1	50.8	63.5	88.9	114.3	139.7	171.4
0.081		0.399	0.406	0.409	0.402	0.379	0.384	0.355	0.340	0.344	0.354	0.329	0.328	0.281	0.300	0.310
0.090		0.411	0.422	0.416	0.411	0.389	0.390	0.359	0.349	0.353	0.358	0.334	0.333	0.292	0.303	0.311
0.100		0.425	0.439	0.424	0.420	0.400	0.397	0.365	0.360	0.363	0.363	0.341	0.339	0.305	0.308	0.313
0.110		0.438	0.455	0.432	0.430	0.410	0.404	0.370	0.369	0.372	0.368	0.347	0.344	0.316	0.312	0.314
0.120		0.451	0.470	0.439	0.438	0.418	0.410	0.376	0.377	0.380	0.373	0.353	0.349	0.325	0.317	0.316
0.130		0.463	0.483	0.447	0.446	0.426	0.417	0.383	0.385	0.388	0.378	0.358	0.355	0.334	0.321	0.317
0.140		0.475	0.496	0.455	0.453	0.431	0.424	0.389	0.391	0.394	0.383	0.364	0.359	0.340	0.325	0.319
0.150		0.486	0.507	0.462	0.460	0.436	0.430	0.396	0.397	0.400	0.388	0.369	0.364	0.346	0.330	0.321
0.160		0.497	0.517	0.469	0.466	0.439	0.437	0.402	0.402	0.406	0.393	0.373	0.368	0.350	0.334	0.322
0.180		0.517	0.534	0.483	0.478	0.451	0.449	0.418	0.414	0.414	0.402	0.381	0.377	0.354	0.343	0.325
0.200		0.535	0.545	0.497	0.495	0.468	0.462	0.434	0.429	0.421	0.411	0.391	0.384	0.360	0.351	0.328
0.250		0.565	0.578	0.534	0.527	0.500	0.490	0.466	0.457	0.445	0.431	0.412	0.402	0.380	0.372	0.335
0.300		0.592	0.602	0.560	0.545	0.524	0.515	0.487	0.475	0.466	0.451	0.430	0.419	0.396	0.391	0.340
0.350		0.612	0.622	0.582	0.573	0.551	0.539	0.515	0.493	0.484	0.469	0.445	0.435	0.409	0.407	0.347
0.400		0.626	0.640	0.604	0.594	0.575	0.562	0.534	0.509	0.499	0.485	0.458	0.447	0.442	0.422	0.355
0.450		0.640	0.650	0.623	0.610	0.599	0.581	0.550	0.527	0.513	0.499	0.470	0.458	0.435	0.436	0.365
0.500		0.650	0.662	0.639	0.627	0.617	0.598	0.566	0.545	0.528	0.511	0.483	0.469	0.448	0.449	0.373
0.600		0.670	0.677	0.663	0.656	0.639	0.625	0.593	0.570	0.551	0.534	0.508	0.489	0.471	0.471	0.389
0.700		0.682	0.688	0.677	0.675	0.658	0.649	0.618	0.593	0.575	0.554	0.529	0.509	0.490	0.490	0.407
0.800		0.693	0.697	0.688	0.688	0.676	0.668	0.638	0.617	0.595	0.573	0.547	0.528	0.507	0.504	0.415
0.900		0.698	0.703	0.695	0.699	0.692	0.683	0.661	0.635	0.611	0.589	0.564	0.543	0.522	0.515	0.421
1.000		0.704	0.710	0.704	0.709	0.703	0.696	0.677	0.653	0.625	0.603	0.580	0.555	0.536	0.528	0.436
1.100		0.713	0.717	0.713	0.718	0.713	0.707	0.689	0.668	0.640	0.617	0.594	0.569	0.548	0.541	0.450
1.200		0.722	0.724	0.721	0.727	0.722	0.719	0.702	0.681	0.654	0.630	0.606	0.583	0.558	0.553	0.464
1.300		0.729	0.730	0.729	0.733	0.728	0.726	0.714	0.691	0.667	0.643	0.619	0.597	0.568	0.563	0.478
1.400		0.737	0.737	0.735	0.740	0.735	0.734	0.724	0.701	0.680	0.656	0.632	0.610	0.581	0.575	0.490
1.600		0.755	0.754	0.751	0.757	0.753	0.751	0.738	0.720	0.701	0.679	0.656	0.632	0.601	0.596	0.513
1.800		0.770	0.767	0.764	0.772	0.767	0.764	0.755	0.739	0.721	0.699	0.675	0.654	0.621	0.615	0.531
2.000		0.784	0.782	0.780	0.786	0.782	0.779	0.770	0.755	0.739	0.717	0.697	0.673	0.638	0.632	0.556
2.500		0.821	0.817	0.814	0.820	0.817	0.815	0.808	0.791	0.778	0.760	0.739	0.718	0.682	0.673	0.603
3.000		0.855	0.849	0.846	0.854	0.852	0.850	0.839	0.825	0.813	0.798	0.778	0.756	0.720	0.710	0.644
3.500		0.888	0.881	0.877	0.885	0.882	0.880	0.871	0.856	0.843	0.829	0.814	0.794	0.760	0.744	0.679
4.000		0.916	0.907	0.903	0.911	0.912	0.907	0.899	0.886	0.872	0.859	0.845	0.828	0.795	0.776	0.713
4.500		0.944	0.935	0.930	0.935	0.938	0.934	0.927	0.913	0.900	0.886	0.875	0.857	0.827	0.807	0.748
5.000		0.967	0.956	0.952	0.957	0.960	0.960	0.953	0.941	0.926	0.913	0.901	0.885	0.854	0.837	0.779

TABLE 6 (continued)
Tables of u/U_1 at Traverse Positions

3·6-1-0·00164

Y (mm)	X (mm)=	-25·4	0·0	3·2	6·3	9·5	12·7	19·0	25·4	38·1	50·8	63·5	88·9	114·3	139·7	171·4
6·000		0·995	0·988	0·986	0·989	0·989	0·992	0·990	0·979	0·970	0·957	0·948	0·933	0·907	0·889	0·839
7·000		0·998	0·998	0·998	1·000	0·998	0·998	1·000	0·997	0·993	0·987	0·983	0·970	0·950	0·931	0·890
8·000		1·000	1·000	1·000	1·000	1·000	1·000	1·000	1·000	0·998	0·997	0·996	0·991	0·980	0·965	0·932
9·000		1·000	1·000	1·000	1·000	1·000	1·000	1·000	1·000	1·000	1·000	1·000	0·998	0·995	0·987	0·964
10·000		1·000	1·000	1·000	1·000	1·000	1·000	1·000	1·000	1·000	1·000	1·000	1·000	0·998	0·996	0·987
11·000		1·000	1·000	1·000	1·000	1·000	1·000	1·000	1·000	1·000	1·000	1·000	1·000	1·000	1·000	0·997
12·000		1·000	1·000	1·000	1·000	1·000	1·000	1·000	1·000	1·000	1·000	1·000	1·000	1·000	1·000	1·000
13·000		1·000	1·000	1·000	1·000	1·000	1·000	1·000	1·000	1·000	1·000	1·000	1·000	1·000	1·000	1·000
14·000		1·000	1·000	1·000	1·000	1·000	1·000	1·000	1·000	1·000	1·000	1·000	1·000	1·000	1·000	1·000
15·000		1·000	1·000	1·000	1·000	1·000	1·000	1·000	1·000	1·000	1·000	1·000	1·000	1·000	1·000	1·000

TABLE 6 (continued)
Tables of u/U_1 at Traverse Positions

3·6-1-0-00294

Y (mm)	X (mm)=	-25·4	0·0	3·2	6·3	9·5	12·7	19·0	25·4	38·1	50·8	63·5	88·9	114·3	139·7
0·081		0·407	0·418	0·380	0·363	0·354	0·354	0·227	0·252	0·295	0·285	0·249	0·252	0·267	0·240
0·090		0·418	0·428	0·385	0·368	0·360	0·359	0·234	0·261	0·299	0·292	0·253	0·255	0·271	0·241
0·100		0·431	0·440	0·392	0·375	0·367	0·364	0·243	0·271	0·303	0·299	0·258	0·258	0·276	0·243
0·110		0·443	0·451	0·398	0·381	0·373	0·370	0·252	0·281	0·307	0·306	0·263	0·261	0·280	0·244
0·120		0·455	0·462	0·405	0·387	0·380	0·376	0·260	0·290	0·312	0·313	0·267	0·265	0·285	0·246
0·130		0·467	0·472	0·412	0·393	0·385	0·381	0·269	0·298	0·316	0·319	0·272	0·268	0·289	0·248
0·140		0·478	0·482	0·420	0·398	0·391	0·387	0·277	0·306	0·320	0·325	0·276	0·271	0·293	0·250
0·150		0·488	0·491	0·427	0·404	0·396	0·393	0·285	0·313	0·324	0·330	0·281	0·274	0·296	0·252
0·160		0·499	0·499	0·435	0·409	0·401	0·398	0·293	0·320	0·328	0·334	0·285	0·277	0·300	0·254
0·180		0·517	0·515	0·450	0·419	0·414	0·410	0·308	0·332	0·336	0·342	0·293	0·282	0·306	0·259
0·200		0·534	0·532	0·463	0·430	0·428	0·421	0·322	0·343	0·343	0·348	0·300	0·287	0·311	0·263
0·250		0·567	0·568	0·492	0·457	0·457	0·445	0·353	0·367	0·356	0·353	0·315	0·299	0·322	0·276
0·300		0·591	0·595	0·523	0·480	0·479	0·469	0·380	0·385	0·372	0·370	0·328	0·311	0·331	0·286
0·350		0·609	0·614	0·549	0·502	0·501	0·491	0·405	0·405	0·390	0·382	0·340	0·324	0·337	0·296
0·400		0·623	0·631	0·576	0·526	0·525	0·506	0·430	0·420	0·403	0·390	0·355	0·338	0·344	0·305
0·450		0·637	0·646	0·602	0·549	0·547	0·526	0·451	0·439	0·417	0·403	0·369	0·350	0·352	0·315
0·500		0·649	0·658	0·621	0·571	0·567	0·543	0·470	0·457	0·431	0·416	0·383	0·359	0·361	0·327
0·600		0·668	0·678	0·653	0·626	0·596	0·575	0·506	0·483	0·454	0·441	0·411	0·378	0·377	0·348
0·700		0·681	0·688	0·672	0·670	0·623	0·602	0·543	0·510	0·474	0·461	0·430	0·395	0·391	0·367
0·800		0·690	0·697	0·689	0·684	0·647	0·630	0·569	0·533	0·497	0·477	0·447	0·409	0·403	0·380
0·900		0·696	0·702	0·699	0·703	0·668	0·651	0·594	0·557	0·517	0·493	0·463	0·424	0·416	0·391
1·000		0·703	0·710	0·707	0·714	0·686	0·672	0·619	0·580	0·536	0·510	0·478	0·440	0·429	0·402
1·100		0·712	0·718	0·716	0·724	0·699	0·691	0·641	0·599	0·554	0·525	0·490	0·455	0·441	0·412
1·200		0·721	0·725	0·725	0·734	0·713	0·705	0·660	0·617	0·569	0·540	0·504	0·466	0·452	0·423
1·300		0·729	0·732	0·734	0·742	0·723	0·715	0·677	0·634	0·585	0·555	0·519	0·480	0·463	0·434
1·400		0·736	0·739	0·741	0·748	0·732	0·726	0·692	0·649	0·600	0·569	0·534	0·494	0·472	0·444
1·600		0·752	0·755	0·756	0·760	0·748	0·744	0·717	0·677	0·629	0·597	0·560	0·519	0·490	0·465
1·800		0·768	0·767	0·772	0·774	0·762	0·760	0·737	0·703	0·656	0·623	0·585	0·542	0·503	0·484
2·000		0·781	0·782	0·787	0·787	0·779	0·773	0·756	0·725	0·681	0·647	0·609	0·564	0·545	0·501
2·500		0·817	0·817	0·821	0·823	0·816	0·812	0·797	0·767	0·787	0·699	0·661	0·614	0·567	0·540
3·000		0·853	0·850	0·853	0·858	0·849	0·847	0·831	0·802	0·769	0·745	0·709	0·664	0·614	0·585
3·500		0·885	0·880	0·878	0·889	0·883	0·881	0·866	0·835	0·815	0·786	0·755	0·709	0·658	0·626
4·000		0·914	0·907	0·907	0·917	0·913	0·908	0·895	0·868	0·846	0·820	0·796	0·752	0·699	0·661
4·500		0·941	0·935	0·932	0·942	0·941	0·936	0·926	0·899	0·877	0·854	0·832	0·791	0·741	0·696
5·000		0·962	0·955	0·957	0·960	0·965	0·962	0·953	0·927	0·905	0·883	0·865	0·826	0·775	0·729

TABLE 6 (continued)
Tables of u/U_1 at Traverse Positions

3·6-1-0-00294

Y (mm)	X (mm)=	-25·4	0·0	3·2	6·3	9·5	12·7	19·0	25·4	38·1	50·8	63·5	88·9	114·3	139·7
6·000		0·992	0·989	0·988	0·992	0·989	0·994	0·992	0·973	0·955	0·935	0·918	0·884	0·840	0·798
7·000		1·000	0·998	1·000	1·000	1·000	1·000	1·000	0·994	0·987	0·974	0·960	0·934	0·897	0·856
8·000		1·000	1·000	1·000	1·000	1·000	1·000	1·000	1·000	0·997	0·995	0·988	0·970	0·942	0·906
9·000		1·000	1·000	1·000	1·000	1·000	1·000	1·000	1·000	1·000	1·000	0·998	0·994	0·974	0·947
10·000		1·000	1·000	1·000	1·000	1·000	1·000	1·000	1·000	1·000	1·000	1·000	1·000	0·993	0·976
11·000		1·000	1·000	1·000	1·000	1·000	1·000	1·000	1·000	1·000	1·000	1·000	1·000	0·998	0·993
12·000		1·000	1·000	1·000	1·000	1·000	1·000	1·000	1·000	1·000	1·000	1·000	1·000	1·000	0·998
13·000		1·000	1·000	1·000	1·000	1·000	1·000	1·000	1·000	1·000	1·000	1·000	1·000	1·000	1·000
14·000		1·000	1·000	1·000	1·000	1·000	1·000	1·000	1·000	1·000	1·000	1·000	1·000	1·000	1·000
15·000		1·000	1·000	1·000	1·000	1·000	1·000	1·000	1·000	1·000	1·000	1·000	1·000	1·000	1·000

TABLE 6 (continued)
Tables of u/U_1 at Traverse Positions

3·6-1-0-00421

Y (mm)	X (mm)=	-25·4	0·0	3·2	6·3	9·5	12·7	19·0	25·4	38·1	50·8	63·5	88·9	114·3	139·7
0·081		0·411	0·428	0·381	0·351	0·341	0·308	0·331	0·237	0·262	0·245	0·208	0·228	0·218	0·217
0·090		0·424	0·438	0·389	0·357	0·344	0·312	0·333	0·242	0·265	0·248	0·211	0·228	0·218	0·217
0·100		0·440	0·449	0·397	0·363	0·347	0·317	0·336	0·248	0·268	0·252	0·214	0·229	0·219	0·218
0·110		0·454	0·460	0·406	0·369	0·351	0·322	0·339	0·253	0·272	0·256	0·218	0·229	0·220	0·219
0·120		0·467	0·471	0·414	0·375	0·355	0·327	0·343	0·259	0·275	0·260	0·221	0·230	0·221	0·220
0·130		0·479	0·481	0·421	0·381	0·358	0·333	0·346	0·264	0·279	0·263	0·224	0·231	0·222	0·221
0·140		0·490	0·491	0·429	0·386	0·362	0·338	0·349	0·269	0·282	0·267	0·228	0·232	0·223	0·222
0·150		0·501	0·501	0·435	0·391	0·366	0·344	0·352	0·274	0·285	0·270	0·231	0·233	0·223	0·223
0·160		0·510	0·510	0·442	0·395	0·370	0·350	0·355	0·279	0·288	0·274	0·234	0·234	0·224	0·224
0·180		0·527	0·527	0·453	0·404	0·377	0·362	0·361	0·287	0·294	0·280	0·241	0·236	0·225	0·226
0·200		0·542	0·543	0·463	0·415	0·386	0·372	0·368	0·295	0·300	0·285	0·247	0·239	0·226	0·227
0·250		0·576	0·573	0·488	0·439	0·409	0·392	0·383	0·312	0·314	0·297	0·260	0·246	0·231	0·229
0·300		0·599	0·598	0·515	0·461	0·432	0·412	0·399	0·328	0·327	0·311	0·269	0·255	0·237	0·231
0·350		0·614	0·619	0·544	0·486	0·453	0·437	0·416	0·343	0·337	0·323	0·277	0·265	0·243	0·234
0·400		0·632	0·634	0·571	0·508	0·474	0·458	0·428	0·356	0·346	0·331	0·285	0·274	0·247	0·240
0·450		0·646	0·648	0·591	0·533	0·495	0·473	0·441	0·371	0·360	0·339	0·297	0·281	0·251	0·244
0·500		0·658	0·661	0·611	0·556	0·514	0·488	0·455	0·387	0·373	0·349	0·305	0·289	0·255	0·248
0·600		0·673	0·679	0·644	0·591	0·544	0·520	0·481	0·418	0·393	0·367	0·320	0·304	0·266	0·256
0·700		0·683	0·691	0·665	0·622	0·574	0·550	0·506	0·441	0·408	0·380	0·338	0·317	0·279	0·262
0·800		0·695	0·699	0·682	0·647	0·606	0·577	0·533	0·460	0·429	0·404	0·352	0·330	0·286	0·264
0·900		0·702	0·706	0·696	0·672	0·633	0·602	0·556	0·484	0·448	0·421	0·365	0·342	0·289	0·269
1·000		0·707	0·714	0·706	0·691	0·657	0·627	0·582	0·507	0·464	0·433	0·380	0·353	0·300	0·275
1·100		0·714	0·722	0·716	0·704	0·678	0·650	0·604	0·529	0·478	0·446	0·398	0·362	0·311	0·284
1·200		0·722	0·728	0·727	0·716	0·696	0·670	0·625	0·549	0·493	0·460	0·413	0·371	0·320	0·294
1·300		0·731	0·735	0·734	0·727	0·709	0·688	0·645	0·568	0·509	0·476	0·426	0·383	0·328	0·302
1·400		0·739	0·743	0·742	0·736	0·722	0·703	0·663	0·586	0·525	0·492	0·437	0·397	0·335	0·310
1·600		0·755	0·756	0·759	0·753	0·742	0·726	0·694	0·622	0·558	0·519	0·461	0·421	0·352	0·326
1·800		0·771	0·770	0·773	0·769	0·758	0·745	0·721	0·651	0·588	0·545	0·487	0·445	0·371	0·338
2·000		0·786	0·785	0·790	0·785	0·775	0·762	0·744	0·678	0·614	0·570	0·516	0·462	0·389	0·348
2·500		0·821	0·818	0·827	0·823	0·813	0·803	0·790	0·735	0·682	0·631	0·575	0·512	0·427	0·376
3·000		0·855	0·852	0·856	0·861	0·851	0·842	0·826	0·777	0·731	0·686	0·627	0·563	0·475	0·411
3·500		0·887	0·882	0·880	0·890	0·883	0·876	0·860	0·813	0·776	0·733	0·677	0·613	0·516	0·442
4·000		0·915	0·908	0·908	0·921	0·916	0·907	0·890	0·847	0·815	0·777	0·729	0·661	0·564	0·480
4·500		0·940	0·935	0·932	0·944	0·944	0·938	0·923	0·882	0·850	0·814	0·772	0·702	0·607	0·517
5·000		0·963	0·955	0·956	0·958	0·970	0·965	0·951	0·914	0·882	0·850	0·811	0·745	0·647	0·553

TABLE 6 (continued)
Tables of u/U_1 at Traverse Positions

3·6-1-0-00421

Y (mm)	X (mm)=	-25·4	0·0	3·2	6·3	9·5	12·7	19·0	25·4	38·1	50·8	63·5	88·9	114·3	139·7
6·000		0·994	0·987	0·989	0·988	0·992	1·000	0·990	0·963	0·935	0·906	0·878	0·820	0·726	0·633
7·000		1·000	0·998	0·998	0·998	1·000	1·000	1·000	0·992	0·997	0·954	0·930	0·884	0·802	0·703
8·000		1·000	1·000	1·000	1·000	1·000	1·000	1·000	1·000	0·995	0·986	0·972	0·935	0·866	0·776
9·000		1·000	1·000	1·000	1·000	1·000	1·000	1·000	1·000	1·000	0·998	0·993	0·972	0·919	0·837
10·000		1·000	1·000	1·000	1·000	1·000	1·000	1·000	1·000	1·000	1·000	1·000	0·993	0·960	0·893
11·000		1·000	1·000	1·000	1·000	1·000	1·000	1·000	1·000	1·000	1·000	1·000	1·000	0·987	0·939
12·000		1·000	1·000	1·000	1·000	1·000	1·000	1·000	1·000	1·000	1·000	1·000	1·000	0·997	0·973
13·000		1·000	1·000	1·000	1·000	1·000	1·000	1·000	1·000	1·000	1·000	1·000	1·000	1·000	0·993
14·000		1·000	1·000	1·000	1·000	1·000	1·000	1·000	1·000	1·000	1·000	1·000	1·000	1·000	1·000
15·000		1·000	1·000	1·000	1·000	1·000	1·000	1·000	1·000	1·000	1·000	1·000	1·000	1·000	1·000

TABLE 6 (continued)
Tables of u/U_1 at Traverse Positions

3-6-2-0-00294

Y (mm)	X (mm)=	-25.4	0.0	3.2	6.3	9.5	12.7	19.0	25.4	38.1	50.8	63.5	88.9	114.3	139.7	171.4
0.081		0.024	0.087	0.038	0.165	0.112	0.076	0.185	0.200	0.257	0.299	0.307	0.169	0.286	0.199	0.166
0.090		0.030	0.094	0.052	0.173	0.146	0.092	0.196	0.211	0.264	0.304	0.316	0.173	0.295	0.220	0.187
0.100		0.038	0.101	0.066	0.183	0.181	0.109	0.209	0.224	0.272	0.310	0.325	0.179	0.305	0.243	0.210
0.110		0.045	0.109	0.080	0.192	0.214	0.125	0.221	0.236	0.281	0.316	0.334	0.185	0.314	0.266	0.232
0.120		0.053	0.116	0.094	0.200	0.244	0.141	0.232	0.248	0.288	0.322	0.343	0.191	0.324	0.286	0.253
0.130		0.060	0.123	0.106	0.208	0.271	0.156	0.243	0.260	0.296	0.328	0.352	0.197	0.333	0.306	0.273
0.140		0.066	0.130	0.119	0.216	0.294	0.170	0.254	0.271	0.304	0.335	0.360	0.203	0.342	0.324	0.292
0.160		0.080	0.143	0.142	0.231	0.332	0.197	0.274	0.291	0.319	0.347	0.376	0.217	0.359	0.356	0.326
0.180		0.092	0.156	0.163	0.244	0.357	0.220	0.292	0.309	0.334	0.359	0.390	0.232	0.375	0.384	0.355
0.200		0.103	0.168	0.181	0.256	0.370	0.240	0.308	0.326	0.348	0.372	0.404	0.248	0.391	0.406	0.381
0.250		0.130	0.194	0.217	0.278	0.348	0.277	0.340	0.359	0.381	0.403	0.432	0.292	0.426	0.439	0.425
0.300		0.154	0.216	0.238	0.292	0.324	0.294	0.359	0.381	0.411	0.436	0.452	0.343	0.455	0.448	0.448
0.350		0.173	0.234	0.245	0.300	0.332	0.302	0.370	0.391	0.438	0.448	0.465	0.400	0.479	0.467	0.467
0.400		0.188	0.247	0.252	0.312	0.339	0.310	0.381	0.390	0.452	0.459	0.471	0.474	0.491	0.484	0.484
0.500		0.207	0.266	0.274	0.330	0.352	0.325	0.399	0.403	0.469	0.477	0.485	0.566	0.509	0.509	0.508
0.600		0.224	0.287	0.292	0.340	0.363	0.339	0.412	0.413	0.481	0.490	0.497	0.557	0.526	0.523	0.520
0.700		0.240	0.310	0.309	0.345	0.369	0.357	0.419	0.421	0.490	0.497	0.509	0.468	0.540	0.538	0.534
0.800		0.255	0.325	0.328	0.355	0.376	0.371	0.424	0.429	0.495	0.503	0.517	0.476	0.544	0.550	0.543
0.900		0.270	0.341	0.343	0.368	0.384	0.380	0.429	0.435	0.498	0.508	0.523	0.485	0.548	0.558	0.549
1.000		0.288	0.358	0.355	0.380	0.393	0.387	0.434	0.439	0.502	0.511	0.527	0.496	0.553	0.561	0.555
1.200		0.314	0.382	0.378	0.390	0.413	0.400	0.442	0.452	0.512	0.516	0.536	0.507	0.566	0.572	0.568
1.400		0.330	0.397	0.392	0.412	0.431	0.412	0.451	0.463	0.517	0.526	0.542	0.516	0.575	0.578	0.574
1.600		0.347	0.408	0.407	0.430	0.446	0.424	0.464	0.474	0.525	0.534	0.548	0.527	0.584	0.582	0.582
1.800		0.368	0.423	0.422	0.443	0.458	0.439	0.479	0.484	0.534	0.540	0.557	0.539	0.593	0.590	0.591
2.000		0.390	0.438	0.436	0.455	0.469	0.455	0.488	0.493	0.542	0.549	0.565	0.544	0.598	0.601	0.601
2.500		0.423	0.470	0.472	0.485	0.496	0.487	0.512	0.518	0.565	0.569	0.582	0.566	0.617	0.617	0.620
3.000		0.463	0.502	0.499	0.515	0.531	0.512	0.538	0.546	0.584	0.595	0.606	0.588	0.633	0.630	0.635
3.500		0.498	0.529	0.532	0.543	0.552	0.546	0.562	0.570	0.605	0.613	0.622	0.609	0.649	0.649	0.651
4.000		0.534	0.561	0.560	0.574	0.582	0.571	0.590	0.592	0.626	0.636	0.643	0.630	0.669	0.664	0.667
4.500		0.568	0.590	0.588	0.600	0.611	0.599	0.615	0.619	0.648	0.659	0.668	0.653	0.686	0.683	0.686
5.000		0.602	0.620	0.619	0.627	0.639	0.628	0.639	0.645	0.673	0.684	0.691	0.677	0.705	0.700	0.700
6.000		0.675	0.676	0.678	0.686	0.695	0.684	0.693	0.697	0.721	0.733	0.735	0.724	0.740	0.734	0.736
7.000		0.743	0.734	0.740	0.739	0.750	0.739	0.744	0.747	0.769	0.778	0.780	0.770	0.782	0.772	0.771
8.000		0.813	0.796	0.799	0.784	0.803	0.793	0.796	0.802	0.819	0.825	0.827	0.818	0.820	0.809	0.805
9.000		0.878	0.856	0.857	0.849	0.856	0.846	0.845	0.851	0.865	0.874	0.873	0.863	0.860	0.847	0.841

TABLE 6 (continued)
Tables of u/U_1 at Traverse Positions

3·6-2-0-00294

Y (mm)	X (mm)=	-25·4	0·0	3·2	6·3	9·5	12·7	19·0	25·4	38·1	50·8	63·5	88·9	114·3	139·7	171·4
10·000		0·937	0·910	0·909	0·902	0·906	0·893	0·893	0·899	0·910	0·915	0·914	0·903	0·895	0·882	0·876
11·000		0·979	0·954	0·951	0·949	0·949	0·936	0·934	0·939	0·950	0·952	0·950	0·942	0·928	0·912	0·909
12·000		0·998	0·983	0·982	0·980	0·979	0·968	0·962	0·968	0·980	0·981	0·981	0·972	0·957	0·937	0·939
13·000		1·000	0·996	0·995	0·995	0·995	0·985	0·978	0·982	0·995	0·999	0·996	0·994	0·979	0·969	0·964
14·000		1·000	0·999	0·999	0·999	0·998	0·990	0·985	0·985	0·999	1·000	1·000	1·000	0·992	0·985	0·982
15·000		1·000	1·000	1·000	1·000	0·999	0·994	0·990	0·986	0·999	1·000	1·000	1·000	0·996	0·994	0·993
16·000		1·000	1·000	1·000	1·000	1·000	0·996	0·993	0·989	1·000	1·000	1·000	1·000	0·998	0·997	0·999
18·000		1·000	1·000	1·000	1·000	1·000	0·999	0·997	0·995	1·000	1·000	1·000	1·000	1·000	0·999	0·999
20·000		1·000	1·000	1·000	1·000	1·000	1·000	0·999	0·999	1·000	1·000	1·000	1·000	1·000	1·000	1·000
22·000		1·000	1·000	1·000	1·000	1·000	1·000	1·000	1·000	1·000	1·000	1·000	1·000	1·000	1·000	1·000

TABLE 7
Tables of T/T_1 at Traverse Positions

Y (mm)	X (mm)=	1·8-0-0-00000					3·6-0-0-00000				
		-25·4	12·7	63·5	114·3	171·4	-25·4	12·7	63·5	114·3	171·4
0·081		1·486	1·488	1·485	1·488	1·467	3·064	3·052	3·020	3·010	2·987
0·090		1·479	1·480	1·479	1·483	1·463	3·039	3·001	2·988	2·984	2·971
0·100		1·471	1·472	1·471	1·477	1·457	3·011	2·949	2·954	2·954	2·951
0·110		1·463	1·463	1·464	1·471	1·452	2·984	2·906	2·921	2·926	2·930
0·120		1·455	1·456	1·458	1·465	1·446	2·958	2·872	2·890	2·900	2·908
0·130		1·448	1·448	1·452	1·460	1·441	2·934	2·845	2·862	2·875	2·886
0·140		1·441	1·442	1·446	1·454	1·436	2·910	2·827	2·835	2·852	2·862
0·150		1·435	1·435	1·440	1·449	1·431	2·888	2·818	2·811	2·830	2·837
0·160		1·429	1·430	1·435	1·444	1·426	2·867	2·817	2·789	2·809	2·812
0·180		1·419	1·420	1·427	1·435	1·417	2·828	2·794	2·750	2·772	2·766
0·200		1·413	1·412	1·417	1·426	1·412	2·784	2·754	2·721	2·741	2·728
0·250		1·397	1·393	1·394	1·403	1·392	2·691	2·669	2·640	2·652	2·643
0·300		1·379	1·376	1·376	1·387	1·368	2·624	2·604	2·575	2·579	2·575
0·350		1·365	1·363	1·361	1·374	1·356	2·562	2·537	2·517	2·520	2·509
0·400		1·350	1·352	1·347	1·359	1·344	2·511	2·495	2·462	2·462	2·449
0·450		1·341	1·343	1·335	1·347	1·337	2·468	2·455	2·422	2·407	2·399
0·500		1·331	1·332	1·324	1·337	1·328	2·427	2·414	2·384	2·367	2·356
0·600		1·313	1·312	1·308	1·322	1·312	2·362	2·343	2·315	2·296	2·285
0·700		1·296	1·296	1·293	1·308	1·298	2·298	2·282	2·258	2·237	2·224
0·800		1·282	1·283	1·279	1·295	1·286	2·239	2·233	2·216	2·190	2·185
0·900		1·270	1·271	1·266	1·283	1·275	2·196	2·184	2·177	2·155	2·152
1·000		1·256	1·262	1·255	1·273	1·265	2·163	2·148	2·141	2·122	2·111
1·100		1·245	1·251	1·247	1·263	1·258	2·130	2·125	2·107	2·093	2·080
1·200		1·237	1·242	1·239	1·256	1·252	2·096	2·100	2·080	2·070	2·058
1·300		1·229	1·235	1·232	1·249	1·245	2·069	2·072	2·059	2·048	2·036
1·400		1·219	1·227	1·225	1·241	1·238	2·044	2·048	2·037	2·023	2·013
1·600		1·200	1·214	1·210	1·227	1·225	1·993	1·998	1·987	1·974	1·970
1·800		1·185	1·199	1·196	1·216	1·215	1·936	1·948	1·945	1·935	1·930
2·000		1·170	1·185	1·183	1·204	1·206	1·887	1·909	1·901	1·893	1·894
2·500		1·137	1·151	1·155	1·177	1·178	1·763	1·788	1·797	1·804	1·804
3·000		1·097	1·118	1·128	1·150	1·155	1·632	1·668	1·697	1·710	1·712
3·500		1·036	1·087	1·102	1·127	1·131	1·523	1·556	1·593	1·616	1·631
4·000		1·037	1·060	1·074	1·105	1·111	1·407	1·451	1·496	1·522	1·551
4·500		1·015	1·033	1·051	1·084	1·090	1·295	1·347	1·402	1·440	1·477
5·000		1·000	1·012	1·029	1·064	1·072	1·185	1·243	1·316	1·355	1·411

TABLE 7 (continued)
Tables of T/T_1 at Traverse Positions

Y (mm)	X (mm)=	1·8-0-0-00000					3·6-0-0-00000				
		-25·4	12·7	63·5	114·3	171·4	-25·4	12·7	63·5	114·3	171·4
6·000		1·000	1·000	1·005	1·033	1·037	1·033	1·079	1·158	1·215	1·274
7·000		1·000	1·000	1·000	1·006	1·012	1·000	1·007	1·044	1·089	1·153
8·000		1·000	1·000	1·000	1·000	1·001	1·000	1·000	1·003	1·020	1·065
9·000		1·000	1·000	1·000	1·000	1·000	1·000	1·000	1·000	1·002	1·016
10·000		1·000	1·000	1·000	1·000	1·000	1·000	1·000	1·000	1·000	1·000
11·000		1·000	1·000	1·000	1·000	1·000	1·000	1·000	1·000	1·000	1·000
12·000		1·000	1·000	1·000	1·000	1·000	1·000	1·000	1·000	1·000	1·000
13·000		1·000	1·000	1·000	1·000	1·000	1·000	1·000	1·000	1·000	1·000
14·000		1·000	1·000	1·000	1·000	1·000	1·000	1·000	1·000	1·000	1·000
15·000		1·000	1·000	1·000	1·000	1·000	1·000	1·000	1·000	1·000	1·000

TABLE 7 (continued)
Tables of T/T_1 at Traverse Positions

1-8-1-0-00174

Y (mm)	X (mm)=	-25.4	0.0	3.2	6.3	9.5	12.7	19.0	25.4	38.1	50.8	63.5	88.9	114.3	139.7	171.4
0.081		1.478	1.475	1.483	1.488	1.486	1.515	1.506	1.517	1.522	1.536	1.540	1.543	1.540	1.543	1.552
0.090		1.473	1.472	1.477	1.484	1.482	1.512	1.501	1.514	1.519	1.533	1.536	1.541	1.538	1.539	1.550
0.100		1.467	1.467	1.470	1.479	1.478	1.507	1.496	1.510	1.514	1.529	1.530	1.538	1.535	1.533	1.548
0.110		1.462	1.462	1.464	1.474	1.473	1.503	1.492	1.506	1.510	1.525	1.525	1.535	1.533	1.528	1.546
0.120		1.456	1.457	1.458	1.469	1.469	1.498	1.488	1.502	1.506	1.521	1.520	1.532	1.530	1.524	1.543
0.130		1.450	1.451	1.452	1.463	1.464	1.494	1.484	1.498	1.501	1.517	1.516	1.528	1.527	1.519	1.541
0.140		1.445	1.445	1.447	1.457	1.460	1.489	1.481	1.494	1.497	1.513	1.511	1.525	1.525	1.516	1.538
0.150		1.440	1.438	1.443	1.452	1.456	1.485	1.479	1.490	1.493	1.509	1.507	1.521	1.522	1.512	1.536
0.160		1.435	1.431	1.438	1.446	1.452	1.480	1.475	1.487	1.489	1.506	1.503	1.517	1.519	1.509	1.533
0.180		1.426	1.417	1.431	1.435	1.445	1.471	1.464	1.478	1.481	1.500	1.495	1.509	1.513	1.503	1.528
0.200		1.418	1.411	1.423	1.426	1.437	1.463	1.454	1.470	1.474	1.493	1.489	1.501	1.508	1.496	1.522
0.250		1.401	1.395	1.402	1.407	1.415	1.442	1.435	1.452	1.457	1.471	1.475	1.483	1.494	1.483	1.511
0.300		1.385	1.377	1.383	1.390	1.399	1.422	1.420	1.436	1.444	1.454	1.461	1.467	1.483	1.472	1.502
0.350		1.370	1.362	1.371	1.374	1.382	1.411	1.404	1.422	1.430	1.441	1.447	1.453	1.472	1.460	1.494
0.400		1.355	1.351	1.353	1.361	1.366	1.394	1.389	1.407	1.418	1.427	1.440	1.444	1.460	1.450	1.483
0.450		1.345	1.343	1.342	1.347	1.356	1.381	1.376	1.393	1.407	1.413	1.426	1.438	1.451	1.440	1.473
0.500		1.334	1.331	1.330	1.335	1.342	1.368	1.364	1.382	1.393	1.399	1.413	1.426	1.442	1.430	1.465
0.600		1.319	1.315	1.311	1.315	1.318	1.348	1.338	1.363	1.372	1.377	1.396	1.406	1.425	1.413	1.450
0.700		1.300	1.298	1.294	1.300	1.300	1.327	1.321	1.342	1.352	1.359	1.378	1.387	1.410	1.400	1.436
0.800		1.286	1.286	1.282	1.286	1.286	1.309	1.305	1.326	1.336	1.346	1.361	1.372	1.395	1.422	
0.900		1.274	1.274	1.269	1.275	1.274	1.296	1.290	1.311	1.322	1.332	1.346	1.357	1.380	1.380	1.408
1.000		1.262	1.265	1.257	1.262	1.264	1.284	1.277	1.298	1.309	1.319	1.335	1.344	1.367	1.367	1.397
1.100		1.251	1.254	1.247	1.253	1.253	1.272	1.267	1.286	1.298	1.306	1.324	1.334	1.357	1.257	1.388
1.200		1.241	1.244	1.239	1.243	1.244	1.263	1.255	1.276	1.288	1.298	1.312	1.324	1.348	1.350	1.379
1.300		1.232	1.235	1.230	1.235	1.232	1.254	1.246	1.265	1.277	1.286	1.303	1.314	1.340	1.344	1.371
1.400		1.223	1.227	1.222	1.226	1.224	1.246	1.239	1.256	1.265	1.278	1.294	1.306	1.333	1.336	1.363
1.600		1.207	1.212	1.207	1.211	1.210	1.228	1.222	1.236	1.248	1.259	1.275	1.289	1.318	1.322	1.349
1.800		1.192	1.198	1.192	1.195	1.199	1.212	1.207	1.220	1.230	1.242	1.258	1.274	1.301	1.311	1.334
2.000		1.175	1.183	1.176	1.180	1.181	1.197	1.194	1.206	1.214	1.225	1.241	1.258	1.284	1.297	1.320
2.500		1.135	1.149	1.144	1.143	1.148	1.161	1.158	1.171	1.179	1.190	1.201	1.218	1.248	1.263	1.291
3.000		1.099	1.116	1.111	1.108	1.117	1.127	1.128	1.140	1.148	1.158	1.167	1.183	1.212	1.232	1.262
3.500		1.066	1.084	1.082	1.079	1.084	1.096	1.097	1.109	1.118	1.128	1.137	1.154	1.181	1.197	1.233
4.000		1.033	1.053	1.054	1.051	1.056	1.065	1.069	1.079	1.090	1.098	1.110	1.126	1.150	1.167	1.204
4.500		1.012	1.025	1.024	1.026	1.031	1.036	1.044	1.049	1.064	1.073	1.082	1.097	1.123	1.137	1.176
5.000		1.001	1.008	1.009	1.007	1.014	1.018	1.020	1.022	1.039	1.051	1.060	1.072	1.095	1.111	1.154

TABLE 7 (continued)
Tables of T/T_1 at Traverse Positions

1·8-1-0-00174

Y (mm)	X (mm)=	-25·4	0·0	3·2	6·3	9·5	12·7	19·0	25·4	38·1	50·8	63·5	88·9	114·3	139·7	171·4
6·000		1·000	1·000	1·000	1·001	1·000	1·000	1·000	1·000	1·005	1·012	1·017	1·030	1·049	1·066	1·104
7·000		1·000	1·000	1·000	1·000	1·000	1·000	1·000	1·000	1·000	1·000	1·002	1·005	1·014	1·029	1·056
8·000		1·000	1·000	1·000	1·000	1·000	1·000	1·000	1·000	1·000	1·000	1·000	1·000	1·000	1·007	1·021
9·000		1·000	1·000	1·000	1·000	1·000	1·000	1·000	1·000	1·000	1·000	1·000	1·000	1·000	1·000	1·004
10·000		1·000	1·000	1·000	1·000	1·000	1·000	1·000	1·000	1·000	1·000	1·000	1·000	1·000	1·000	1·000
11·000		1·000	1·000	1·000	1·000	1·000	1·000	1·000	1·000	1·000	1·000	1·000	1·000	1·000	1·000	1·000
12·000		1·000	1·000	1·000	1·000	1·000	1·000	1·000	1·000	1·000	1·000	1·000	1·000	1·000	1·000	1·000
13·000		1·000	1·000	1·000	1·000	1·000	1·000	1·000	1·000	1·000	1·000	1·000	1·000	1·000	1·000	1·000
14·000		1·000	1·000	1·000	1·000	1·000	1·000	1·000	1·000	1·000	1·000	1·000	1·000	1·000	1·000	1·000
15·000		1·000	1·000	1·000	1·000	1·000	1·000	1·000	1·000	1·000	1·000	1·000	1·000	1·000	1·000	1·000

TABLE 7 (continued)
Tables of T/T_1 at Traverse Positions

1·8-1-0·00311

Y (mm)	X (mm)=	-25·4	0·0	3·2	6·3	9·5	12·7	19·0	25·4	38·1	50·8	63·5	88·9	114·3	139·7	171·4
0·081		1·474	1·470	1·498	1·502	1·510	1·507	1·516	1·526	1·526	1·543	1·560	1·565	1·556	1·558	1·550
0·090		1·469	1·468	1·494	1·498	1·506	1·504	1·514	1·523	1·524	1·542	1·557	1·564	1·554	1·556	1·549
0·100		1·463	1·466	1·490	1·493	1·502	1·500	1·512	1·520	1·521	1·539	1·553	1·561	1·552	1·554	1·547
0·110		1·458	1·462	1·485	1·487	1·497	1·496	1·509	1·516	1·518	1·536	1·550	1·559	1·549	1·551	1·545
0·120		1·452	1·459	1·481	1·482	1·493	1·492	1·506	1·513	1·515	1·534	1·546	1·557	1·547	1·549	1·543
0·130		1·447	1·454	1·477	1·477	1·488	1·488	1·503	1·509	1·512	1·531	1·543	1·555	1·545	1·546	1·542
0·140		1·441	1·450	1·473	1·471	1·484	1·484	1·499	1·506	1·508	1·527	1·540	1·553	1·542	1·543	1·540
0·150		1·436	1·445	1·468	1·466	1·479	1·479	1·496	1·502	1·505	1·524	1·537	1·551	1·540	1·541	1·539
0·160		1·432	1·439	1·462	1·460	1·475	1·475	1·492	1·499	1·501	1·520	1·534	1·549	1·538	1·538	1·538
0·180		1·425	1·427	1·451	1·450	1·466	1·466	1·484	1·493	1·493	1·513	1·528	1·544	1·534	1·533	1·536
0·200		1·419	1·413	1·442	1·443	1·458	1·461	1·476	1·487	1·485	1·505	1·522	1·540	1·530	1·527	1·535
0·250		1·399	1·391	1·425	1·424	1·439	1·446	1·464	1·470	1·472	1·490	1·508	1·531	1·521	1·515	1·530
0·300		1·381	1·377	1·404	1·404	1·423	1·427	1·447	1·452	1·458	1·475	1·494	1·520	1·513	1·505	1·525
0·350		1·366	1·364	1·386	1·387	1·405	1·411	1·433	1·440	1·447	1·460	1·484	1·510	1·504	1·494	1·523
0·400		1·352	1·354	1·373	1·368	1·386	1·395	1·419	1·430	1·436	1·446	1·474	1·501	1·495	1·485	1·517
0·450		1·341	1·343	1·359	1·356	1·375	1·381	1·407	1·416	1·427	1·434	1·462	1·493	1·488	1·477	1·512
0·500		1·332	1·333	1·345	1·343	1·360	1·370	1·393	1·407	1·416	1·422	1·451	1·484	1·483	1·469	1·508
0·600		1·315	1·317	1·328	1·323	1·337	1·349	1·372	1·388	1·396	1·402	1·437	1·469	1·470	1·458	1·497
0·700		1·302	1·302	1·310	1·305	1·319	1·328	1·349	1·364	1·381	1·382	1·418	1·454	1·456	1·443	1·486
0·800		1·286	1·289	1·296	1·293	1·301	1·310	1·330	1·346	1·361	1·364	1·400	1·440	1·444	1·433	1·477
0·900		1·274	1·277	1·285	1·282	1·286	1·295	1·313	1·330	1·346	1·348	1·384	1·426	1·435	1·424	1·467
1·000		1·263	1·267	1·273	1·267	1·276	1·280	1·301	1·314	1·334	1·335	1·371	1·415	1·424	1·414	1·457
1·100		1·252	1·257	1·262	1·257	1·264	1·271	1·287	1·300	1·322	1·323	1·358	1·404	1·411	1·404	1·447
1·200		1·245	1·247	1·252	1·250	1·254	1·258	1·276	1·290	1·308	1·314	1·348	1·394	1·402	1·397	1·439
1·300		1·236	1·238	1·244	1·240	1·244	1·249	1·266	1·278	1·297	1·303	1·338	1·385	1·393	1·390	1·432
1·400		1·229	1·231	1·235	1·231	1·235	1·242	1·256	1·267	1·286	1·293	1·326	1·373	1·384	1·383	1·426
1·600		1·208	1·214	1·219	1·213	1·219	1·224	1·240	1·250	1·267	1·275	1·306	1·355	1·368	1·371	1·416
1·800		1·193	1·200	1·203	1·197	1·204	1·209	1·224	1·233	1·249	1·258	1·288	1·337	1·353	1·360	1·403
2·000		1·176	1·185	1·187	1·181	1·189	1·194	1·207	1·215	1·230	1·242	1·270	1·319	1·337	1·348	1·389
2·500		1·141	1·149	1·151	1·149	1·155	1·160	1·172	1·177	1·189	1·200	1·229	1·280	1·297	1·317	1·357
3·000		1·107	1·114	1·118	1·113	1·119	1·126	1·135	1·145	1·152	1·167	1·193	1·239	1·261	1·285	1·332
3·500		1·072	1·085	1·085	1·081	1·086	1·095	1·109	1·114	1·125	1·135	1·156	1·200	1·226	1·251	1·303
4·000		1·042	1·053	1·058	1·053	1·057	1·066	1·079	1·083	1·097	1·105	1·125	1·166	1·191	1·218	1·274
4·500		1·018	1·029	1·027	1·029	1·040	1·048	1·056	1·069	1·078	1·095	1·135	1·159	1·189	1·244	
5·000		1·004	1·010	1·011	1·008	1·010	1·016	1·025	1·028	1·043	1·055	1·069	1·107	1·131	1·159	1·220

TABLE 7 (continued)
Tables of T/T₁ at Traverse Positions

1·8-1-0-00311

Y (mm)	X (mm)=	-25·4	0·0	3·2	6·3	9·5	12·7	19·0	25·4	38·1	50·8	63·5	88·9	114·3	139·7	171·4
6·000	1·000	1·000	1·000	1·000	1·000	1·000	1·001	1·002	1·009	1·016	1·027	1·056	1·078	1·102	1·167	
7·000	1·000	1·000	1·000	1·000	1·000	1·000	1·000	1·000	1·000	1·001	1·005	1·016	1·036	1·053	1·115	
8·000	1·000	1·000	1·000	1·000	1·000	1·000	1·000	1·000	1·000	1·000	1·000	1·001	1·008	1·020	1·069	
9·000	1·000	1·000	1·000	1·000	1·000	1·000	1·000	1·000	1·000	1·000	1·000	1·000	1·001	1·001	1·030	
10·000	1·000	1·000	1·000	1·000	1·000	1·000	1·000	1·000	1·000	1·000	1·000	1·000	1·000	1·000	1·007	
11·000	1·000	1·000	1·000	1·000	1·000	1·000	1·000	1·000	1·000	1·000	1·000	1·000	1·000	1·000	1·002	
12·000	1·000	1·000	1·000	1·000	1·000	1·000	1·000	1·000	1·000	1·000	1·000	1·000	1·000	1·000	1·000	
13·000	1·000	1·000	1·000	1·000	1·000	1·000	1·000	1·000	1·000	1·000	1·000	1·000	1·000	1·000	1·000	
14·000	1·000	1·000	1·000	1·000	1·000	1·000	1·000	1·000	1·000	1·000	1·000	1·000	1·000	1·000	1·000	
15·000	1·000	1·000	1·000	1·000	1·000	1·000	1·000	1·000	1·000	1·000	1·000	1·000	1·000	1·000	1·000	

TABLE 7 (continued)
Tables of T/T_1 at Traverse Positions

1·8-1-0-00446

Y (mm)	X (mm)=	-25·4	0·0	3·2	6·3	9·5	12·7	19·0	25·4	38·1	50·8	63·5	88·9	114·3	139·7	171·4
0·081		1·481	1·459	1·500	1·515	1·509	1·520	1·524	1·531	1·540	1·567	1·574	1·579	1·556	1·552	1·496
0·090		1·476	1·456	1·497	1·514	1·506	1·517	1·522	1·528	1·537	1·563	1·571	1·578	1·555	1·551	1·496
0·100		1·469	1·451	1·493	1·511	1·501	1·513	1·519	1·524	1·534	1·558	1·568	1·577	1·554	1·549	1·496
0·110		1·463	1·447	1·489	1·509	1·497	1·509	1·516	1·520	1·530	1·554	1·565	1·575	1·553	1·548	1·496
0·120		1·457	1·442	1·484	1·506	1·493	1·506	1·513	1·516	1·527	1·550	1·562	1·574	1·551	1·546	1·496
0·130		1·451	1·438	1·479	1·502	1·489	1·502	1·510	1·513	1·524	1·547	1·559	1·572	1·550	1·545	1·496
0·140		1·445	1·434	1·474	1·498	1·485	1·498	1·507	1·511	1·521	1·545	1·556	1·570	1·548	1·543	1·495
0·150		1·440	1·429	1·468	1·495	1·482	1·494	1·503	1·508	1·518	1·542	1·553	1·568	1·546	1·542	1·495
0·160		1·434	1·425	1·464	1·490	1·478	1·492	1·500	1·506	1·515	1·541	1·551	1·566	1·545	1·541	1·495
0·180		1·423	1·416	1·457	1·481	1·471	1·487	1·493	1·502	1·510	1·537	1·546	1·561	1·542	1·539	1·494
0·200		1·413	1·406	1·449	1·472	1·464	1·481	1·486	1·496	1·505	1·531	1·542	1·556	1·538	1·537	1·493
0·250		1·397	1·386	1·427	1·452	1·447	1·466	1·472	1·483	1·492	1·517	1·530	1·548	1·529	1·531	1·490
0·300		1·381	1·370	1·405	1·436	1·430	1·449	1·461	1·470	1·478	1·506	1·519	1·539	1·522	1·525	1·490
0·350		1·367	1·354	1·388	1·421	1·415	1·435	1·445	1·459	1·467	1·494	1·509	1·528	1·519	1·489	
0·400		1·355	1·345	1·372	1·400	1·398	1·418	1·430	1·450	1·458	1·480	1·498	1·520	1·513	1·512	1·489
38	0·450	1·346	1·335	1·359	1·385	1·385	1·404	1·421	1·441	1·446	1·471	1·490	1·513	1·508	1·507	1·487
0·500		1·335	1·323	1·348	1·367	1·375	1·391	1·409	1·431	1·435	1·461	1·481	1·505	1·503	1·503	1·485
0·600		1·318	1·308	1·327	1·347	1·344	1·369	1·383	1·409	1·419	1·442	1·464	1·492	1·493	1·490	1·482
0·700		1·300	1·291	1·314	1·326	1·323	1·346	1·365	1·389	1·398	1·428	1·450	1·478	1·483	1·482	1·481
0·800		1·288	1·278	1·299	1·311	1·307	1·327	1·347	1·368	1·385	1·411	1·436	1·465	1·474	1·472	1·479
0·900		1·275	1·269	1·285	1·296	1·292	1·311	1·327	1·352	1·366	1·393	1·423	1·452	1·465	1·464	1·476
1·000		1·265	1·257	1·272	1·281	1·279	1·296	1·310	1·335	1·352	1·381	1·410	1·441	1·456	1·458	1·474
1·100		1·255	1·247	1·261	1·269	1·267	1·284	1·294	1·319	1·338	1·367	1·396	1·431	1·449	1·449	1·472
1·200		1·244	1·238	1·253	1·258	1·257	1·272	1·283	1·308	1·327	1·353	1·385	1·421	1·440	1·442	1·470
1·300		1·234	1·230	1·244	1·243	1·247	1·261	1·272	1·295	1·316	1·343	1·374	1·411	1·432	1·435	1·467
1·400		1·225	1·222	1·237	1·237	1·238	1·251	1·261	1·282	1·304	1·334	1·363	1·403	1·427	1·427	1·464
1·600		1·208	1·205	1·220	1·224	1·222	1·235	1·242	1·263	1·283	1·315	1·339	1·386	1·411	1·414	1·459
1·800		1·192	1·192	1·202	1·206	1·209	1·220	1·225	1·242	1·264	1·297	1·323	1·367	1·399	1·403	1·455
2·000		1·176	1·176	1·185	1·190	1·195	1·205	1·208	1·225	1·245	1·278	1·306	1·353	1·383	1·394	1·451
2·500		1·141	1·141	1·149	1·153	1·160	1·172	1·171	1·188	1·202	1·232	1·261	1·315	1·352	1·368	1·436
3·000		1·105	1·110	1·114	1·119	1·127	1·136	1·138	1·155	1·164	1·192	1·220	1·272	1·317	1·341	1·420
3·500		1·070	1·080	1·083	1·086	1·095	1·105	1·106	1·122	1·134	1·157	1·182	1·233	1·279	1·311	1·401
4·000		1·040	1·051	1·050	1·054	1·066	1·073	1·075	1·091	1·102	1·127	1·146	1·194	1·243	1·279	1·384
4·500		1·016	1·029	1·026	1·025	1·037	1·044	1·049	1·062	1·075	1·098	1·116	1·157	1·209	1·247	1·360
5·000		1·004	1·012	1·010	1·007	1·015	1·021	1·027	1·034	1·049	1·073	1·087	1·127	1·173	1·218	1·338

TABLE 7 (continued)
Tables of T/T₁ at Traverse Positions

1·8-1-0·00446

Y (mm)	X (mm)=	-25·4	0·0	3·2	6·3	9·5	12·7	19·0	25·4	38·1	50·8	63·5	88·9	114·3	139·7	171·4
6·000		1·000	1·000	1·001	1·001	1·000	1·000	1·002	1·005	1·011	1·028	1·040	1·072	1·112	1·152	1·294
7·000		1·000	1·000	1·000	1·000	1·000	1·000	1·000	1·000	1·005	1·005	1·009	1·030	1·063	1·095	1·243
8·000		1·000	1·000	1·000	1·000	1·000	1·000	1·000	1·000	1·000	1·000	1·000	1·007	1·024	1·049	1·189
9·000		1·000	1·000	1·000	1·000	1·000	1·000	1·000	1·000	1·000	1·000	1·000	1·000	1·005	1·017	1·137
10·000		1·000	1·000	1·000	1·000	1·000	1·000	1·000	1·000	1·000	1·000	1·000	1·000	1·000	1·002	1·085
11·000		1·000	1·000	1·000	1·000	1·000	1·000	1·000	1·000	1·000	1·000	1·000	1·000	1·000	1·000	1·043
12·000		1·000	1·000	1·000	1·000	1·000	1·000	1·000	1·000	1·000	1·000	1·000	1·000	1·000	1·000	1·012
13·000		1·000	1·000	1·000	1·000	1·000	1·000	1·000	1·000	1·000	1·000	1·000	1·000	1·000	1·000	1·003
14·000		1·000	1·000	1·000	1·000	1·000	1·000	1·000	1·000	1·000	1·000	1·000	1·000	1·000	1·000	1·000
15·000		1·000	1·000	1·000	1·000	1·000	1·000	1·000	1·000	1·000	1·000	1·000	1·000	1·000	1·000	1·000

TABLE 7 (continued)
Tables of T/T₁ at Traverse Positions

3·6-1-0-00164

Y (mm)	X (mm)=	-25·4	0·0	3·2	6·3	9·5	12·7	19·0	25·4	38·1	50·8	63·5	88·9	114·3	139·7	171·4
0·081		3·154	3·121	3·110	3·136	3·167	3·123	3·167	3·145	3·169	3·155	3·156	3·190	3·293	3·275	3·264
0·090		3·129	3·088	3·095	3·116	3·149	3·111	3·159	3·128	3·152	3·146	3·145	3·182	3·276	3·269	3·261
0·100		3·101	3·052	3·077	3·095	3·129	3·097	3·148	3·110	3·133	3·136	3·133	3·172	3·257	3·261	3·258
0·110		3·072	3·018	3·059	3·074	3·111	3·083	3·137	3·093	3·116	3·126	3·122	3·163	3·240	3·253	3·254
0·120		3·045	2·986	3·042	3·055	3·094	3·069	3·125	3·077	3·100	3·116	3·111	3·153	3·225	3·245	3·250
0·130		3·018	2·956	3·024	3·036	3·079	3·055	3·112	3·063	3·085	3·106	3·100	3·144	3·211	3·236	3·246
0·140		2·991	2·928	3·007	3·019	3·065	3·041	3·099	3·050	3·071	3·096	3·090	3·135	3·199	3·228	3·243
0·150		2·965	2·903	2·990	3·004	3·053	3·027	3·085	3·038	3·059	3·086	3·081	3·127	3·189	3·219	3·239
0·160		2·940	2·879	2·973	2·989	3·042	3·012	3·070	3·028	3·047	3·076	3·072	3·118	3·180	3·211	3·235
0·180		2·890	2·837	2·939	2·962	3·010	2·984	3·037	3·001	3·029	3·056	3·056	3·102	3·168	3·193	3·227
0·200		2·844	2·803	2·906	2·919	2·972	2·955	3·003	2·971	3·014	3·037	3·037	3·087	3·154	3·175	3·220
0·250		2·751	2·710	2·812	2·835	2·892	2·886	2·931	2·908	2·960	2·991	2·993	3·047	3·112	3·128	3·201
0·300		2·669	2·636	2·738	2·782	2·827	2·818	2·875	2·861	2·907	2·939	2·952	3·006	3·076	3·088	3·184
0·350		2·610	2·571	2·667	2·704	2·753	2·751	2·802	2·812	2·857	2·893	2·913	2·965	3·046	3·049	3·165
0·400		2·556	2·512	2·596	2·639	2·681	2·684	2·747	2·767	2·817	2·852	2·876	2·932	3·014	3·011	3·143
0·450		2·498	2·473	2·537	2·581	2·607	2·625	2·699	2·717	2·776	2·811	2·842	2·902	2·981	2·977	3·119
0·500		2·462	2·426	2·481	2·520	2·549	2·572	2·650	2·668	2·735	2·773	2·809	2·871	2·945	2·941	3·097
0·600		2·388	2·357	2·389	2·417	2·467	2·479	2·559	2·590	2·654	2·701	2·736	2·811	2·875	2·874	3·052
0·700		2·314	2·301	2·328	2·340	2·387	2·390	2·471	2·513	2·579	2·635	2·671	2·751	2·819	2·817	3·002
0·800		2·259	2·250	2·275	2·280	2·307	2·313	2·392	2·429	2·508	2·574	2·610	2·692	2·765	2·762	2·965
0·900		2·221	2·209	2·226	2·224	2·236	2·246	2·313	2·360	2·445	2·511	2·551	2·637	2·711	2·711	2·934
1·000		2·189	2·170	2·182	2·176	2·188	2·191	2·248	2·300	2·390	2·449	2·492	2·587	2·658	2·665	2·890
1·100		2·149	2·136	2·140	2·137	2·147	2·147	2·197	2·245	2·340	2·394	2·439	2·541	2·611	2·621	2·849
1·200		2·119	2·108	2·104	2·104	2·111	2·106	2·152	1·199	2·292	2·349	2·396	2·493	2·573	2·580	2·810
1·300		2·093	2·080	2·075	2·077	2·086	2·082	2·115	2·163	2·246	2·307	2·360	2·445	2·538	2·541	2·774
1·400		2·064	2·054	2·049	2·054	2·058	2·052	2·081	2·129	2·206	2·264	2·319	2·401	2·498	2·504	2·741
1·600		2·004	1·993	1·995	1·993	1·995	1·993	2·025	2·067	2·134	2·194	2·248	2·331	2·431	2·442	2·687
1·800		1·950	1·946	1·952	1·940	1·945	1·942	1·969	2·004	2·073	2·130	2·189	2·269	2·374	2·393	2·638
2·000		1·902	1·893	1·901	1·894	1·897	1·894	1·913	1·950	2·010	2·071	2·121	2·208	2·322	2·339	2·573
2·500		1·771	1·773	1·781	1·773	1·773	1·767	1·783	1·831	1·883	1·934	1·988	2·075	2·184	2·217	2·441
3·000		1·644	1·651	1·663	1·647	1·644	1·641	1·671	1·714	1·759	1·804	1·859	1·952	2·056	2·106	2·323
3·500		1·516	1·534	1·549	1·531	1·533	1·537	1·560	1·604	1·651	1·696	1·739	1·825	1·937	1·999	2·216
4·000		1·406	1·427	1·444	1·427	1·419	1·426	1·453	1·497	1·547	1·586	1·628	1·706	1·820	1·892	2·111
4·500		1·286	1·318	1·336	1·330	1·316	1·321	1·342	1·394	1·441	1·485	1·525	1·597	1·706	1·786	1·995
5·000		1·186	1·218	1·236	1·230	1·211	1·214	1·234	1·285	1·335	1·392	1·426	1·496	1·608	1·677	1·886

TABLE 7 (continued)
Tables of T/T₁ at Traverse Positions

3·6-1-0-00164

Y (mm)	X (mm)=	-25·4	0·0	3·2	6·3	9·5	12·7	19·0	25·4	38·1	50·8	63·5	88·9	114·3	139·7	171·4
6·000		1·030	1·059	1·064	1·062	1·059	1·051	1·059	1·107	1·151	1·204	1·240	1·314	1·415	1·484	1·687
7·000		1·000	1·003	1·004	1·004	1·002	1·004	1·004	1·015	1·032	1·066	1·087	1·157	1·240	1·322	1·494
8·000		1·000	1·000	1·000	1·000	1·000	1·000	1·000	1·000	1·003	1·012	1·015	1·049	1·108	1·180	1·335
9·000		1·000	1·000	1·000	1·000	1·000	1·000	1·000	1·000	1·000	1·000	1·000	1·009	1·030	1·077	1·196
10·000		1·000	1·000	1·000	1·000	1·000	1·000	1·000	1·000	1·000	1·000	1·000	1·000	1·002	1·023	1·089
11·000		1·000	1·000	1·000	1·000	1·000	1·000	1·000	1·000	1·000	1·000	1·000	1·000	1·000	1·000	1·028
12·000		1·000	1·000	1·000	1·000	1·000	1·000	1·000	1·000	1·000	1·000	1·000	1·000	1·000	1·000	1·006
13·000		1·000	1·000	1·000	1·000	1·000	1·000	1·000	1·000	1·000	1·000	1·000	1·000	1·000	1·000	1·002
14·000		1·000	1·000	1·000	1·000	1·000	1·000	1·000	1·000	1·000	1·000	1·000	1·000	1·000	1·000	1·000
15·000		1·000	1·000	1·000	1·000	1·000	1·000	1·000	1·000	1·000	1·000	1·000	1·000	1·000	1·000	1·000

TABLE 7 (continued)
Tables of T/T_1 at Traverse Positions

3·6-1-0-00294

Y (mm)	X (mm)=	-25·4	0·0	3·2	6·3	9·5	12·7	19·0	25·4	38·1	50·8	63·5	88·9	114·3	139·7
0·081		3·070	3·096	3·196	2·900	3·184	3·163	3·390	3·201	3·175	3·177	3·250	3·257	3·223	3·289
0·090		3·047	3·073	3·184	2·891	3·172	3·153	3·381	3·189	3·169	3·167	3·245	3·252	3·217	3·286
0·100		3·020	3·047	3·170	2·880	3·158	3·141	3·369	3·175	3·161	3·156	3·238	3·246	3·210	2·282
0·110		2·994	3·021	3·155	2·870	3·145	3·128	3·358	3·162	3·154	3·145	3·231	3·240	3·204	3·278
0·120		2·969	2·997	3·139	2·859	3·132	3·116	3·346	3·149	3·146	3·135	3·224	3·234	3·197	3·274
0·130		2·944	2·973	3·124	2·849	3·120	3·105	3·334	3·137	3·139	3·126	3·217	3·228	3·191	3·269
0·140		2·919	2·950	3·108	2·839	3·108	3·093	3·321	3·125	3·131	3·117	3·211	3·223	3·184	3·265
0·150		2·895	2·928	3·092	2·829	3·097	3·081	3·309	3·113	3·124	3·109	3·204	3·217	3·178	3·261
0·160		2·872	2·907	3·075	2·820	3·086	3·070	3·296	3·103	3·117	3·101	3·198	3·212	3·173	3·257
0·180		2·826	2·866	3·041	2·802	3·059	3·047	3·269	3·082	3·103	3·088	3·185	3·202	3·161	3·248
0·200		2·782	2·823	3·012	2·783	3·028	3·025	3·242	3·062	3·090	3·077	3·172	3·193	3·151	3·240
0·250		2·691	2·726	2·940	2·731	2·961	2·969	3·190	3·017	3·062	3·059	3·144	3·173	3·127	3·218
0·300		2·617	2·649	2·859	2·683	2·906	2·911	3·138	2·978	3·028	3·026	3·118	3·152	3·106	3·200
0·350		2·559	2·587	2·789	2·634	2·847	2·854	3·082	2·935	2·989	2·999	3·092	3·127	3·088	3·180
0·400		2·512	2·530	2·709	2·581	2·783	2·810	3·025	2·901	2·960	2·977	3·062	3·099	3·073	3·157
0·450		2·461	2·476	2·627	2·525	2·718	2·753	2·974	2·859	2·928	2·947	3·034	3·073	3·056	3·133
0·500		2·416	2·428	2·566	2·471	2·659	2·703	2·923	2·815	2·895	2·916	3·007	3·051	3·034	3·110
0·600		2·337	2·350	2·456	2·533	2·563	2·604	2·822	2·742	2·834	2·853	2·946	3·003	2·997	3·064
0·700		2·274	2·300	2·380	2·600	2·470	2·512	2·714	2·668	2·776	2·800	2·895	2·959	2·960	3·022
0·800		2·226	2·251	2·315	2·430	2·379	2·413	2·630	2·602	2·712	2·751	2·847	2·918	2·921	2·981
0·900		2·190	2·208	2·261	2·350	2·298	2·333	2·541	2·525	2·653	2·701	2·799	2·873	2·885	2·946
1·000		2·152	2·168	2·213	2·297	2·230	2·261	2·456	2·454	2·599	2·651	2·757	2·826	2·848	2·913
1·100		2·116	2·132	2·165	2·241	2·176	2·202	2·383	2·394	2·547	2·603	2·716	2·783	2·810	2·882
1·200		2·087	2·101	2·129	2·188	2·127	2·152	2·323	2·342	2·495	2·557	2·670	2·747	2·778	2·851
1·300		2·063	2·074	2·092	2·139	2·091	2·111	2·261	2·294	2·447	2·511	2·625	2·707	2·749	2·823
1·400		2·038	2·050	2·061	2·097	2·059	2·073	2·207	2·247	2·403	2·467	2·582	2·667	2·721	2·796
1·600		1·985	1·992	2·003	2·026	1·998	2·010	2·125	2·161	2·320	2·387	2·505	2·607	2·668	2·742
1·800		1·934	1·950	1·949	1·964	1·950	1·957	2·056	2·089	2·242	2·313	2·436	2·546	2·631	2·695
2·000		1·888	1·898	1·898	1·910	1·895	1·908	1·989	2·022	2·175	2·245	2·366	2·484	2·532	2·654
2·500		1·760	1·771	1·778	1·777	1·769	1·773	1·840	1·882	1·834	2·092	2·221	2·349	2·464	2·553
3·000		1·628	1·650	1·662	1·647	1·645	1·654	1·716	1·764	1·889	1·948	2·077	2·208	2·337	2·438
3·500		1·505	1·534	1·564	1·524	1·519	1·532	1·585	1·650	1·736	1·818	1·930	2·072	2·212	2·322
4·000		1·396	1·430	1·447	1·414	1·405	1·421	1·473	1·542	1·626	1·703	1·798	1·936	2·091	2·217
4·500		1·280	1·318	1·344	1·314	1·294	1·309	1·355	1·424	1·512	1·586	1·674	1·810	1·966	2·118
5·000		1·184	1·217	1·235	1·235	1·186	1·200	1·244	1·319	1·409	1·478	1·559	1·689	1·854	2·009

TABLE 7 (continued)
Tables of T/T_1 at Traverse Positions

3·6-1-0-00294

Y (mm)	X (mm)=	-25·4	0·0	3·2	6·3	9·5	12·7	19·0	25·4	38·1	50·8	63·5	88·9	114·3	139·7
6·000		1·027	1·056	1·063	1·073	1·055	1·038	1·058	1·132	1·213	1·290	1·363	1·486	1·638	1·793
7·000		1·000	1·004	1·005	1·007	1·006	1·000	1·003	1·021	1·065	1·132	1·190	1·302	1·436	1·589
8·000		1·000	1·000	1·000	1·002	1·000	1·000	1·000	1·000	1·005	1·030	1·060	1·149	1·262	1·410
9·000		1·000	1·000	1·000	1·000	1·000	1·000	1·000	1·000	1·000	1·004	1·009	1·042	1·128	1·253
10·000		1·000	1·000	1·000	1·000	1·000	1·000	1·000	1·000	1·000	1·000	1·000	1·007	1·038	1·129
11·000		1·000	1·000	1·000	1·000	1·000	1·000	1·000	1·000	1·000	1·000	1·000	1·000	1·003	1·043
12·000		1·000	1·000	1·000	1·000	1·000	1·000	1·000	1·000	1·000	1·000	1·000	1·000	1·000	1·008
13·000		1·000	1·000	1·000	1·000	1·000	1·000	1·000	1·000	1·000	1·000	1·000	1·000	1·000	1·000
14·000		1·000	1·000	1·000	1·000	1·000	1·000	1·000	1·000	1·000	1·000	1·000	1·000	1·000	1·000
15·000		1·000	1·000	1·000	1·000	1·000	1·000	1·000	1·000	1·000	1·000	1·000	1·000	1·000	1·000

TABLE 7 (continued)
Tables of T/T₁ at Traverse Positions

3·6-1-0-00421

Y (mm)	X (mm)=	-25·4	0·0	3·2	6·3	9·5	12·7	19·0	25·4	38·1	50·8	63·5	88·9	114·3	139·7
0·081		3·120	3·071	3·170	3·214	3·178	3·243	3·203	3·195	3·169	3·179	3·206	3·269	3·219	3·163
0·090		3·091	3·049	3·155	3·203	3·172	3·235	3·198	3·189	3·165	3·174	3·202	3·267	3·217	3·163
0·100		3·059	3·023	3·137	3·190	3·164	3·225	3·192	3·181	3·159	3·168	3·197	3·265	3·214	3·162
0·110		3·029	2·998	3·120	3·178	3·156	3·215	3·185	3·173	3·153	3·162	3·192	3·262	3·211	3·161
0·120		3·000	2·974	3·104	3·166	3·148	3·205	3·179	3·166	3·148	3·157	3·187	3·260	3·209	3·160
0·130		2·972	2·949	3·088	3·154	3·140	3·195	3·172	3·159	3·142	3·151	3·183	3·258	3·206	3·159
0·140		2·946	2·926	3·073	3·144	3·132	3·185	3·166	3·151	3·137	3·146	3·178	3·255	3·205	3·158
0·150		2·921	2·903	2·058	3·133	3·124	3·175	3·159	3·145	3·132	2·141	3·173	3·253	3·203	3·157
0·160		2·898	2·880	3·045	3·123	3·115	3·165	3·152	3·138	3·126	3·136	3·168	3·251	3·202	3·155
0·180		2·855	2·836	3·018	3·103	3·099	3·144	3·138	3·125	3·115	3·127	3·159	3·246	3·200	3·153
0·200		2·814	2·794	2·995	3·080	3·084	3·126	3·123	3·113	3·105	3·119	3·150	3·242	3·198	3·150
0·250		2·719	2·709	2·930	3·023	3·038	3·082	3·092	3·083	3·080	3·102	3·130	3·229	3·189	3·144
0·300		2·640	2·635	2·858	2·969	2·981	3·035	3·056	3·052	3·059	3·075	3·116	3·211	3·179	3·139
0·350		2·582	2·567	2·781	2·905	2·930	2·982	3·016	3·024	3·038	3·052	3·100	3·195	3·169	3·132
0·400		2·523	2·515	2·705	2·848	2·881	2·933	2·982	2·998	3·016	3·033	3·082	3·181	3·161	3·123
0·450		2·466	2·464	2·643	2·780	2·828	2·892	2·945	2·967	2·989	3·013	3·065	3·164	3·152	3·116
0·500		2·418	2·415	2·579	2·712	2·775	2·853	2·911	2·930	2·961	2·993	3·048	3·148	3·144	3·108
0·600		2·349	2·341	2·466	2·601	2·687	2·767	2·841	2·858	2·912	2·954	3·010	3·117	3·124	3·094
0·700		2·288	2·284	2·382	2·500	2·595	2·675	2·766	2·802	2·869	2·918	2·972	3·088	3·101	3·080
0·800		2·229	2·238	2·311	2·413	2·496	2·590	2·689	2·755	2·814	2·863	2·940	3·063	3·085	3·070
0·900		2·186	2·200	2·249	2·318	2·406	2·510	2·609	2·688	2·767	2·823	2·910	3·034	3·072	3·058
1·000		2·157	2·158	2·196	2·247	2·323	2·426	2·530	2·625	2·724	2·790	2·872	3·005	3·047	3·044
1·100		2·128	2·122	2·147	2·194	2·252	2·345	2·459	2·568	2·680	2·751	2·827	2·978	3·024	3·027
1·200		2·103	2·095	2·102	2·147	2·192	2·275	2·391	2·510	2·638	2·713	2·788	2·952	3·004	3·009
1·300		2·070	2·072	2·074	2·108	2·138	2·213	2·328	2·461	2·597	2·670	2·756	2·923	2·986	2·992
1·400		2·042	2·043	2·045	2·074	2·100	2·162	2·271	2·412	2·554	2·627	2·729	2·892	2·970	2·975
1·600		1·990	1·995	1·984	2·011	2·028	2·081	2·172	2·311	2·469	2·556	2·671	2·835	2·934	2·941
1·800		1·936	1·946	1·938	1·958	1·973	2·006	2·085	2·232	2·391	2·491	2·612	2·779	2·893	2·914
2·000		1·884	1·893	1·878	1·902	1·916	1·953	2·006	2·150	2·322	2·425	2·537	2·732	2·856	2·892
2·500		1·760	1·772	1·750	1·768	1·783	1·807	1·845	1·977	2·131	2·261	2·396	2·616	2·772	2·833
3·000		1·633	1·650	1·642	1·629	1·646	1·668	1·717	1·842	1·984	2·106	2·257	2·488	2·666	2·767
3·500		1·511	1·534	1·550	1·514	1·522	1·544	1·593	1·724	1·839	1·969	2·117	2·353	2·572	2·698
4·000		1·401	1·430	1·439	1·392	1·403	1·422	1·473	1·609	1·712	1·833	1·967	2·216	2·449	2·612
4·500		1·285	1·317	1·333	1·301	1·288	1·303	1·352	1·486	1·594	1·711	1·834	2·088	2·339	2·528
5·000		1·180	1·216	1·227	1·227	1·175	1·190	1·239	1·369	1·477	1·588	1·707	1·954	2·226	2·442

TABLE 7 (continued)
Tables of T/T_1 at Traverse Positions

3·6-1-0-00421

Y (mm)	X (mm)=	-25·4	0·0	3·2	6·3	9·5	12·7	19·0	25·4	38·1	50·8	63·5	88·9	114·3	139·7
6·000		1·028	1·054	1·056	1·065	1·050	1·028	1·059	1·178	1·285	1·385	1·484	1·707	1·994	2·233
7·000		1·000	1·004	1·003	1·005	1·002	1·003	1·006	1·034	1·110	1·205	1·289	1·482	1·755	2·031
8·000		1·000	1·000	1·000	1·000	1·000	1·000	1·000	1·000	1·016	1·062	1·125	1·294	1·534	1·814
9·000		1·000	1·000	1·000	1·000	1·000	1·000	1·000	1·000	1·000	1·005	1·032	1·143	1·345	1·617
10·000		1·000	1·000	1·000	1·000	1·000	1·000	1·000	1·000	1·000	1·000	1·002	1·042	1·188	1·426
11·000		1·000	1·000	1·000	1·000	1·000	1·000	1·000	1·000	1·000	1·000	1·000	1·003	1·069	1·264
12·000		1·000	1·000	1·000	1·000	1·000	1·000	1·000	1·000	1·000	1·000	1·000	1·000	1·012	1·132
13·000		1·000	1·000	1·000	1·000	1·000	1·000	1·000	1·000	1·000	1·000	1·000	1·000	1·000	1·046
14·000		1·000	1·000	1·000	1·000	1·000	1·000	1·000	1·000	1·000	1·000	1·000	1·000	1·000	1·009
15·000		1·000	1·000	1·000	1·000	1·000	1·000	1·000	1·000	1·000	1·000	1·000	1·000	1·000	1·000

TABLE 7 (continued)
Tables of T/T₁ at Traverse Positions

3·6-2-0-00294

Y (mm)	X (mm)=	-25·4	0·0	3·2	6·3	9·5	12·7	19·0	25·4	38·1	50·8	63·5	88·9	114·3	139·7	171·4
0·081		3·405	3·408	3·438	3·376	3·475	3·409	3·330	3·344	3·374	3·347	3·319	3·515	3·294	3·386	3·399
0·090		3·401	3·402	3·429	3·367	3·448	3·401	3·318	3·328	3·363	3·338	3·303	3·511	3·279	3·361	3·379
0·100		3·397	3·396	3·420	3·357	3·419	3·391	3·304	3·311	3·351	3·327	3·286	3·506	3·263	3·334	3·356
0·110		3·393	3·389	3·410	3·348	3·392	3·381	3·290	3·294	3·339	3·316	3·269	3·501	3·246	3·307	3·334
0·120		3·389	3·383	3·401	3·339	3·368	3·372	3·277	3·278	3·327	3·305	3·252	3·494	3·230	3·282	3·312
0·130		3·385	3·377	3·392	3·330	3·345	3·362	3·265	3·262	3·315	3·294	3·236	3·488	3·214	3·258	3·290
0·140		3·380	3·371	3·384	3·321	3·324	3·352	3·252	3·247	3·303	3·282	3·221	3·480	3·199	3·234	3·268
0·160		3·372	3·359	3·367	3·305	3·289	3·332	3·228	3·218	3·279	3·259	3·191	3·463	3·168	3·190	3·225
0·180		3·364	3·347	3·351	3·289	3·262	3·312	3·206	3·192	3·255	3·235	3·163	3·443	3·137	3·150	3·183
0·200		3·355	3·335	3·336	3·275	3·244	3·292	3·184	3·167	3·230	3·210	3·137	3·421	3·108	3·113	3·143
0·250		3·334	3·307	3·302	3·242	3·233	3·241	3·137	3·115	3·169	3·146	3·080	3·353	3·038	3·039	3·045
0·300		3·313	3·280	3·273	3·216	3·231	3·198	3·097	3·076	3·106	3·077	3·035	3·269	3·973	2·987	2·977
0·350		3·291	3·254	3·249	3·193	3·211	3·181	3·065	3·051	3·044	3·042	3·002	3·168	2·913	2·938	2·929
0·400		3·269	3·230	3·227	3·167	3·192	3·164	3·038	3·038	3·005	3·012	2·980	3·000	2·876	2·896	2·886
0·500		3·237	3·191	3·181	3·125	3·151	3·128	2·990	2·994	2·955	2·957	2·932	2·771	2·819	2·825	2·817
0·600		3·202	3·147	3·138	3·094	3·111	3·090	2·951	2·957	2·912	2·912	2·888	2·779	2·759	2·776	2·766
0·700		3·164	3·096	3·093	3·072	3·082	3·046	2·923	2·927	2·878	2·879	2·846	2·969	2·704	2·721	2·717
0·800		3·134	3·060	3·044	3·044	3·053	3·008	2·901	2·895	2·850	2·850	2·810	2·933	2·678	2·677	2·678
0·900		3·105	3·027	3·008	3·007	3·026	2·975	2·878	2·866	2·826	2·825	2·779	2·895	2·651	2·645	2·648
1·000		3·075	2·993	2·984	2·973	2·999	2·954	2·855	2·841	2·800	2·801	2·755	2·855	2·621	2·621	2·614
1·200		2·076	2·945	2·938	2·940	2·948	2·920	2·816	2·799	2·745	2·758	2·704	2·797	2·566	2·568	2·561
1·400		3·003	2·911	2·908	2·888	2·905	2·889	2·786	2·766	2·716	2·718	2·669	2·744	2·534	2·532	2·536
1·600		2·973	2·884	2·875	2·849	2·869	2·860	2·754	2·741	2·689	2·689	2·645	2·700	2·506	2·513	2·509
1·800		2·936	2·853	2·844	2·821	2·840	2·822	2·720	2·715	2·659	2·667	2·617	2·667	2·477	2·493	2·475
2·000		2·895	2·819	2·814	2·796	2·813	2·785	2·696	2·691	2·640	2·639	2·593	2·647	2·461	2·466	2·449
2·500		2·827	2·745	2·731	2·727	2·746	2·718	2·638	2·626	2·568	2·577	2·537	2·588	2·408	2·403	2·392
3·000		2·738	2·673	2·665	2·649	2·656	2·650	2·570	2·556	2·514	2·507	2·469	2·526	2·356	2·363	2·341
3·500		2·661	2·606	2·592	2·581	2·595	2·571	2·512	2·492	2·452	2·448	2·424	2·462	2·308	2·309	2·287
4·000		2·573	2·521	2·517	2·501	2·514	2·498	2·438	2·430	2·385	2·384	2·356	2·398	2·243	2·258	2·237
4·500		2·485	2·438	2·440	2·423	2·430	2·422	2·369	2·357	2·320	2·309	2·280	2·325	2·189	2·203	2·181
5·000		2·397	2·360	2·358	2·349	2·352	2·342	2·298	2·285	2·240	2·230	2·209	2·247	2·131	2·144	2·131
6·000		2·186	2·195	2·190	2·178	2·175	2·174	2·143	2·132	2·088	2·069	2·061	2·100	2·015	2·033	2·017
7·000		1·977	2·016	2·003	2·001	1·997	2·007	1·983	1·972	1·926	1·913	1·905	1·944	1·875	1·907	1·893
8·000		1·751	1·819	1·821	1·787	1·816	1·826	1·809	1·792	1·746	1·743	1·739	1·775	1·738	1·777	1·773
9·000		1·524	1·610	1·617	1·635	1·623	1·646	1·642	1·622	1·580	1·570	1·574	1·613	1·601	1·643	1·650

TABLE 7 (continued)
Tables of T/T₁ at Traverse Positions

3·6-2-0·00294

Y (mm)	X (mm) =	-25·4	0·0	3·2	6·3	9·5	12·7	19·0	25·4	38·1	50·8	63·5	88·9	114·3	139·7	171·4
10·000		1·304	1·413	1·410	1·439	1·433	1·474	1·468	1·447	1·414	1·403	1·411	1·455	1·477	1·517	1·518
11·000		1·126	1·234	1·223	1·255	1·258	1·302	1·314	1·296	1·253	1·259	1·264	1·306	1·345	1·402	1·398
12·000		1·029	1·090	1·080	1·111	1·115	1·157	1·193	1·167	1·123	1·127	1·134	1·179	1·226	1·306	1·284
13·000		1·004	1·025	1·021	1·037	1·037	1·076	1·110	1·101	1·041	1·035	1·051	1·078	1·128	1·173	1·190
14·000		1·000	1·002	1·003	1·010	1·010	1·043	1·067	1·076	1·008	1·014	1·014	1·027	1·061	1·097	1·112
15·000		1·000	1·000	1·000	1·003	1·004	1·026	1·042	1·058	1·002	1·001	1·002	1·007	1·026	1·051	1·054
16·000		1·000	1·000	1·000	1·000	1·000	1·014	1·026	1·044	1·000	1·000	1·000	1·001	1·011	1·022	1·021
18·000		1·000	1·000	1·000	1·000	1·000	1·003	1·010	1·019	1·000	1·000	1·000	1·000	1·001	1·000	1·002
20·000		1·000	1·000	1·000	1·000	1·000	1·000	1·001	1·003	1·000	1·000	1·000	1·000	1·000	1·000	1·000
22·000		1·000	1·000	1·000	1·000	1·000	1·000	1·000	1·000	1·000	1·000	1·000	1·000	1·000	1·000	1·000

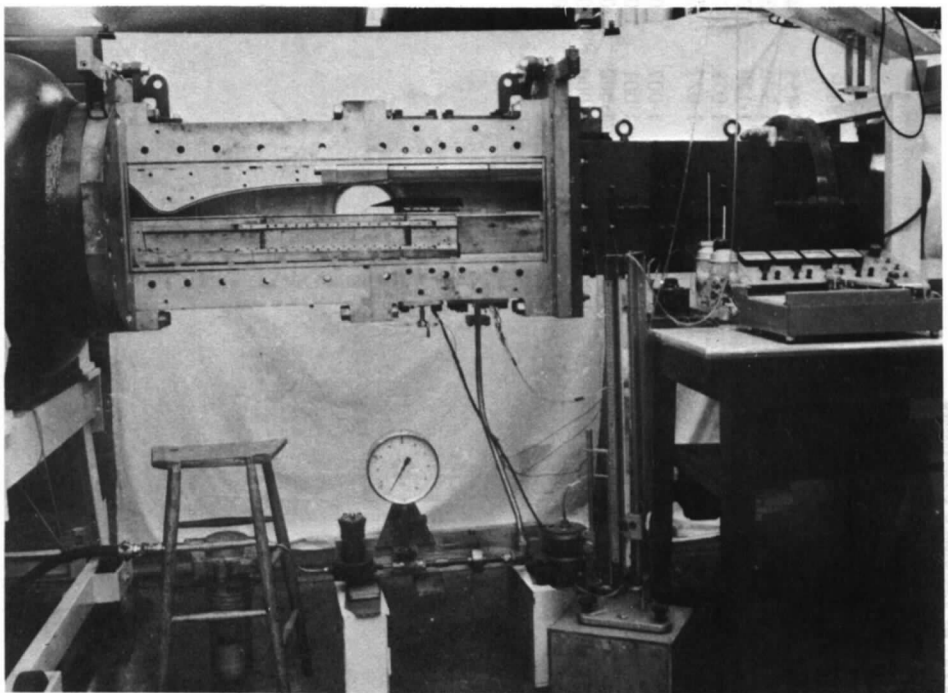


FIG. 1 Photograph of tunnel.

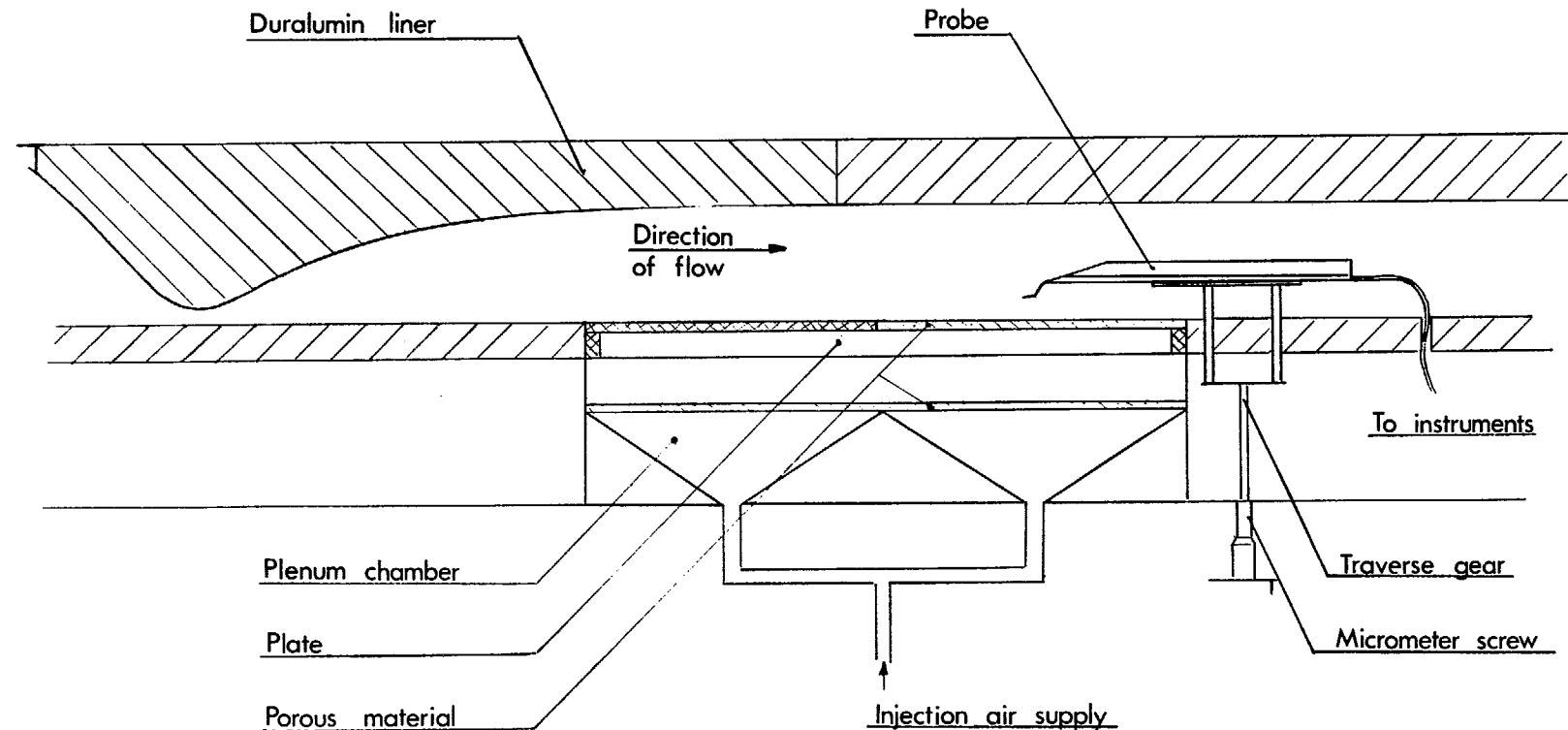


FIG. 2. Sketch of the working section.

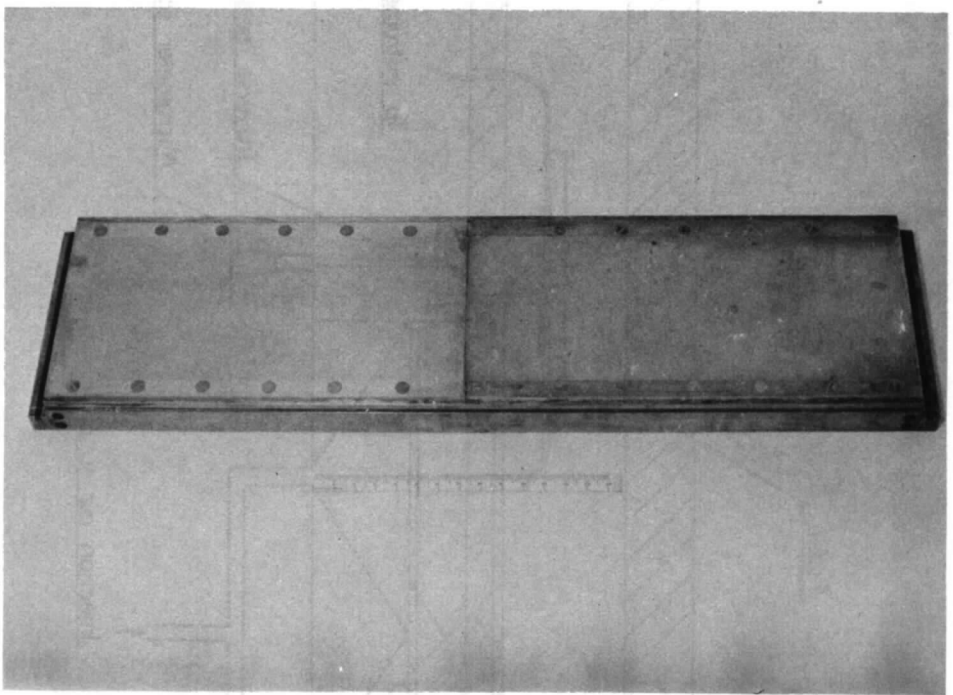


FIG. 3. Photograph of plate.

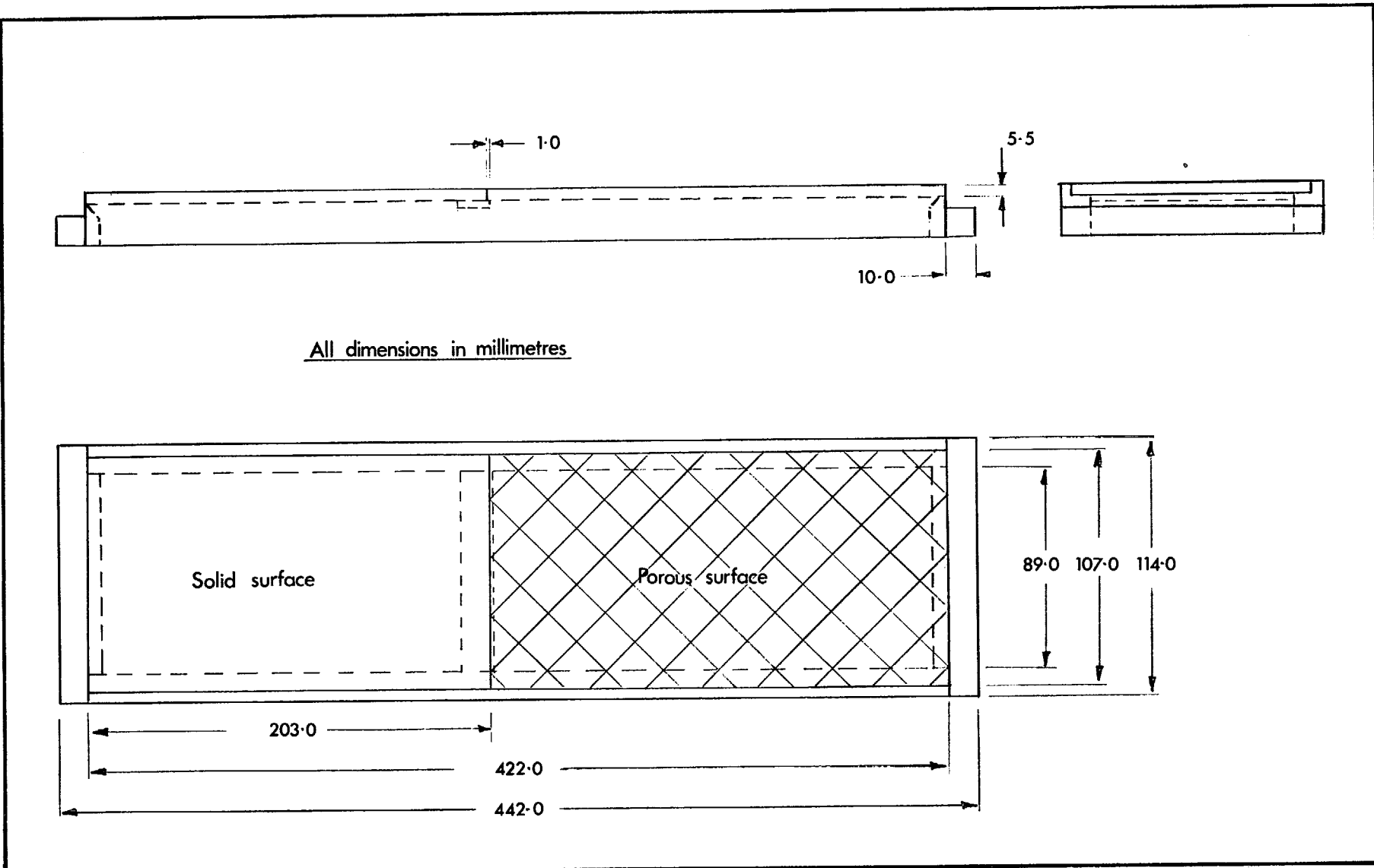
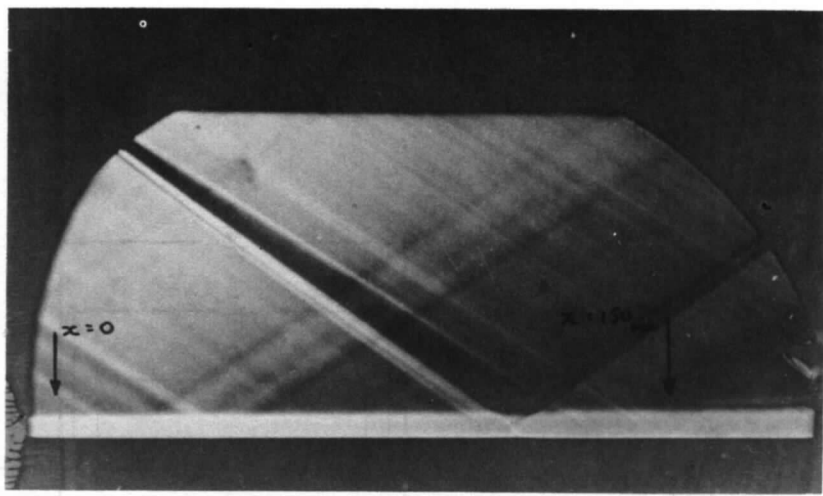
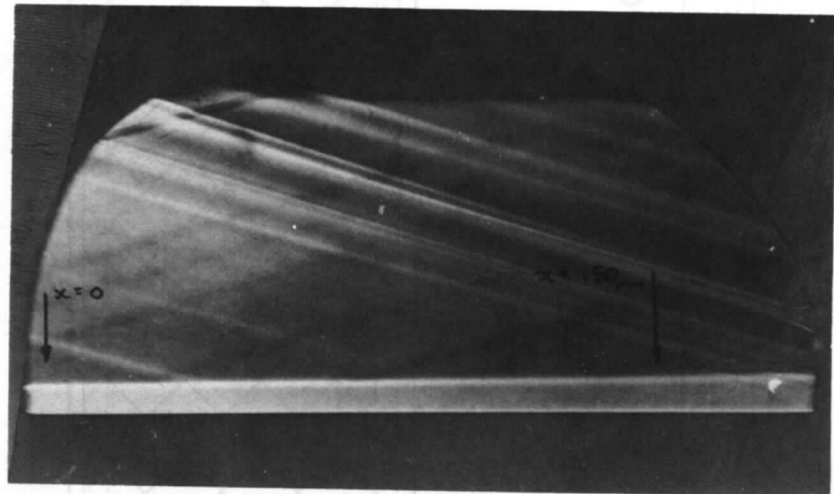


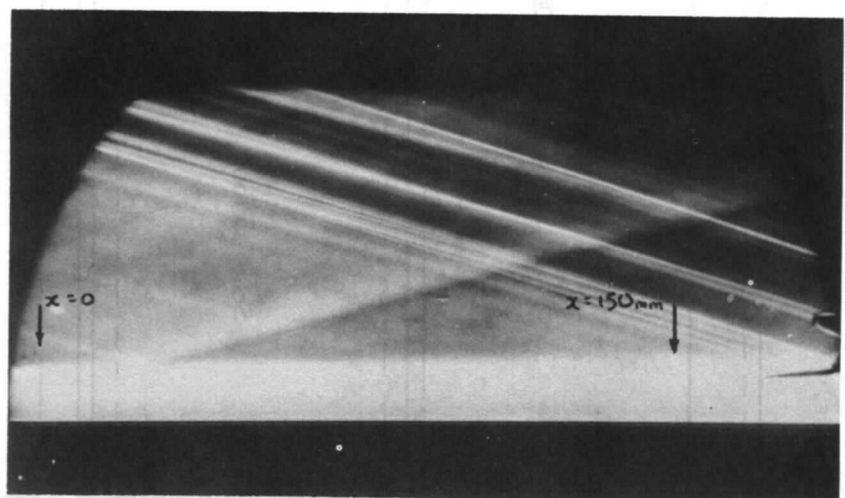
FIG. 4. Dimensions of the plate.



(a) Mach 1.8 solid surface.

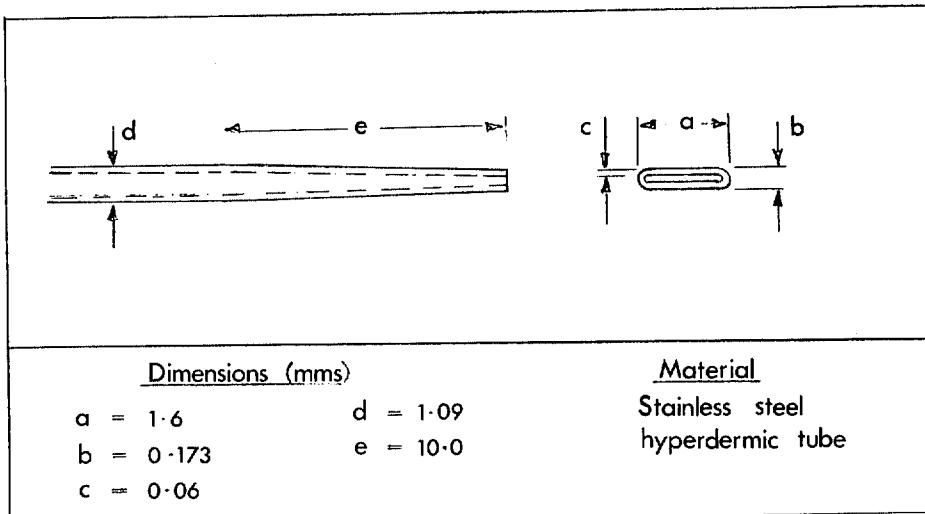


(b) Mach 3.6 solid surface.

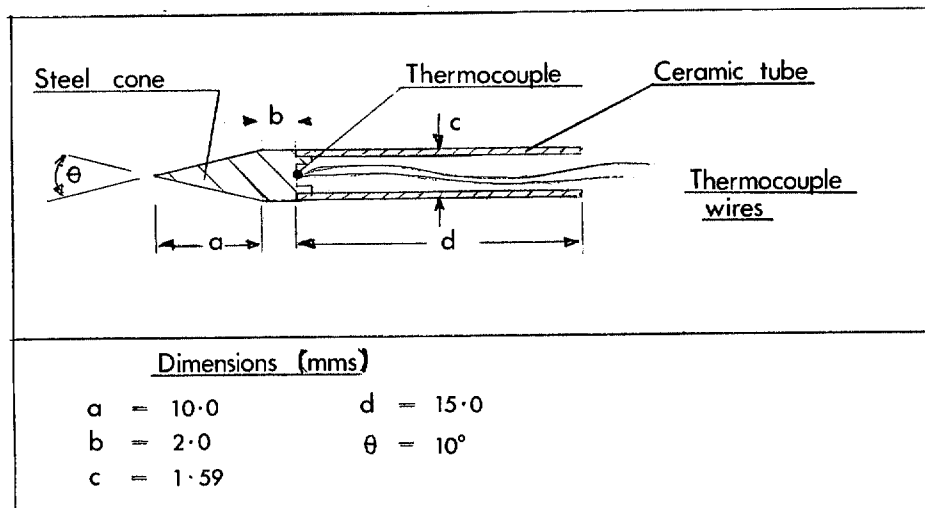


(c) Mach 3.6 porous solid ($F = 0.00294$).

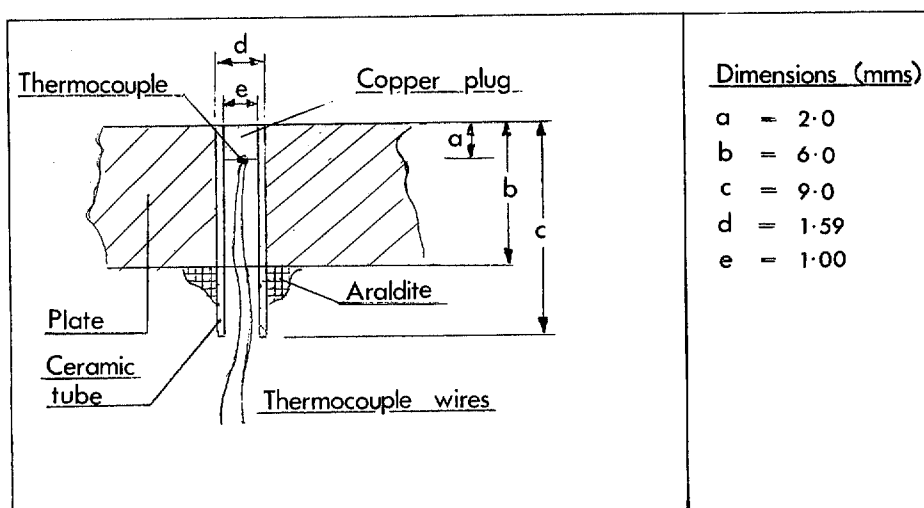
FIG. 5. Schlieren photographs.



(a) Dimensions of the pitot probe



(b) Dimensions of the temperature probe



(c) Dimensions of the wall thermocouples

FIG. 6. Instrument dimensions.

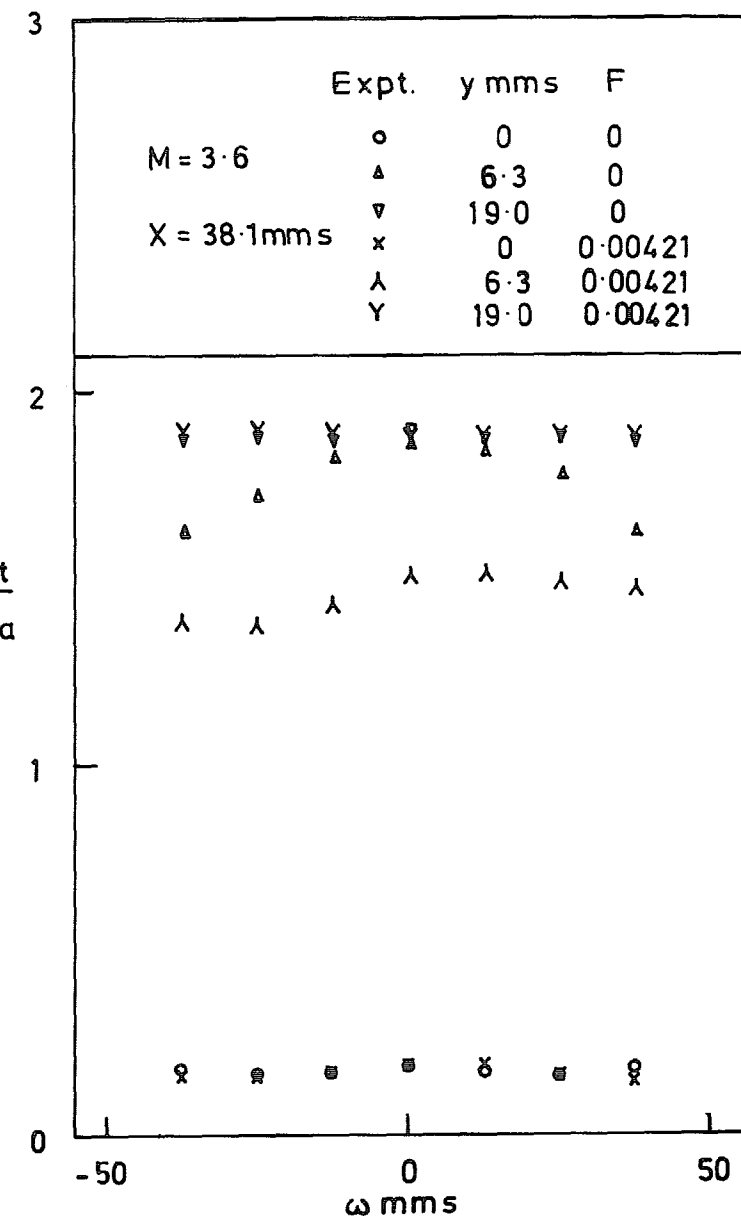
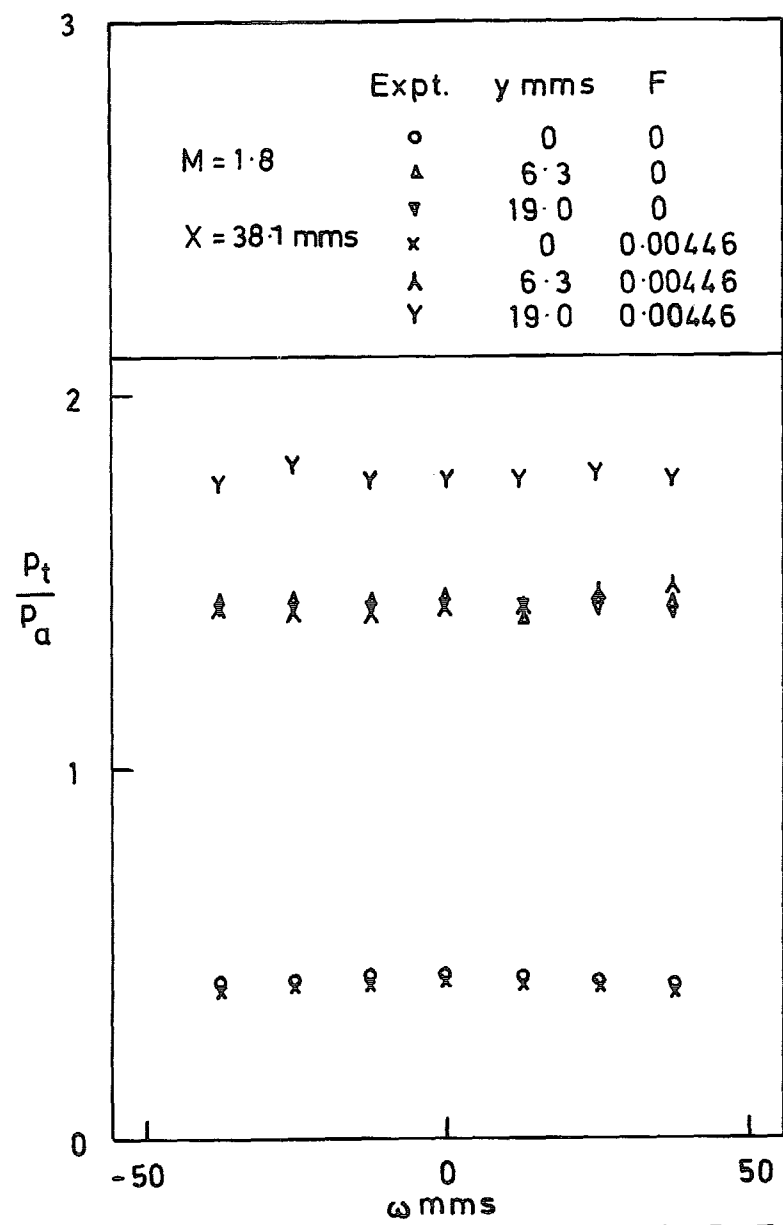


FIG. 7. Total pressure variation across plate.

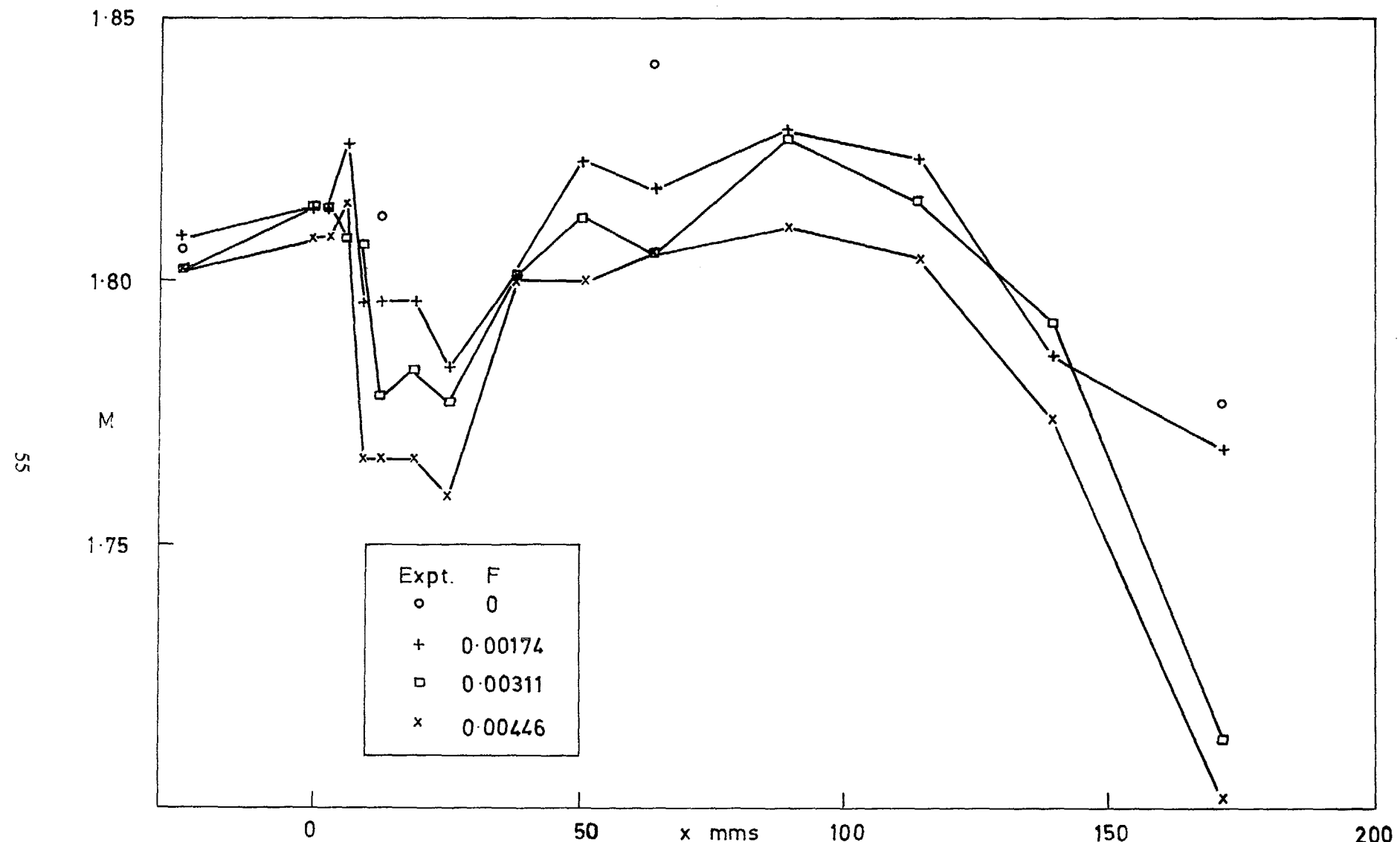


FIG. 8. Mach number distribution.

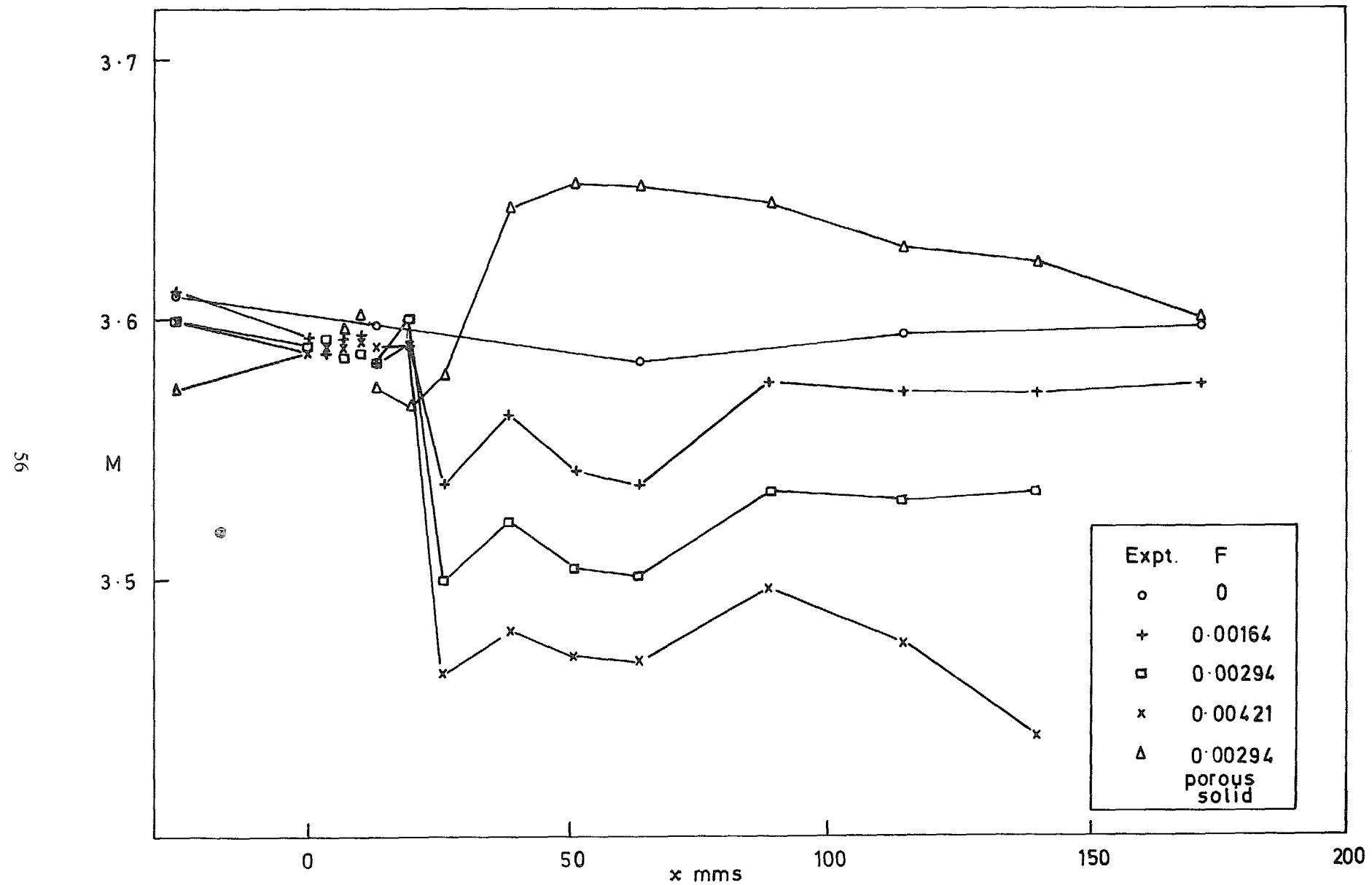


FIG. 9. Mach number distribution.

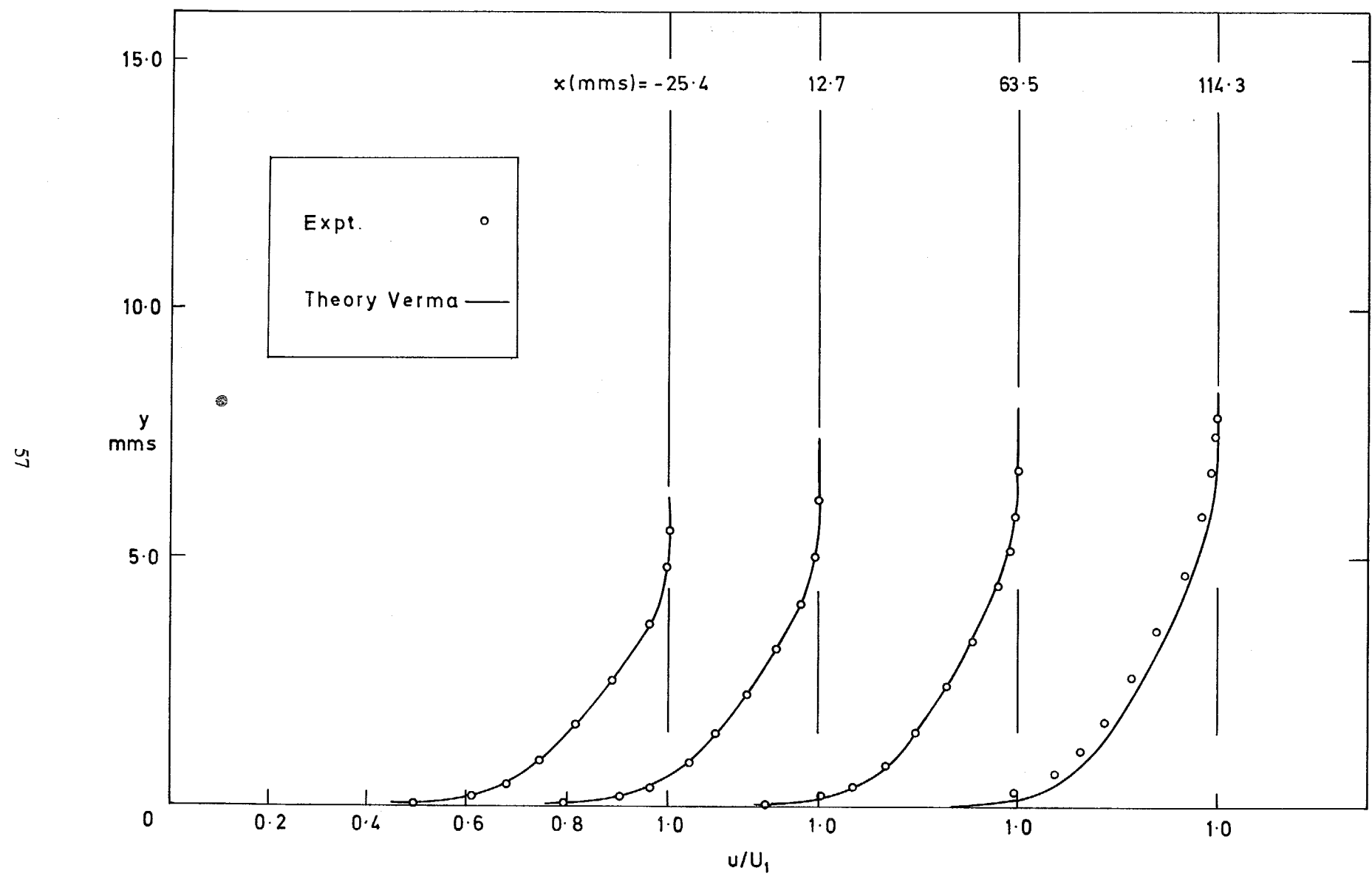


FIG. 10. Velocity profiles ($M = 1.8$; $F = 0$).

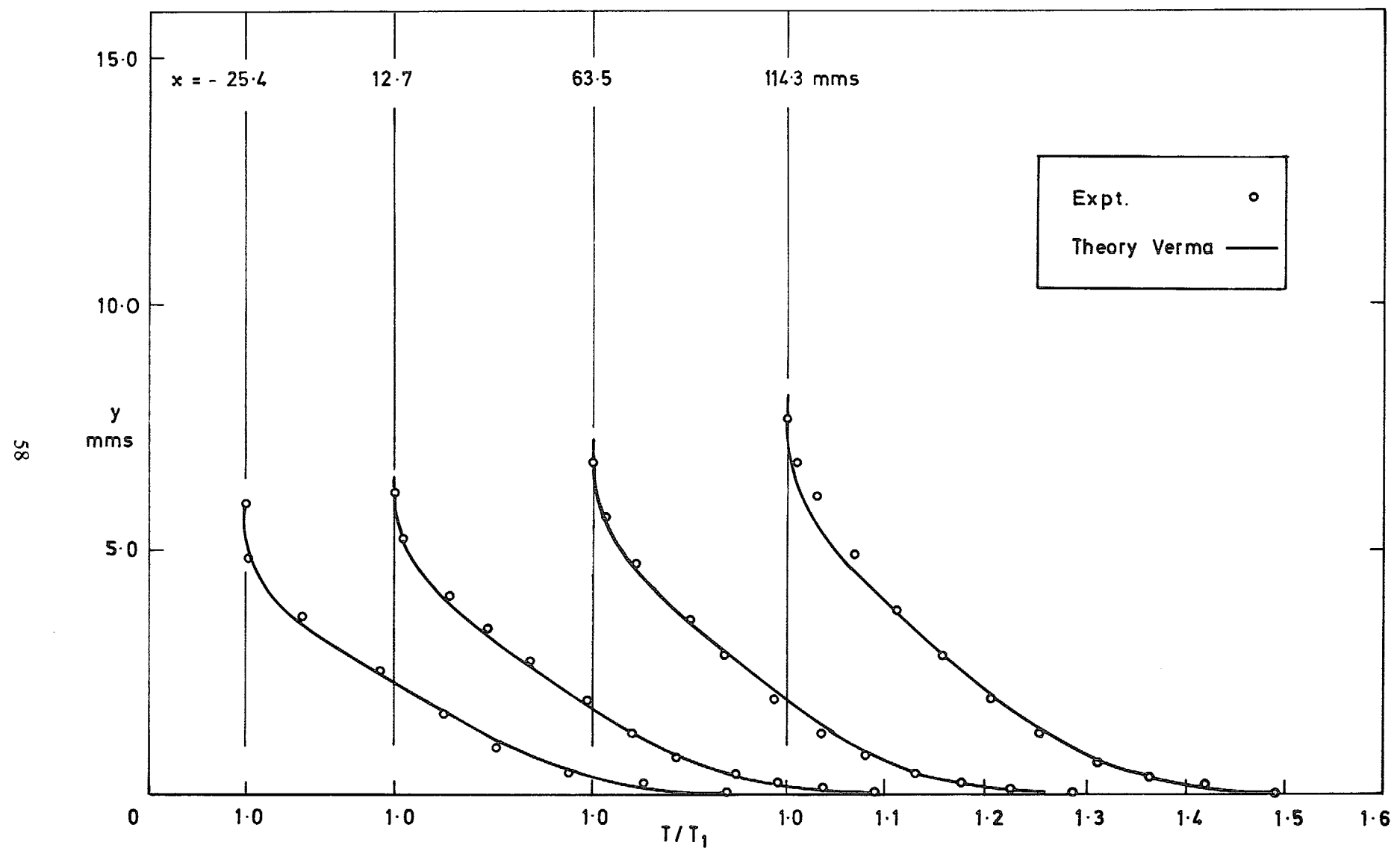


FIG. 11. Temperature profiles ($M = 1.8; F = 0$).

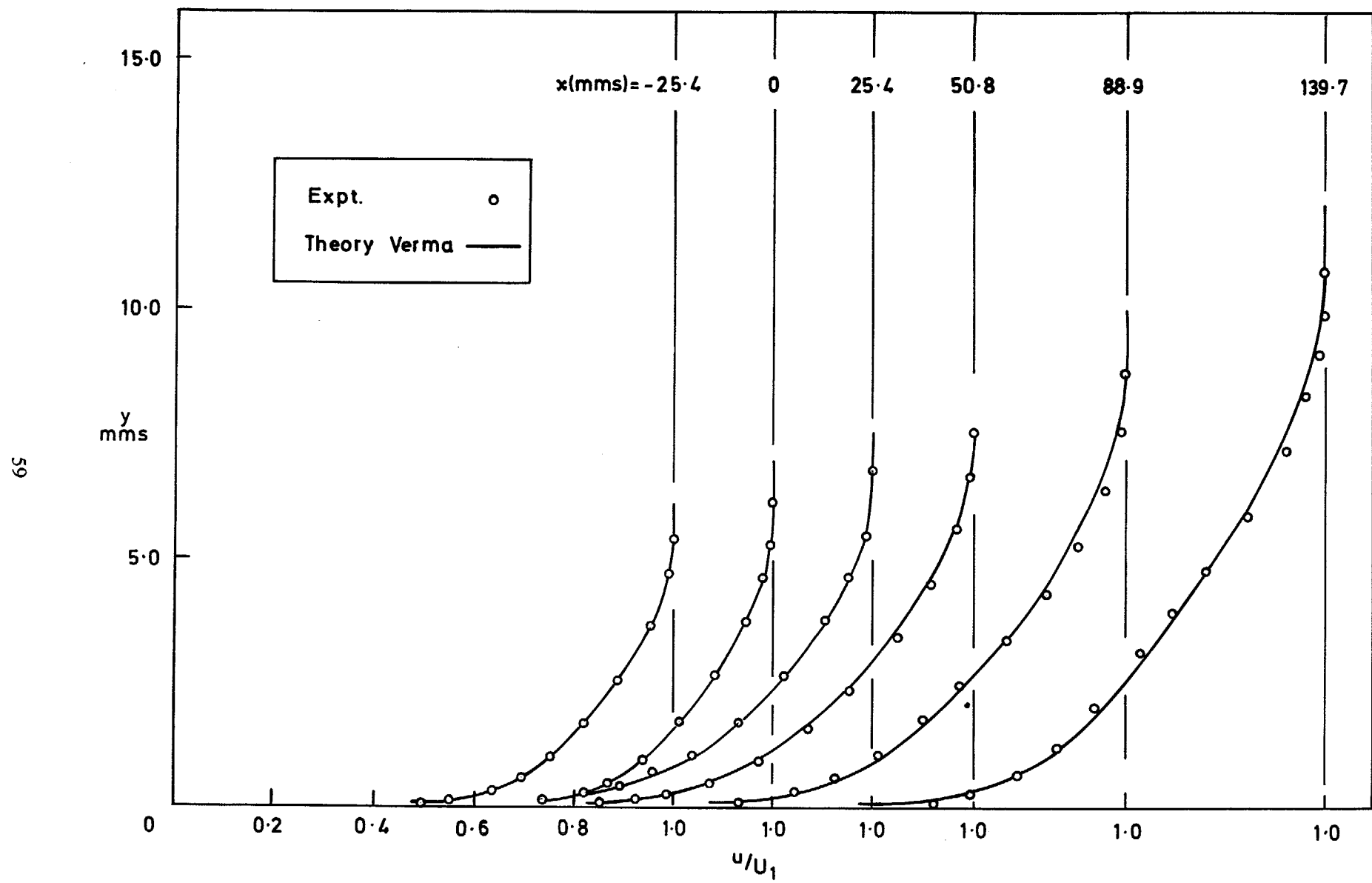


FIG. 12. Velocity profiles ($M = 1.8$; $F = 0.00446$).

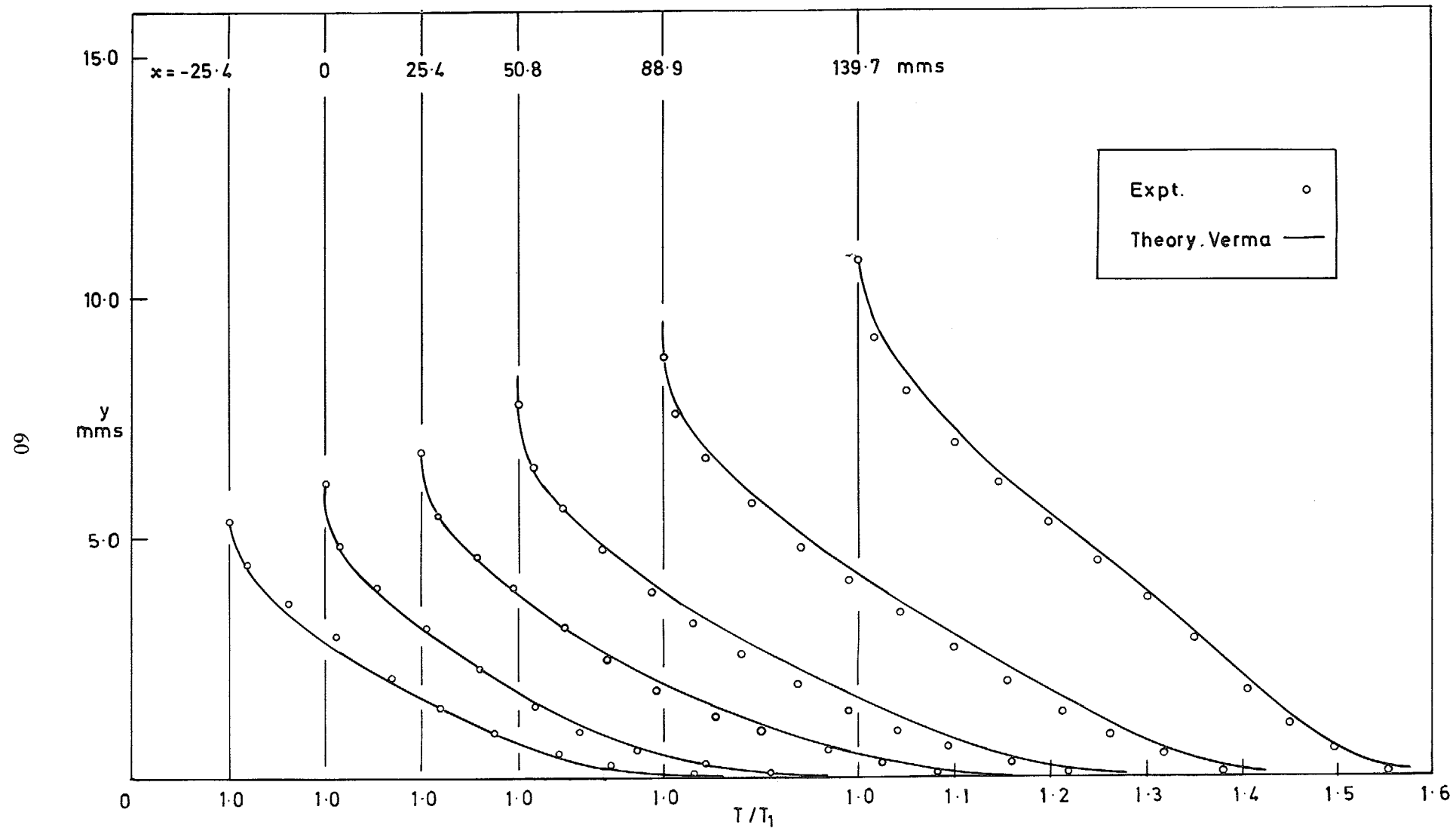


FIG. 13. Temperature profiles ($M = 1.8; F = 0.00446$).

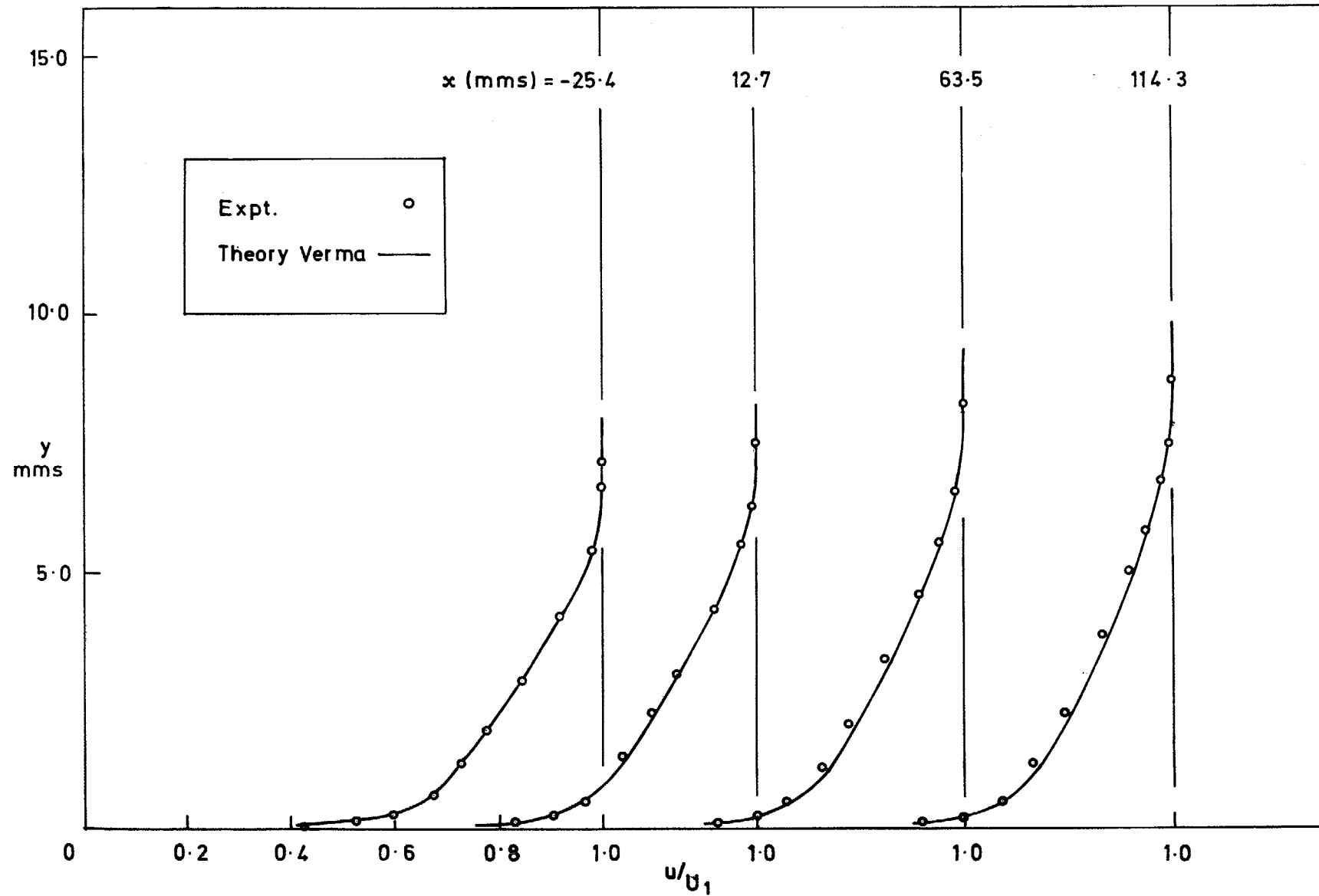


FIG. 14. Velocity profiles ($M = 3.6; F = 0$).

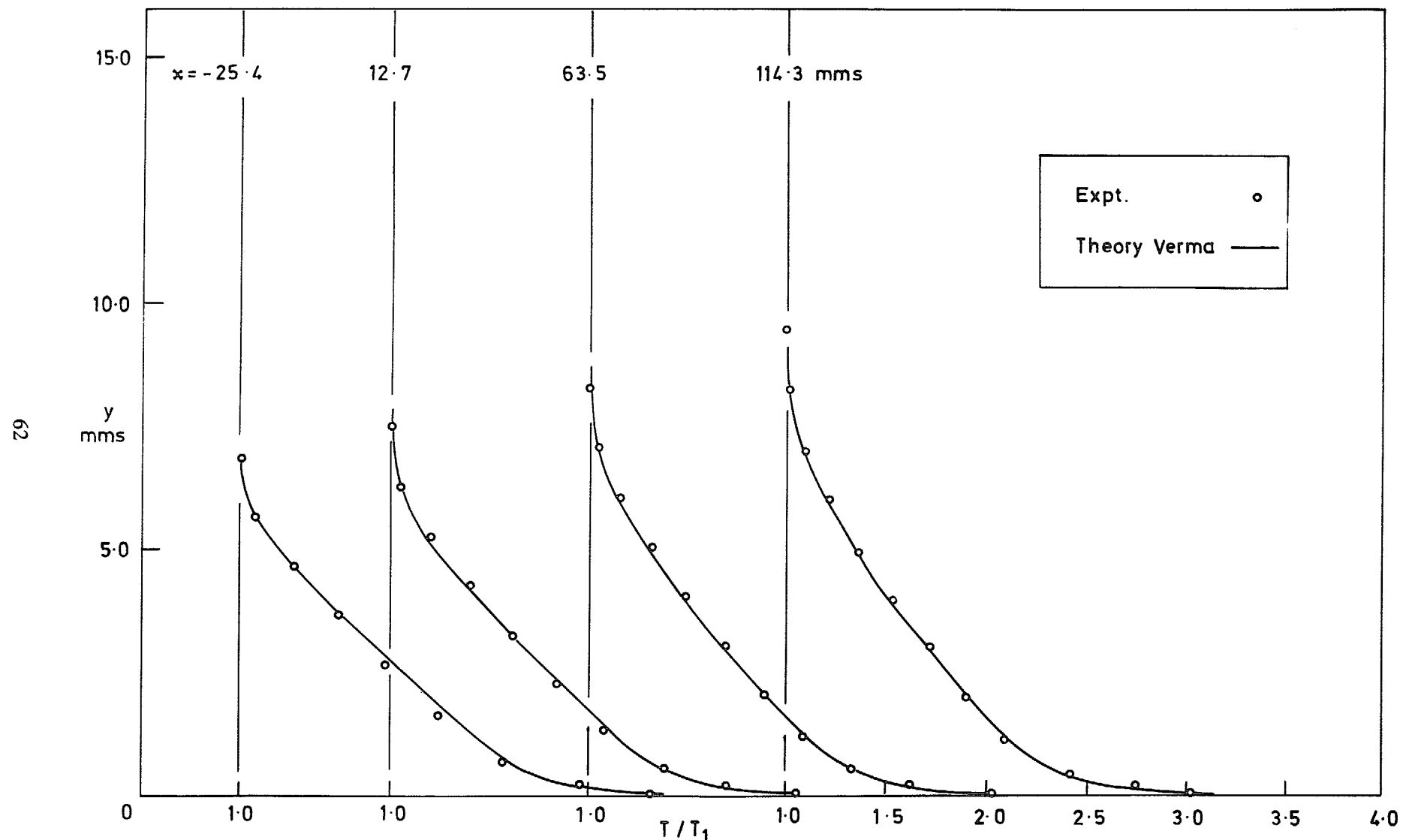


FIG. 15. Temperature profiles ($M = 3.6$; $F = 0$).

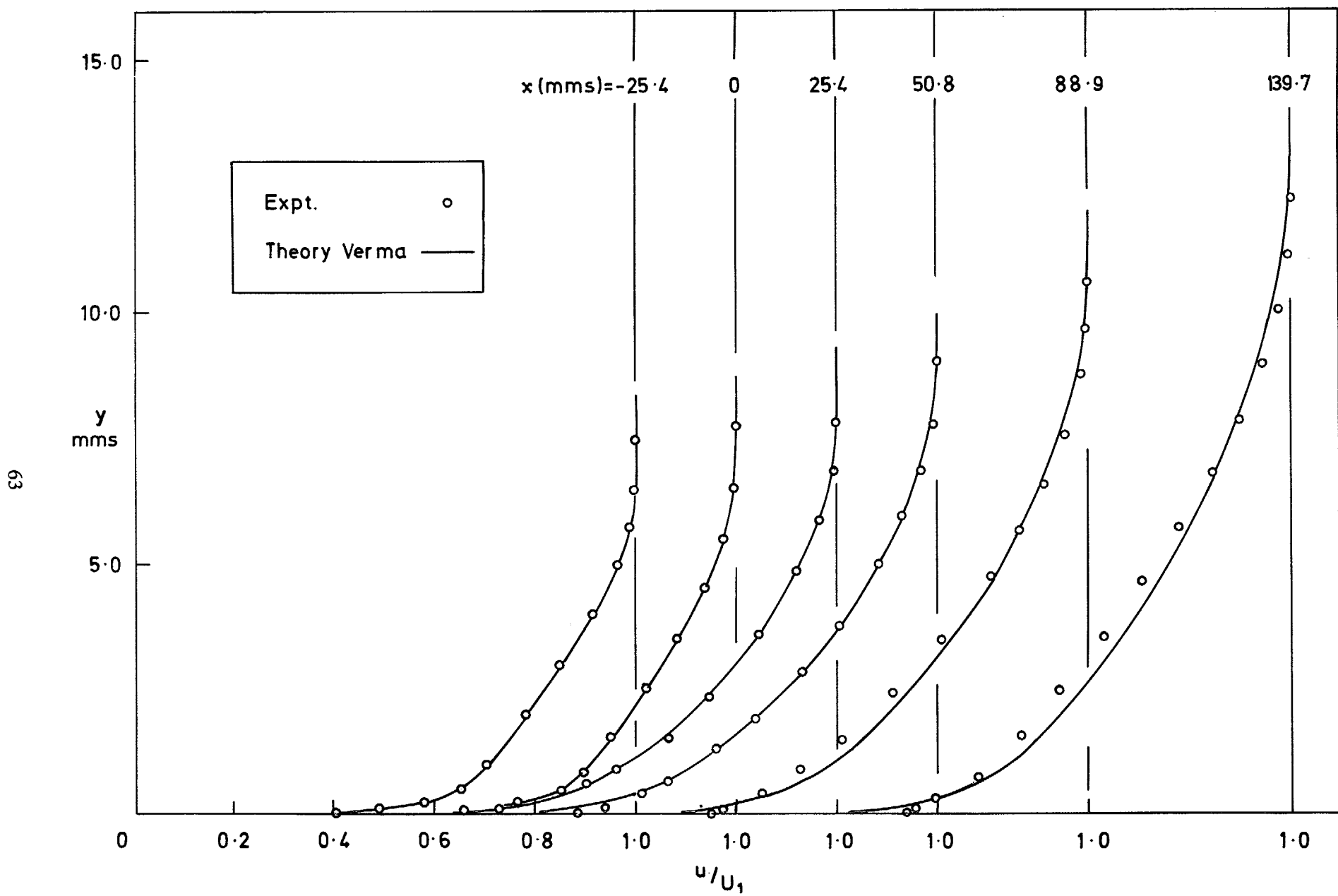


FIG. 16. Velocity profiles ($M = 3.6; F = 0.00294$).

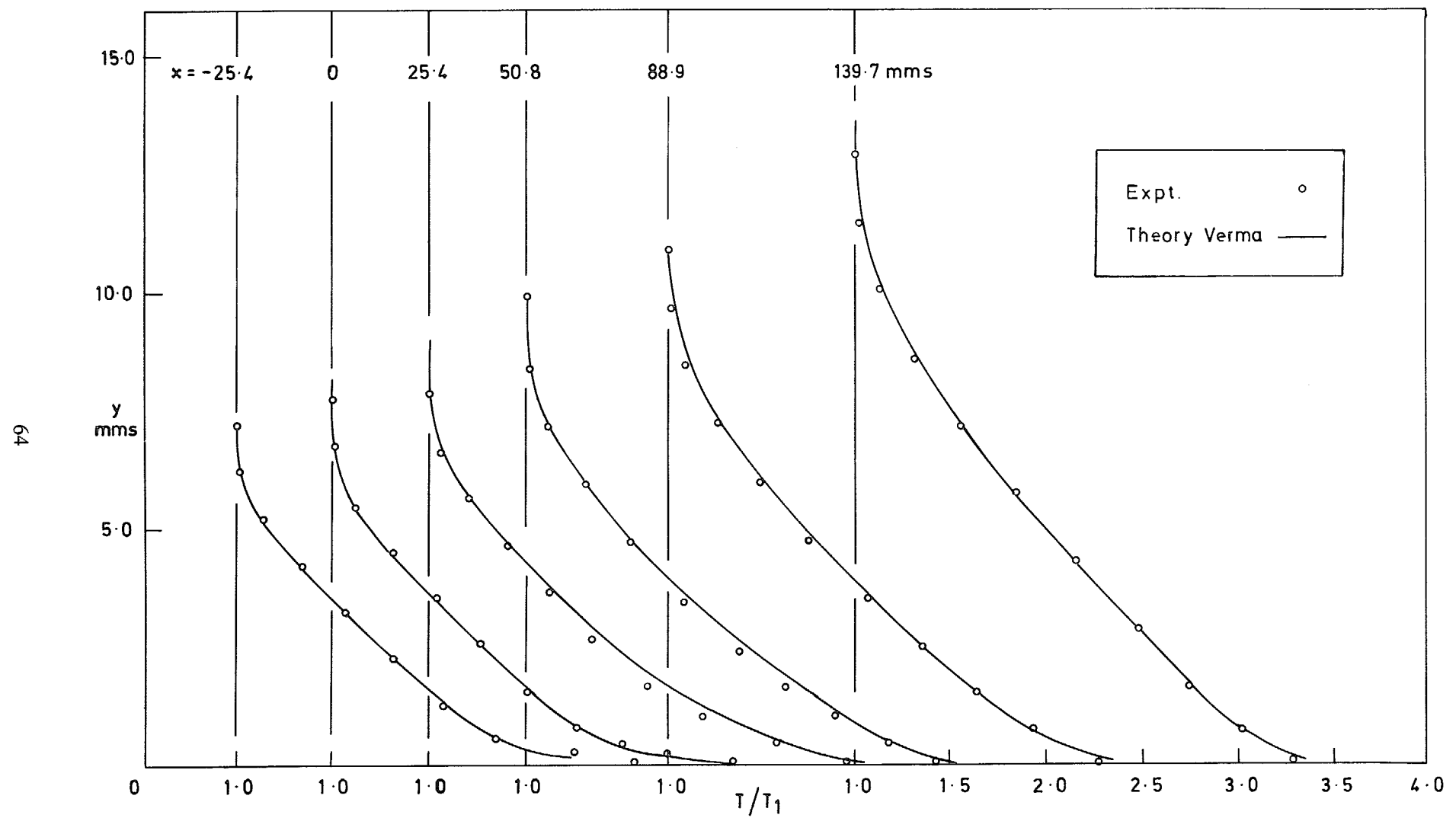


FIG. 17. Temperature profiles ($M = 3.6; F = 0.00294$).

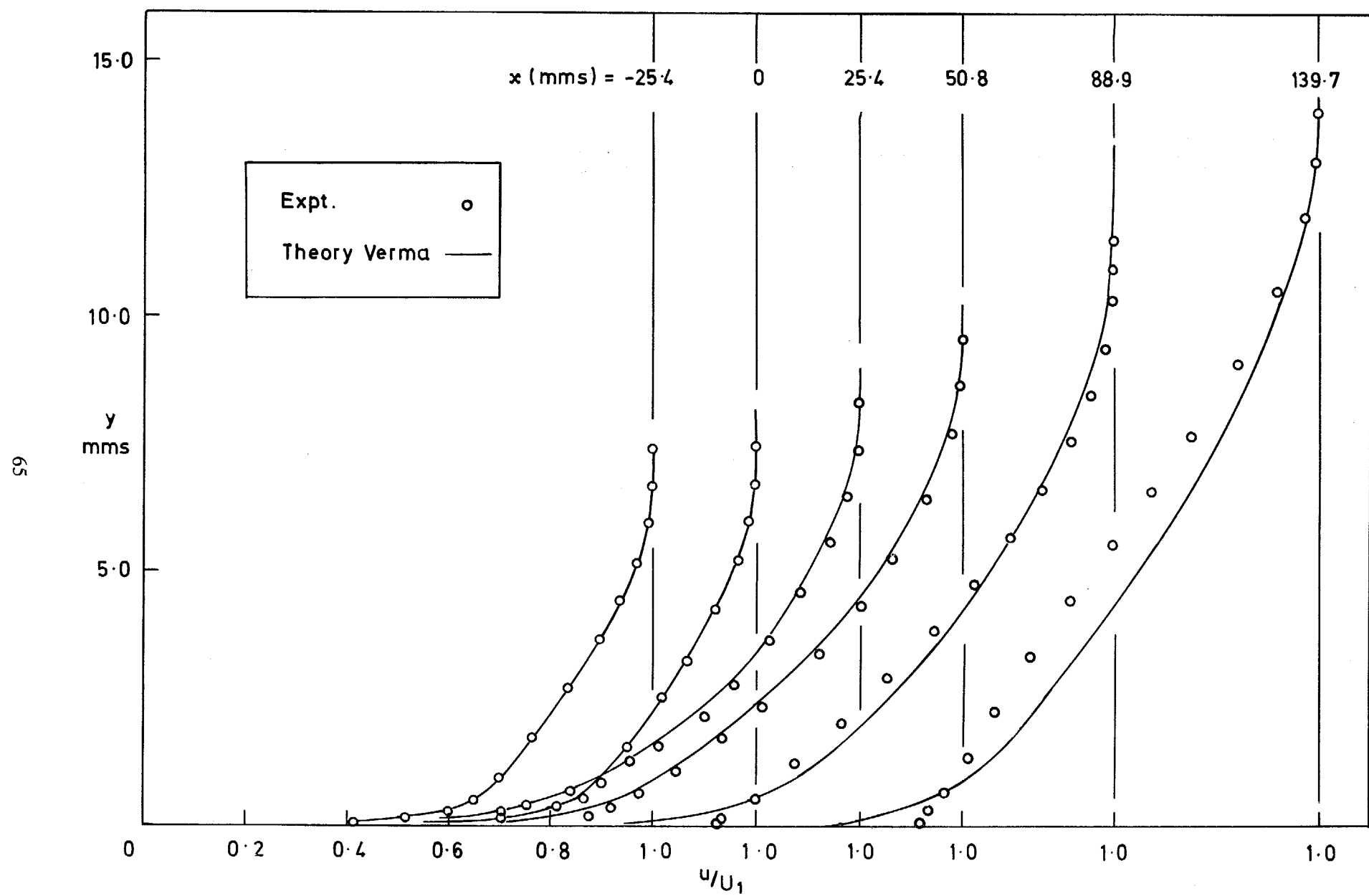


FIG. 18. Velocity profiles ($M = 3.6$; $F = 0.00421$).

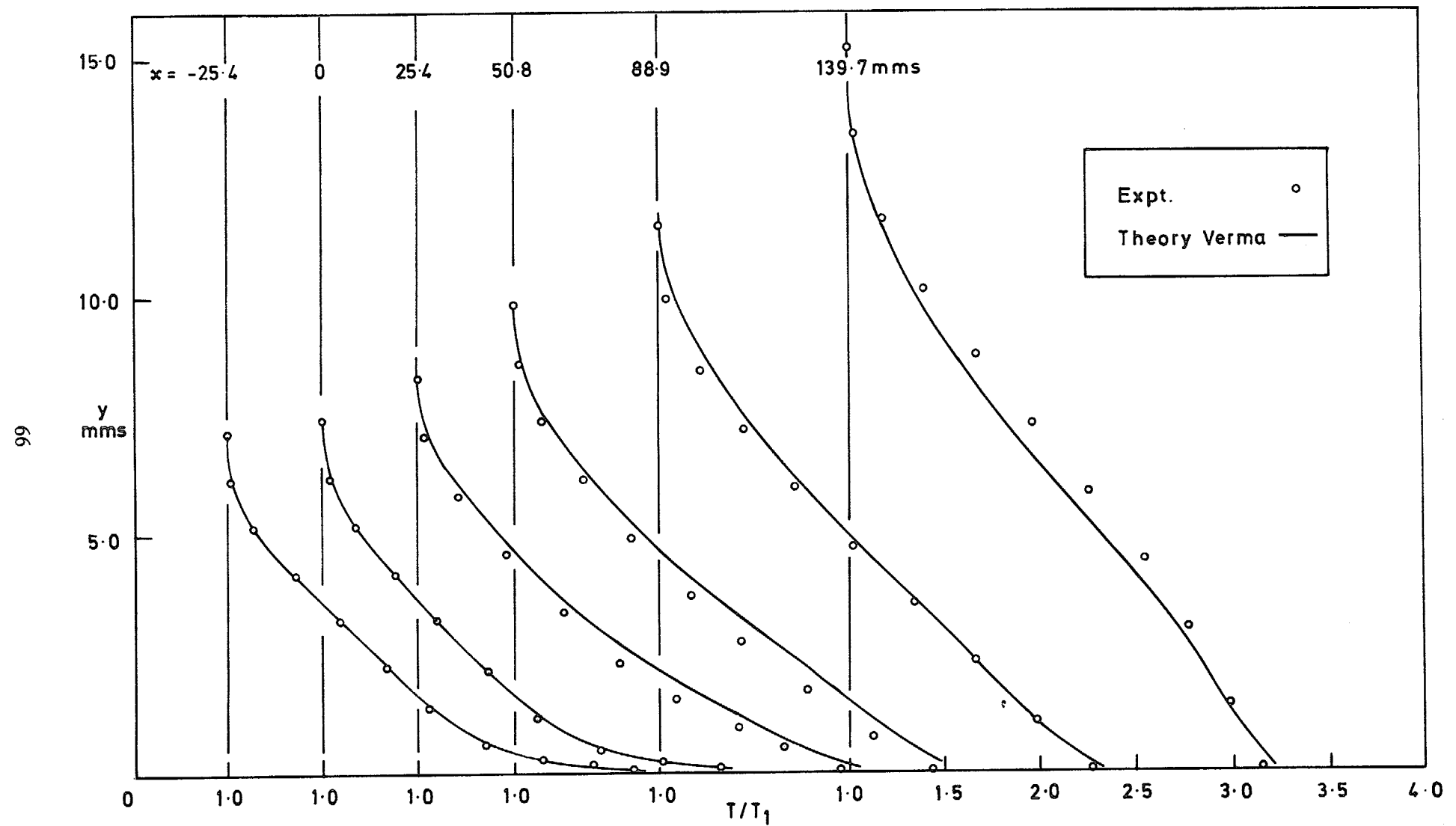


FIG. 19. Temperature profiles ($M = 3.6$; $F = 0.00421$).

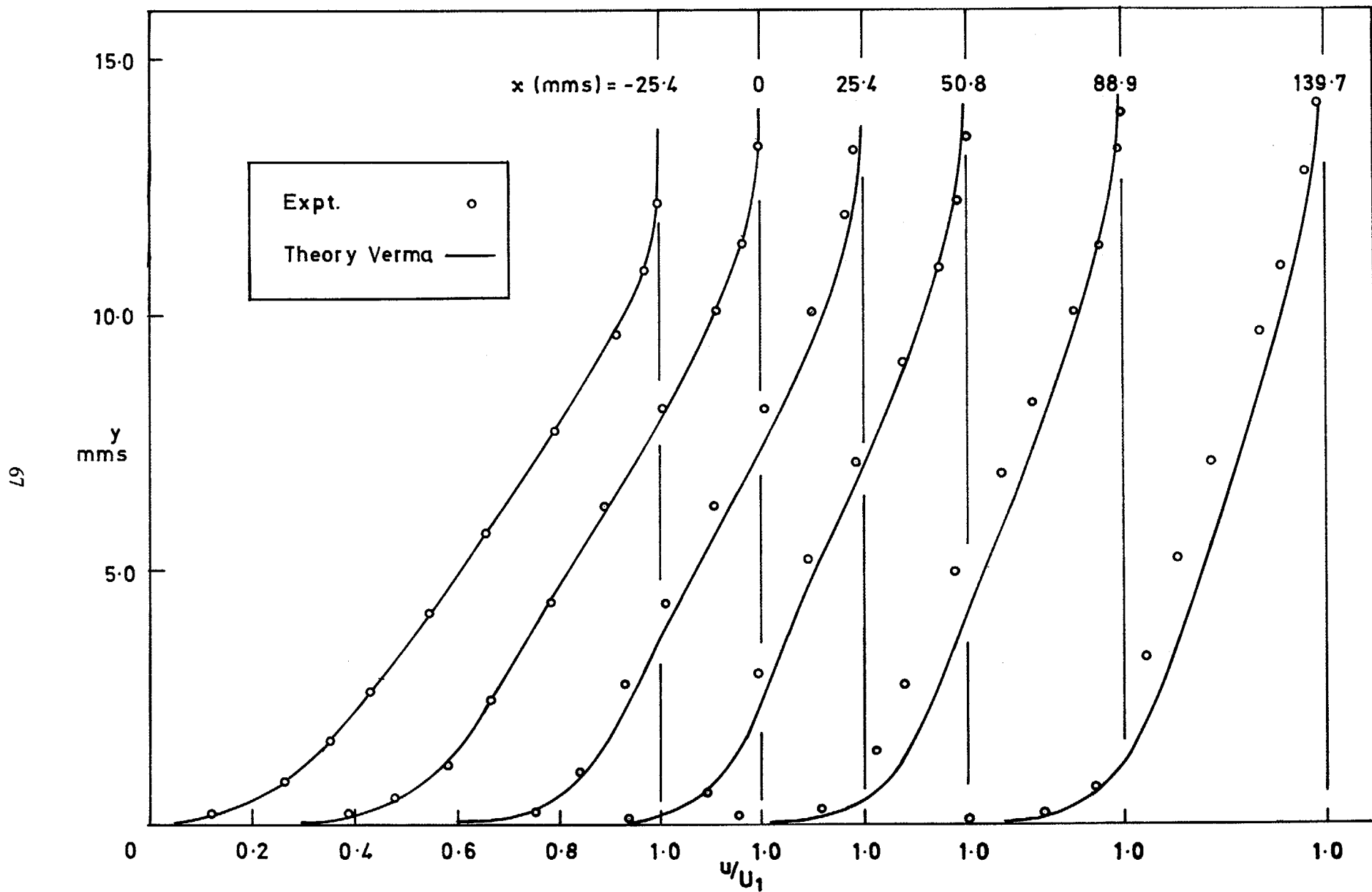


FIG. 20. Velocity profiles ($M = 3.6$; $F = 0.00294$ porous-solid).

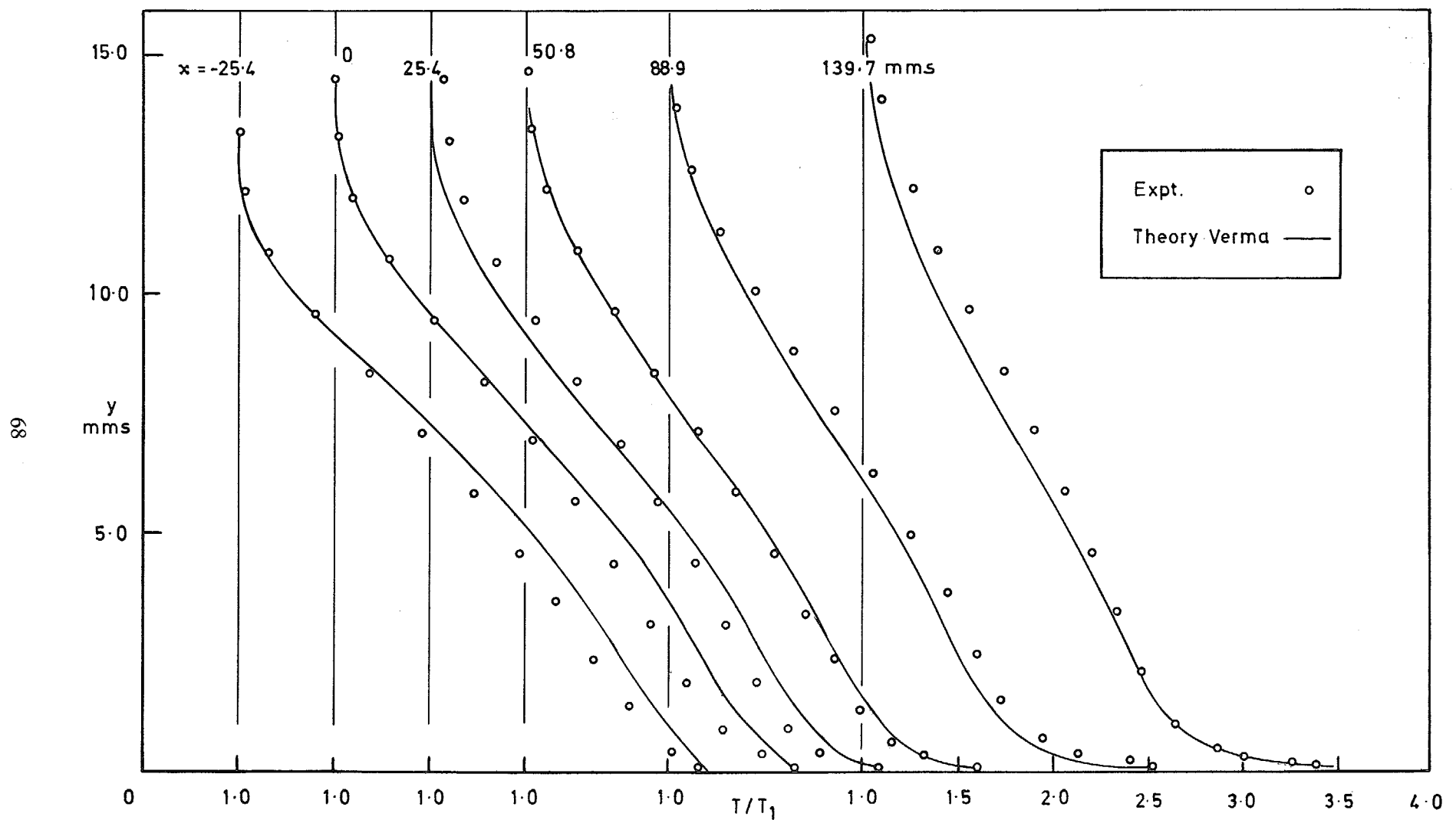
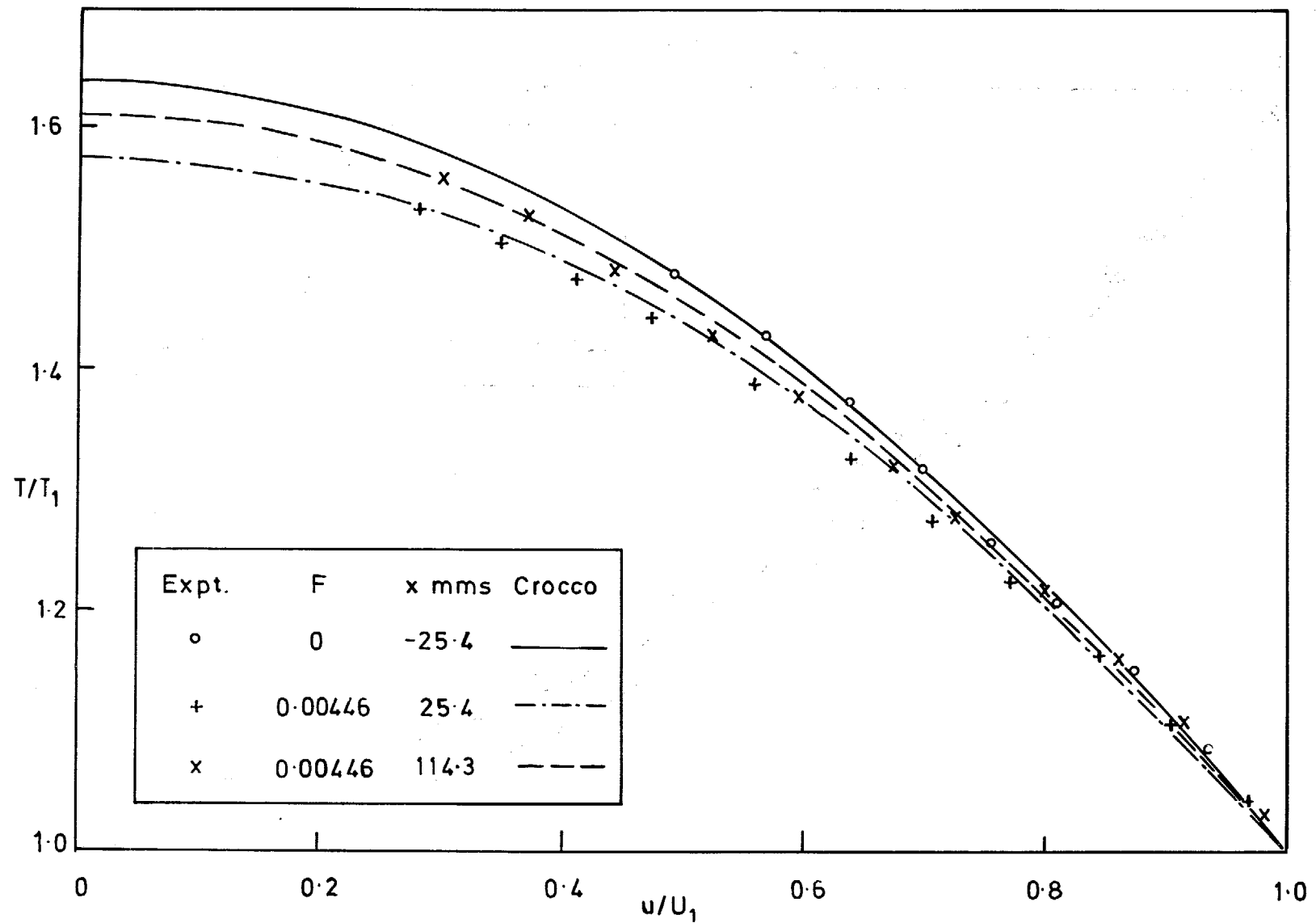


FIG. 21. Temperature profiles ($M = 3.6$; $F = 0.00294$ porous-solid).

FIG. 22. T/T_1 vs u/U_1 ($M = 1.8$).

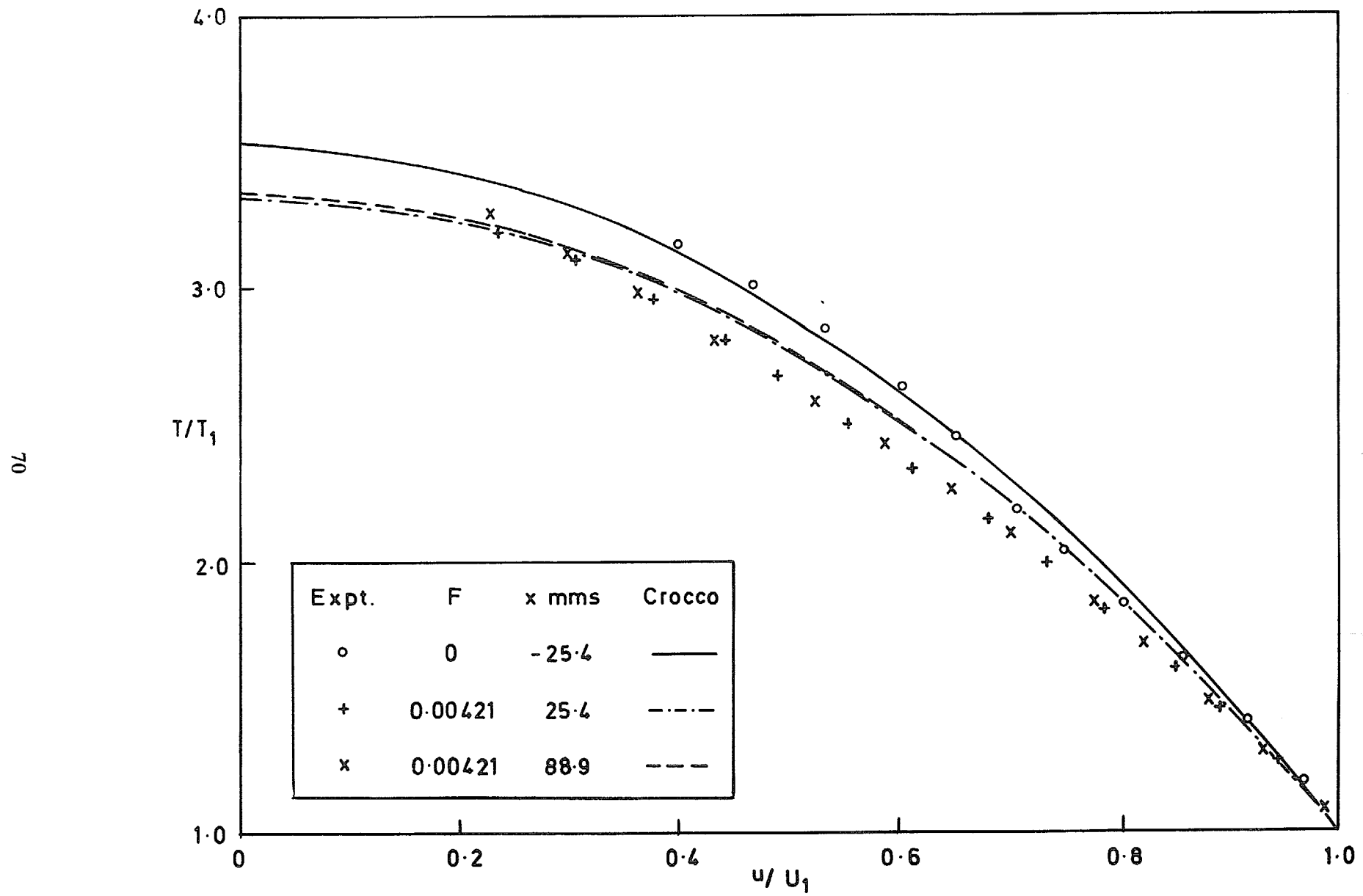


FIG. 23. T/T_1 vs u/u_1 ($M = 3.6$).

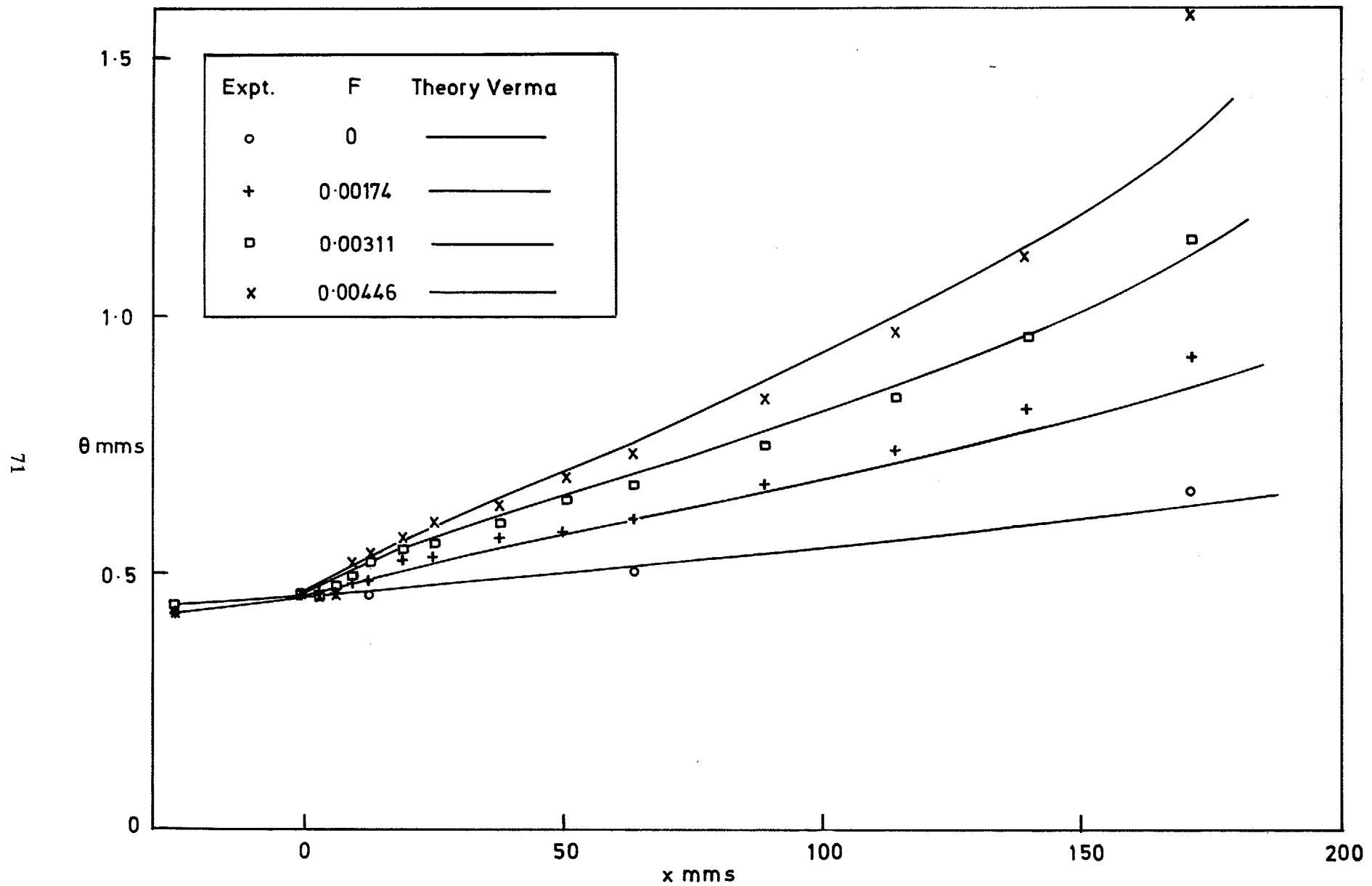


FIG. 24. Momentum thickness development ($M = 1.8$).

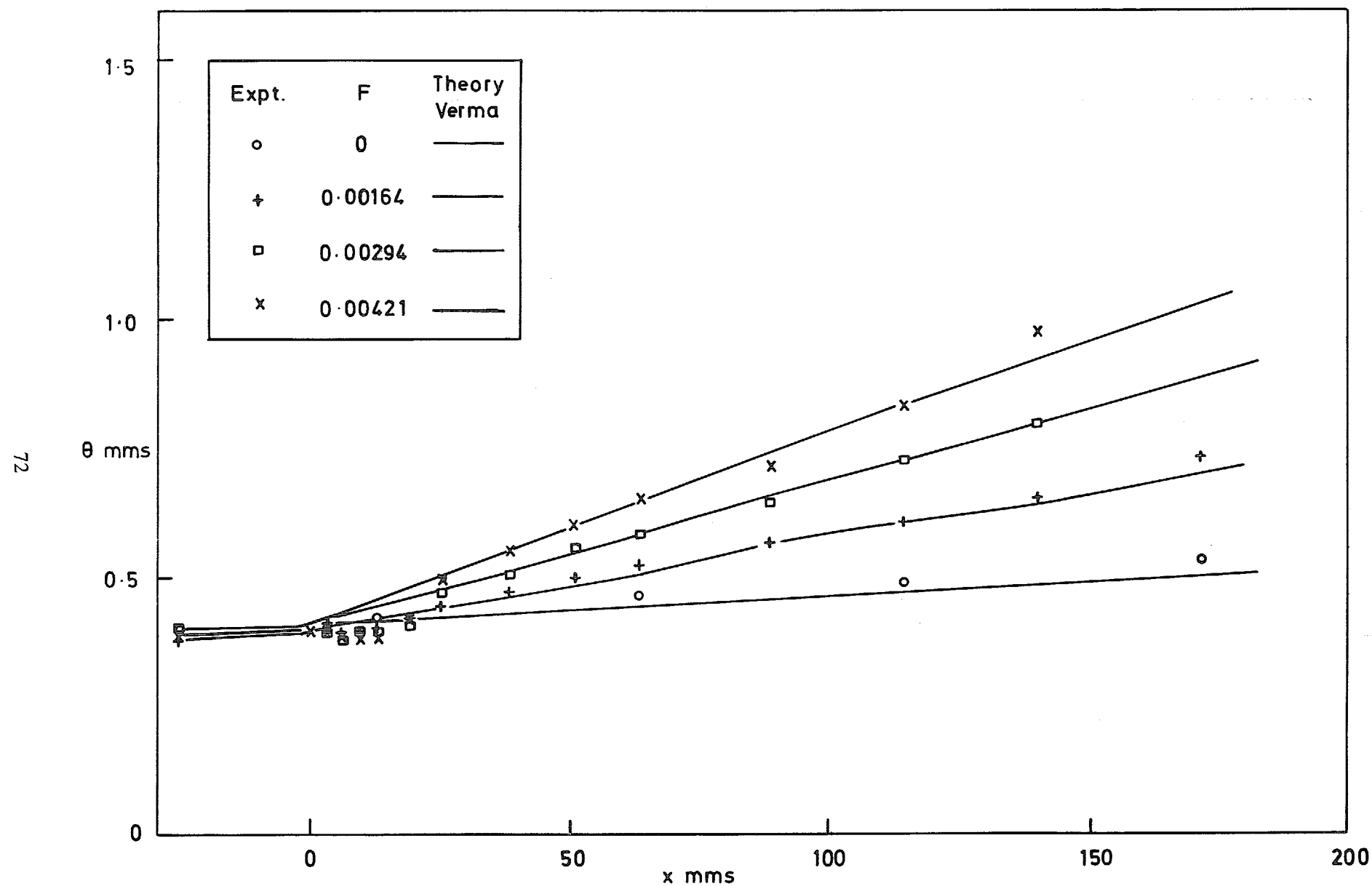


FIG. 25. Momentum thickness development ($M = 3.6$).

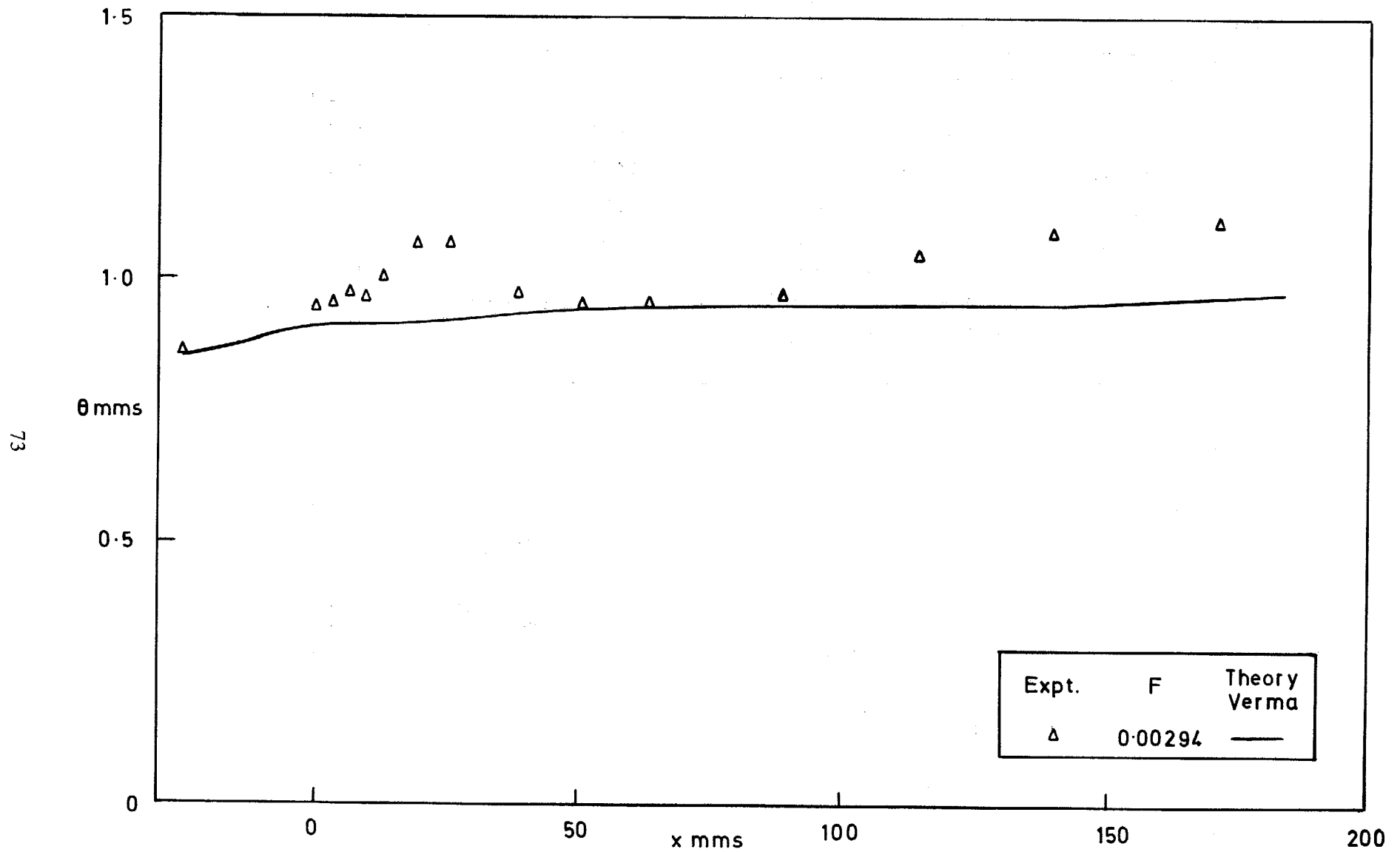
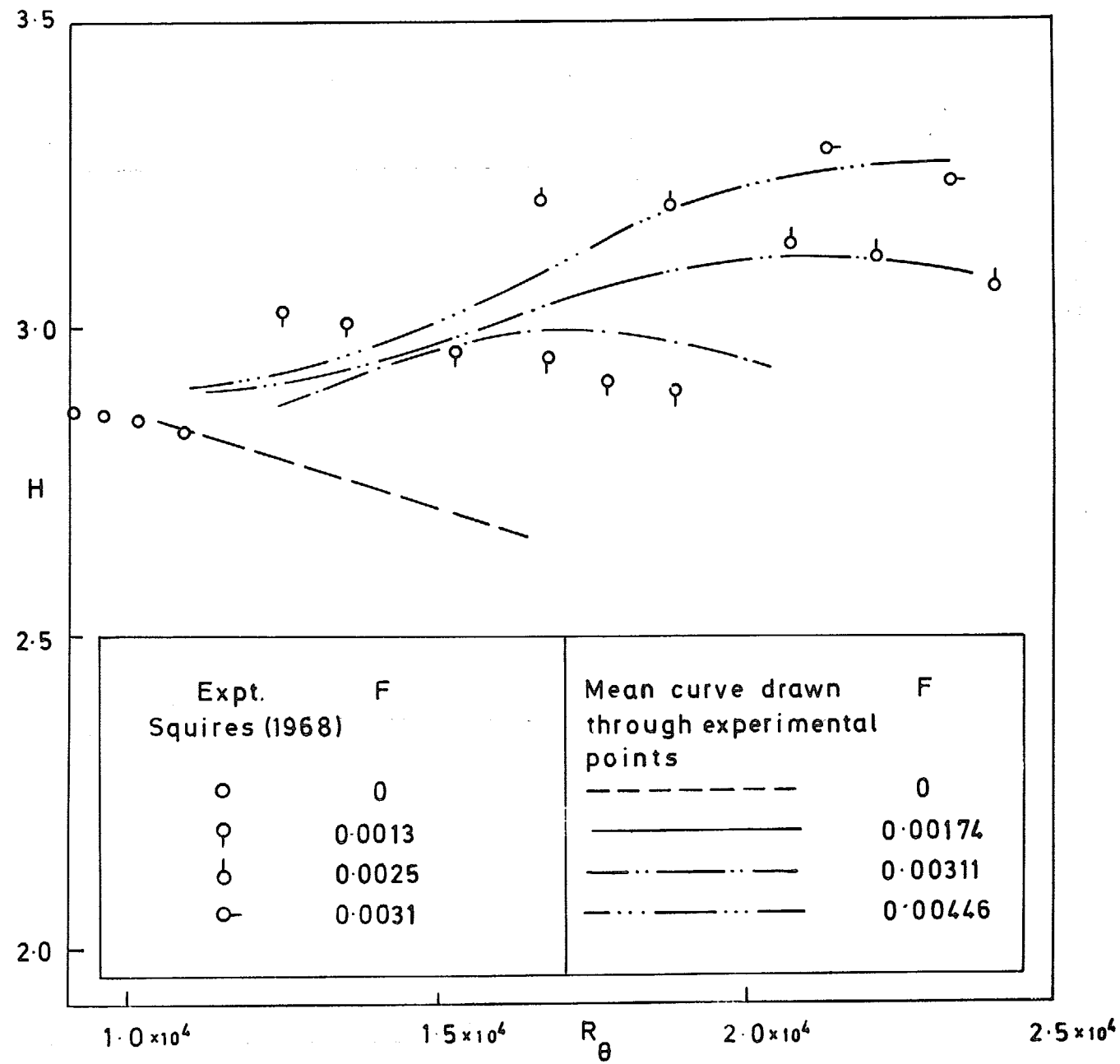


FIG. 26. Momentum thickness development ($M = 3.6$ porous-solid).

FIG. 27. H vs R_θ ($M = 1.8$).

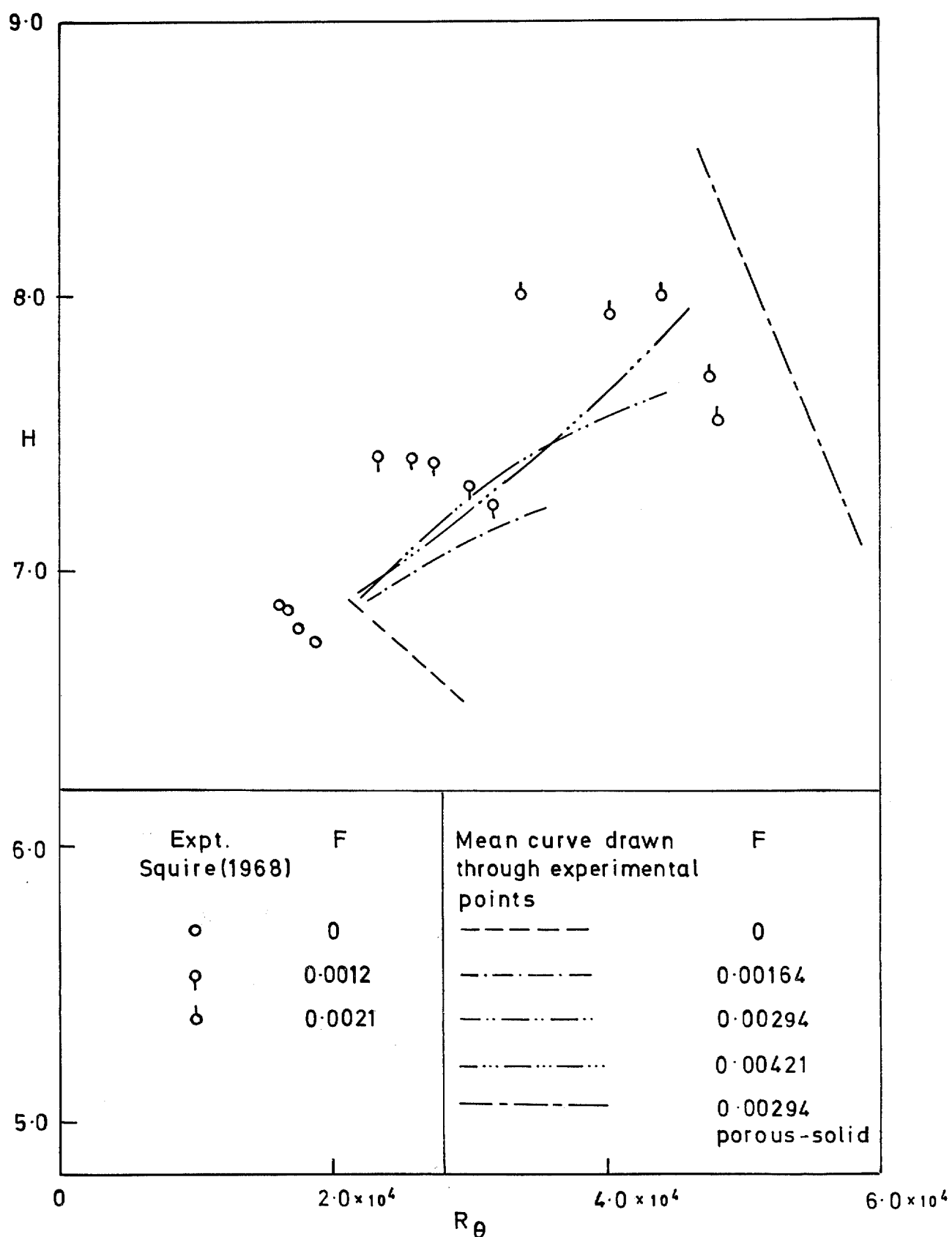


FIG. 28. H vs R_θ ($M = 3.6$).

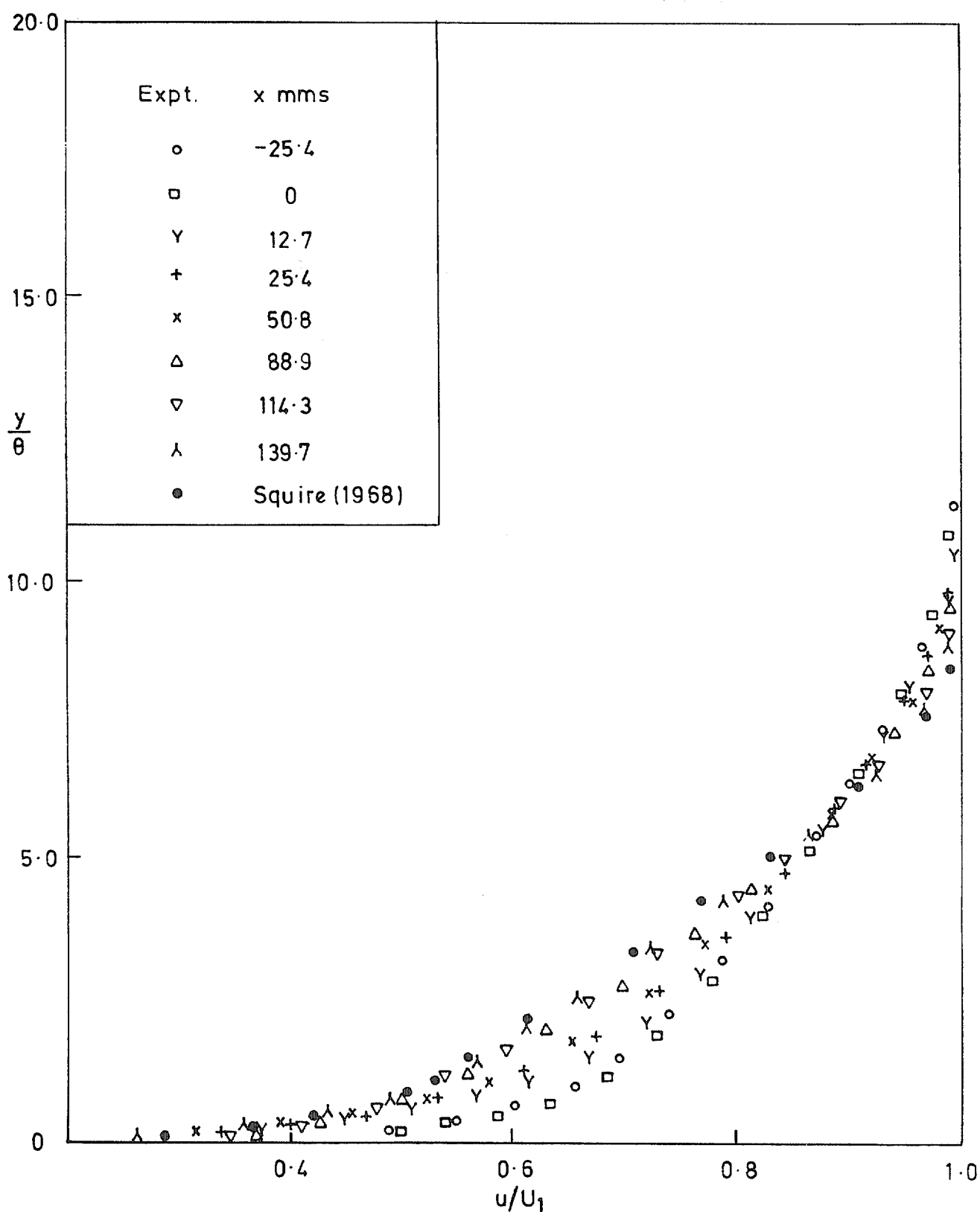


FIG. 29. y/θ vs u/U_1 ($M = 1.8$; $F = 0.00311$).

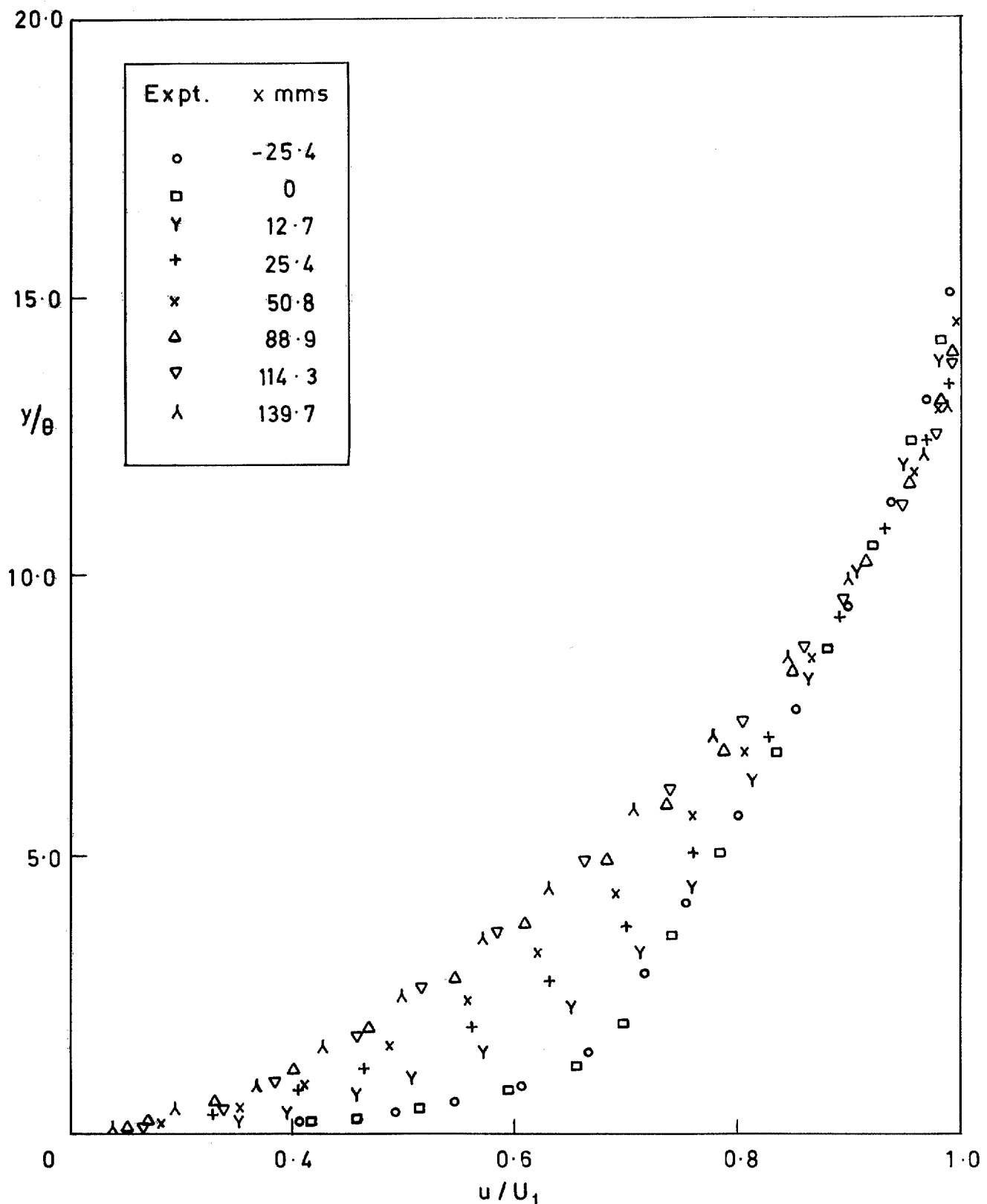


FIG. 30. y/θ vs u/U_1 ($M = 3.6$; $F = 0.00294$).

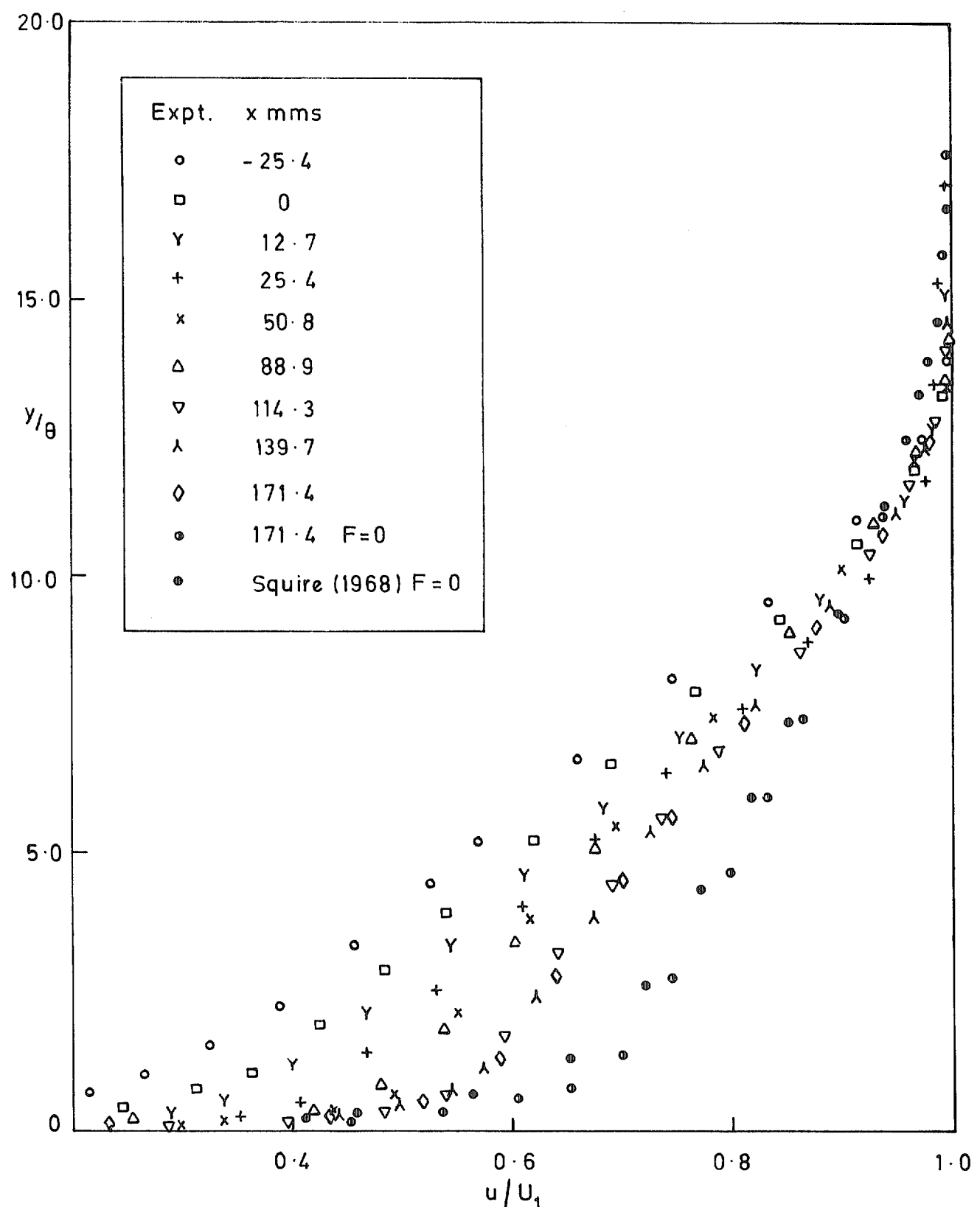


FIG. 31. y/θ vs u/U_1 ($M = 3.6$; $F = 0.00294$ porous-solid).

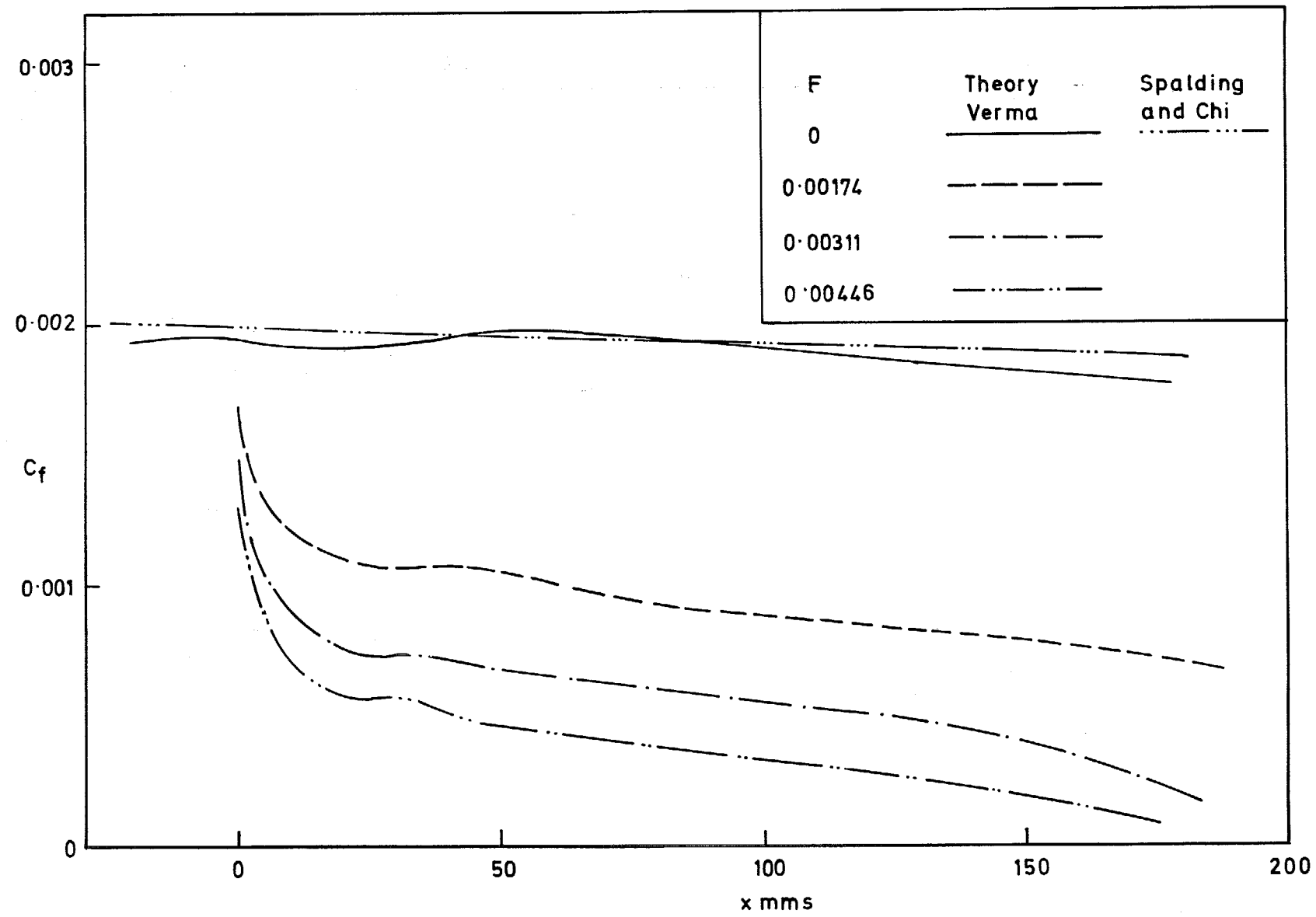


FIG. 32. Theoretical skin friction development ($M = 1.8$).

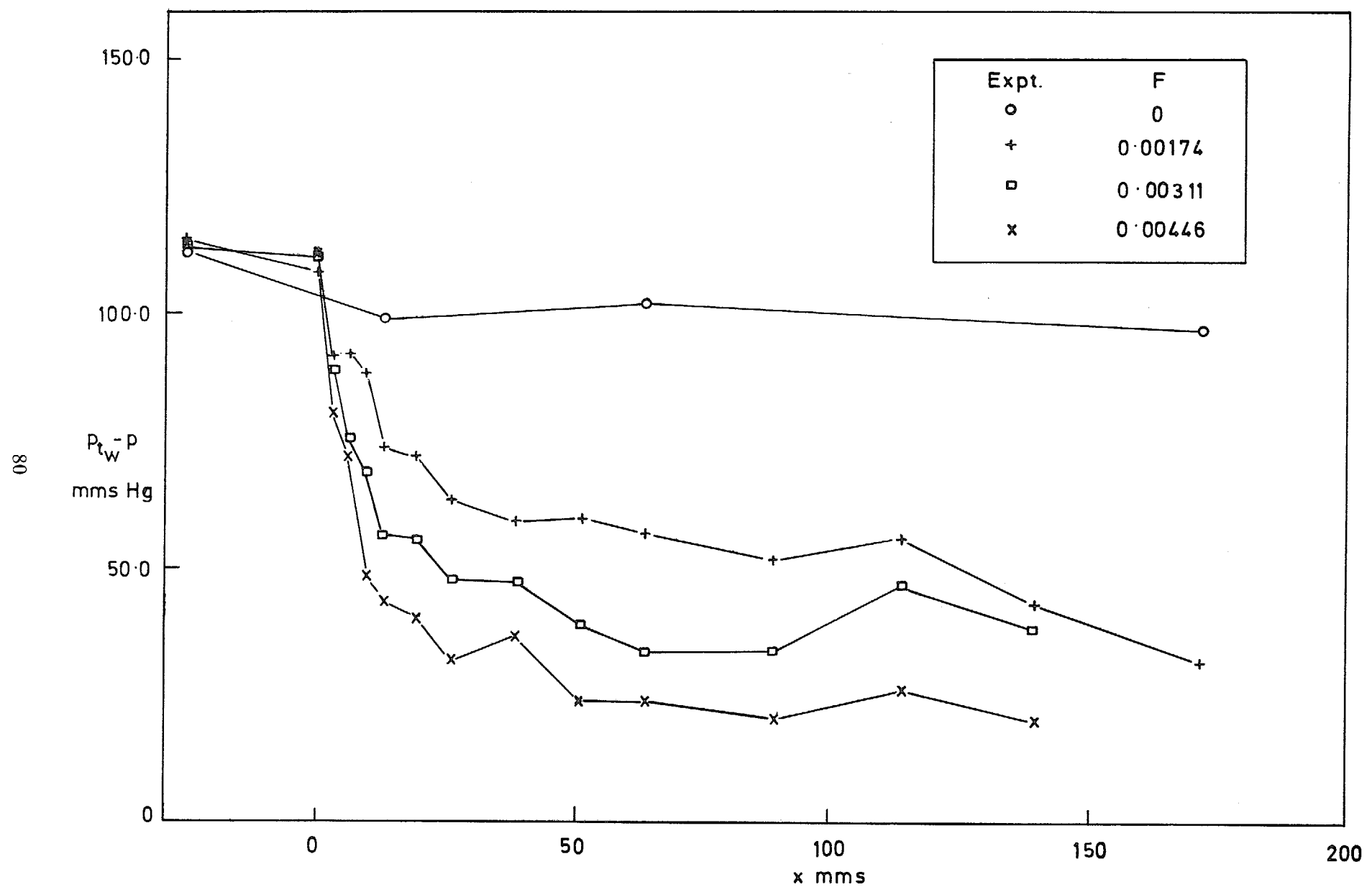


FIG. 33. Variation of dynamic pressure at the wall ($M = 1.8$).

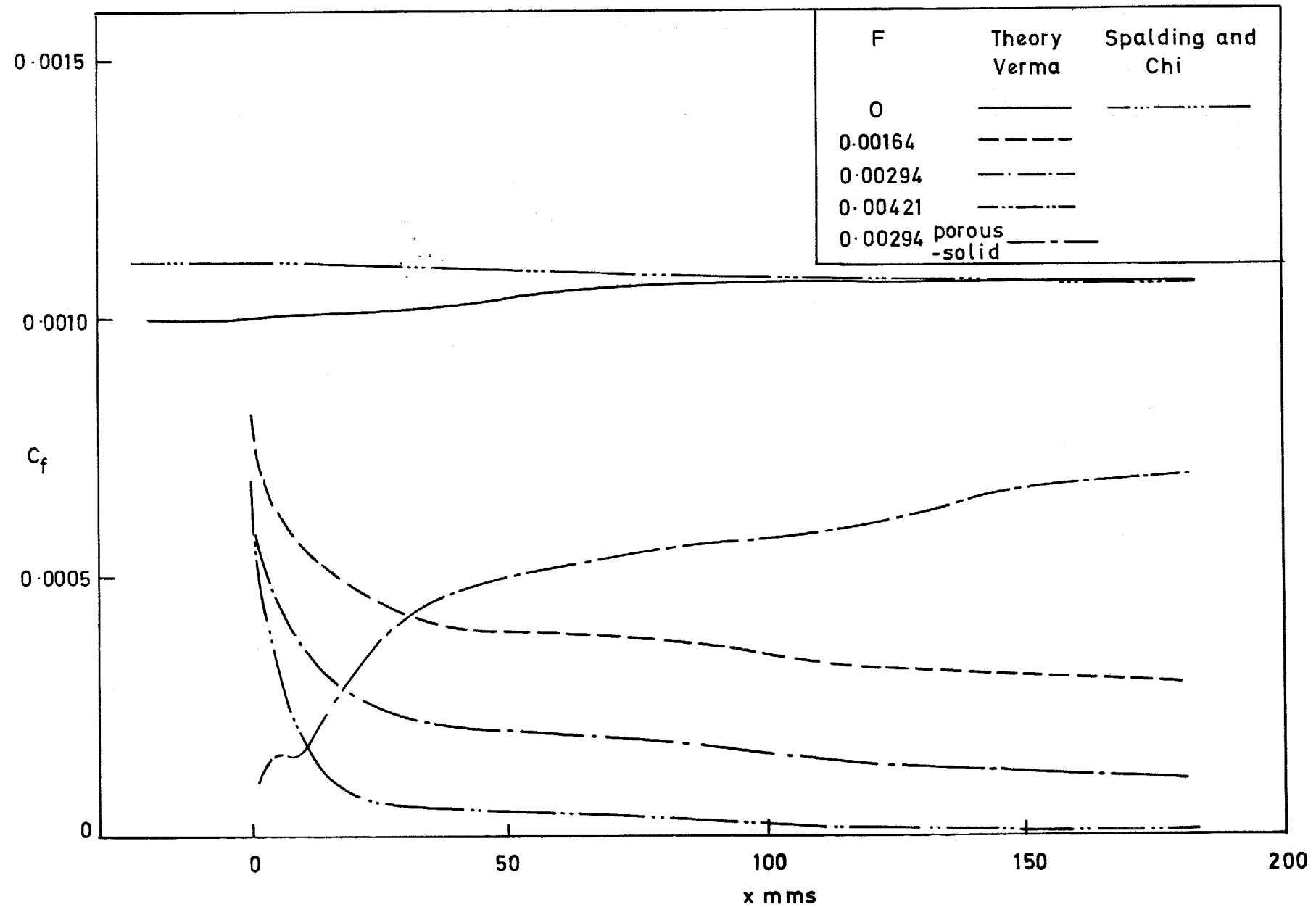


FIG. 34. Theoretical skin friction development ($M = 3.6$).

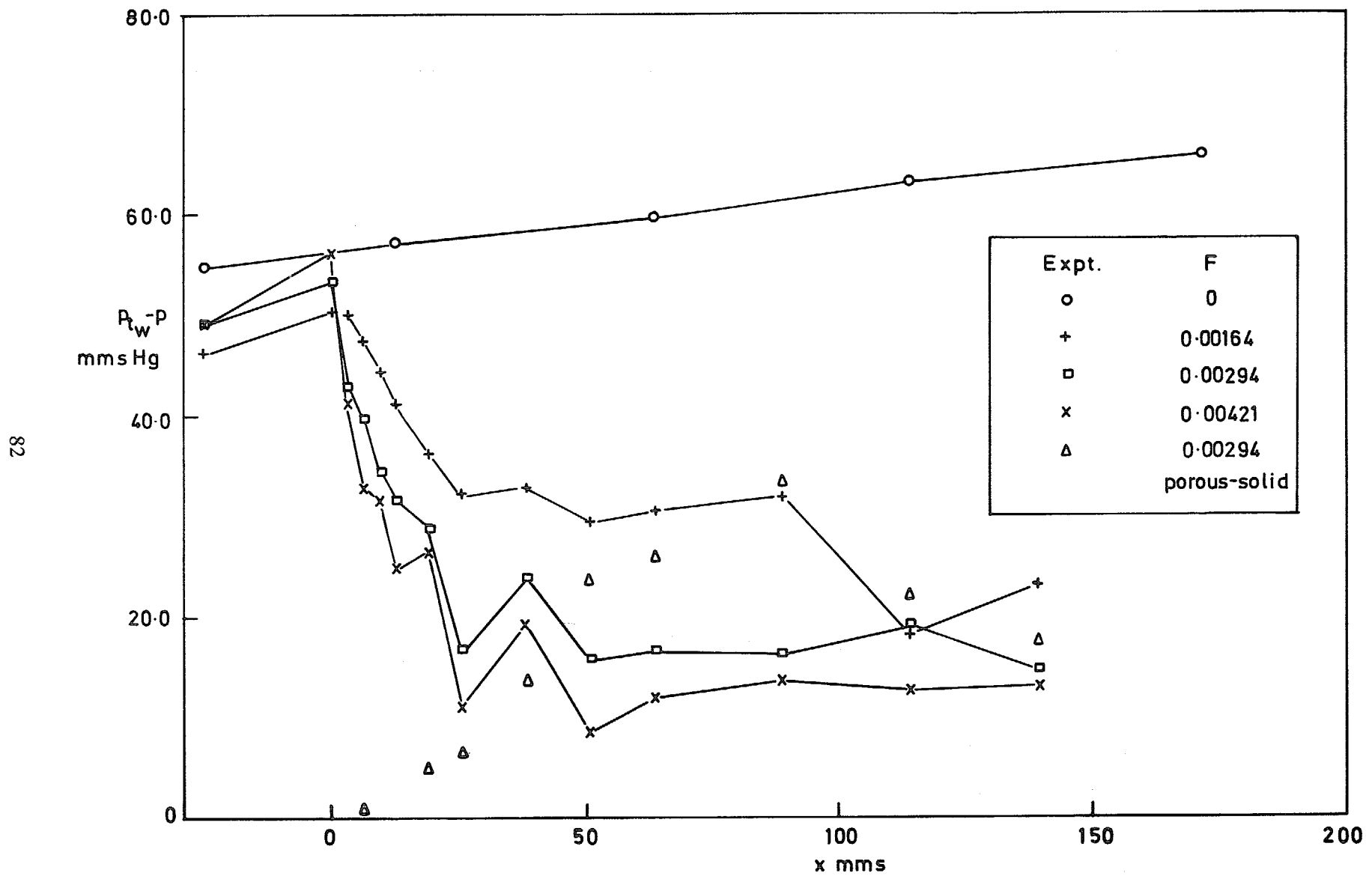


FIG. 35. Variation of dynamic pressure at the wall ($M = 3.6$).

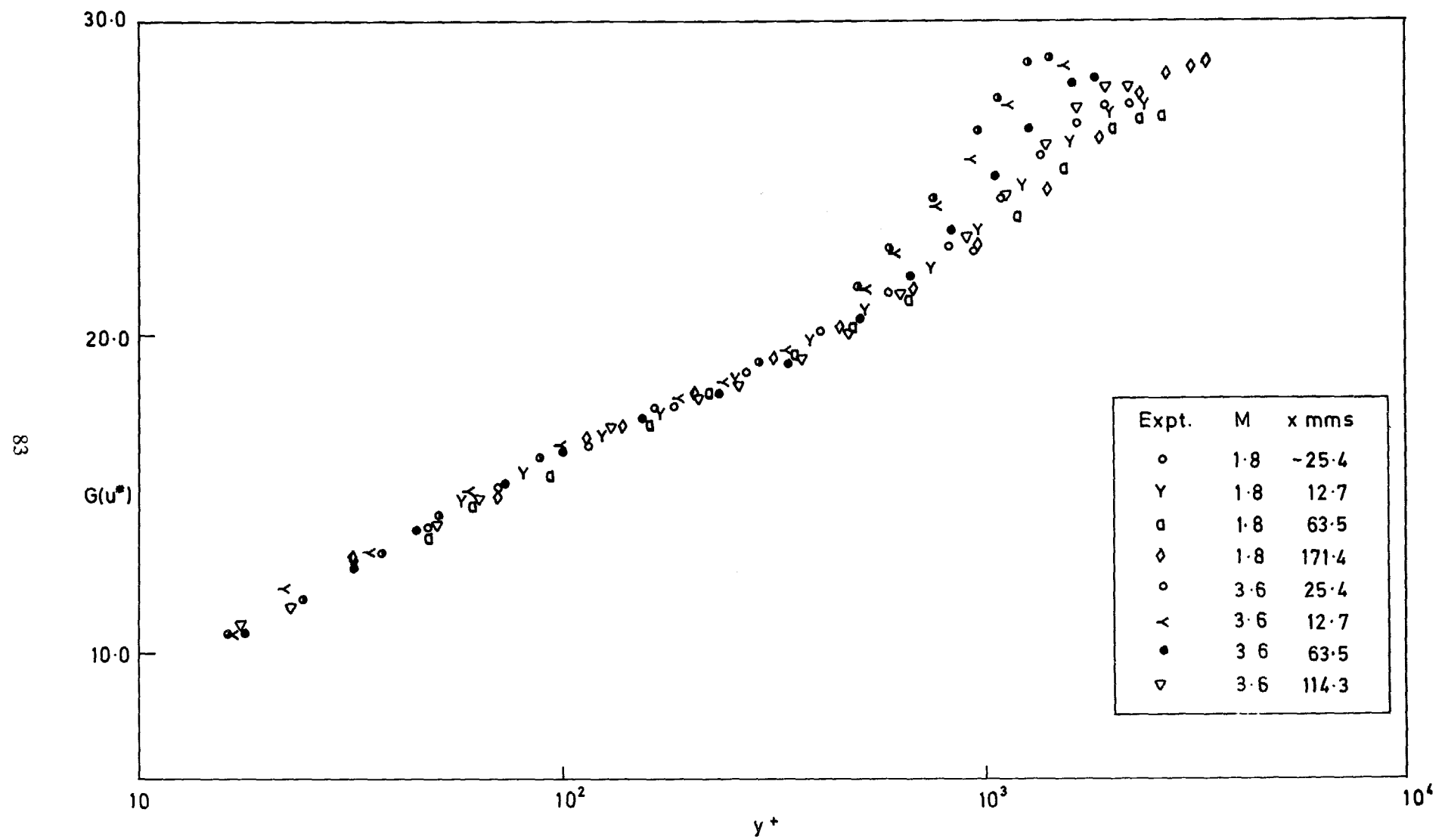


FIG. 36. $G(u^*)$ vs $\log(yU_r/\nu_w)$ ($M = 1.8; 3.6; F = 0$).

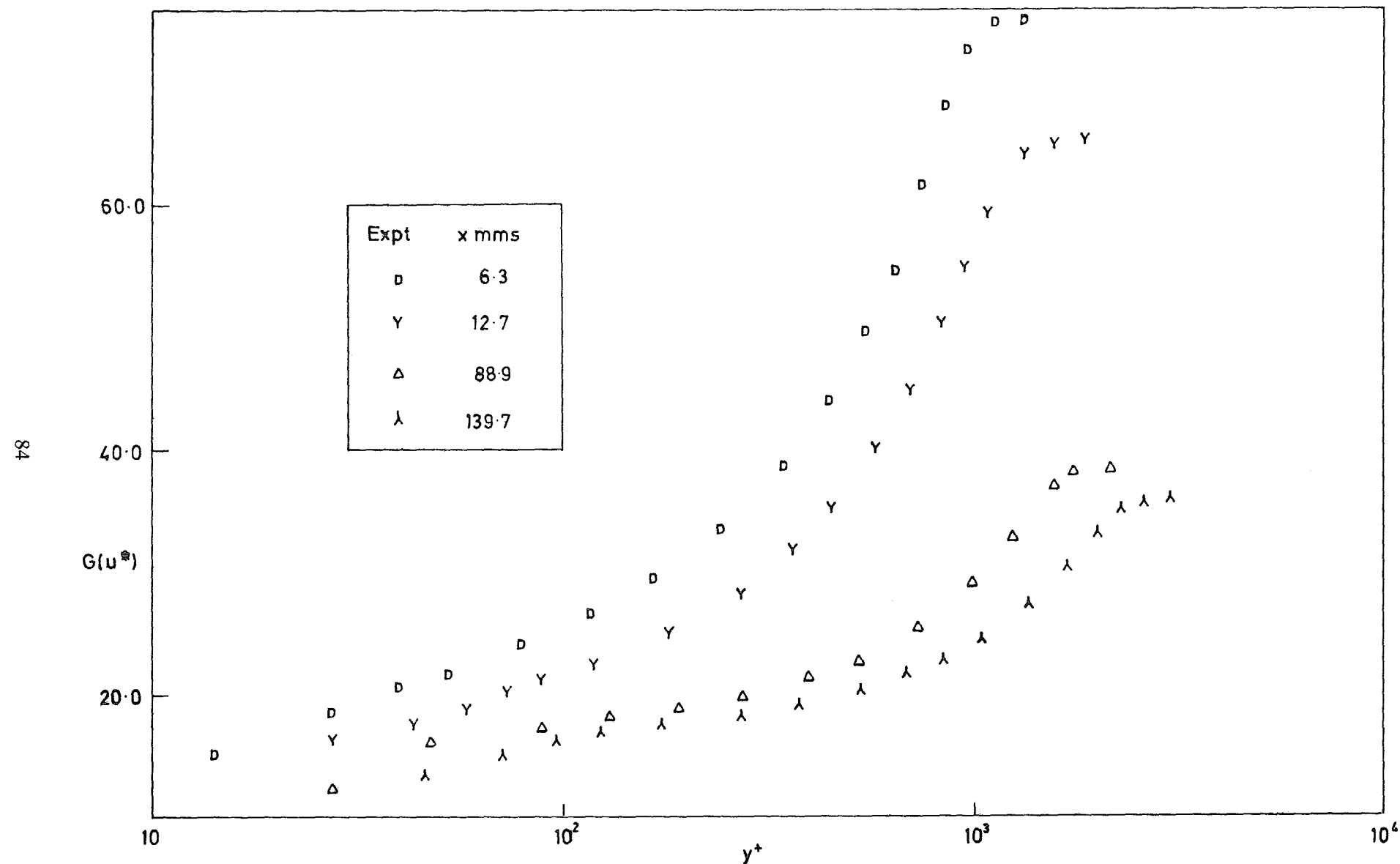


FIG. 37. $G(u^*)$ vs $\log(yU_\tau/\nu_w)$ ($M = 3.6; F = 0.00294$ porous-solid).

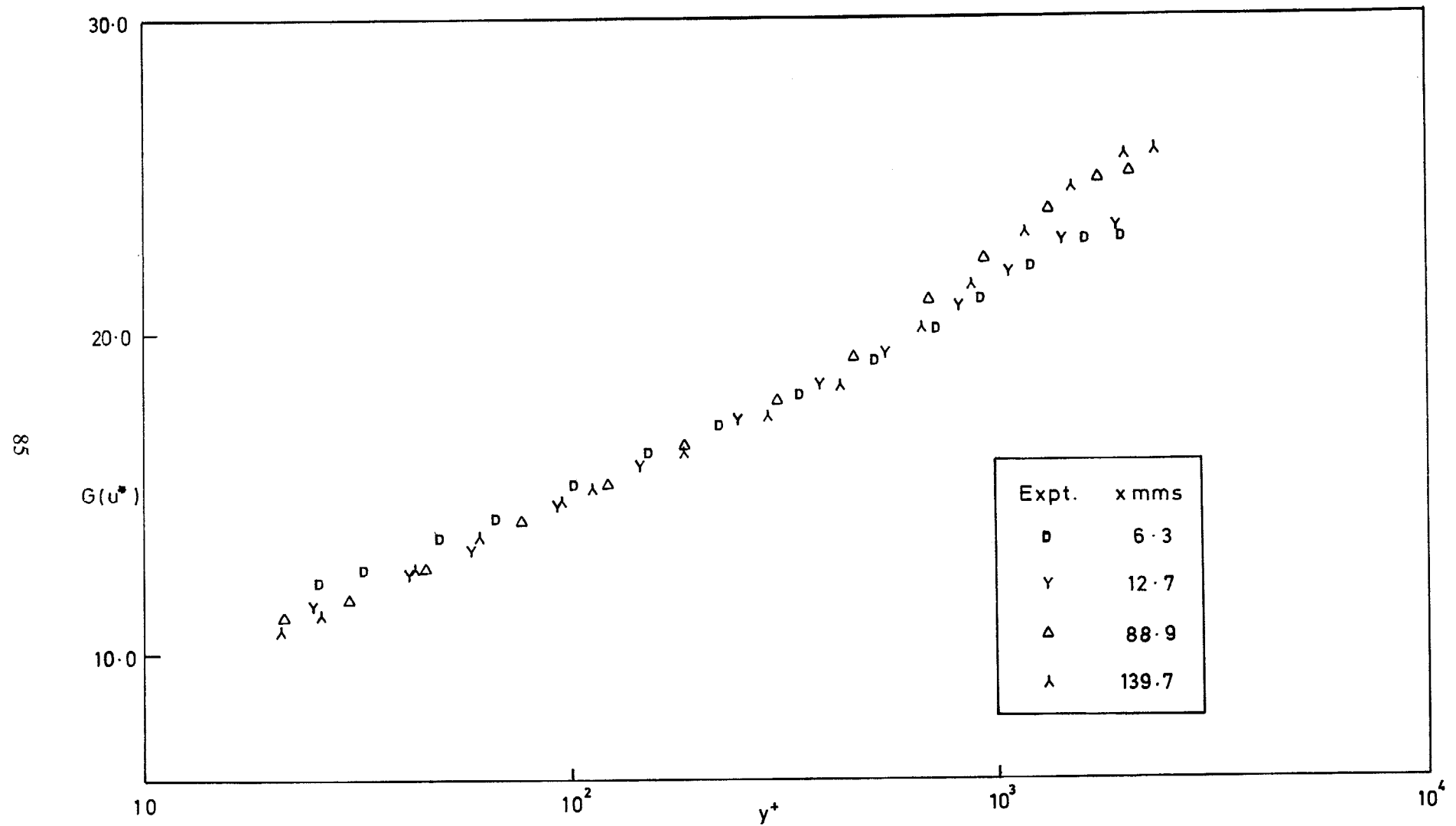


FIG. 38. $G(u^*)$ vs $(\log(yU_r/\nu_w))$ ($M = 1.8; F = 0.00174$).

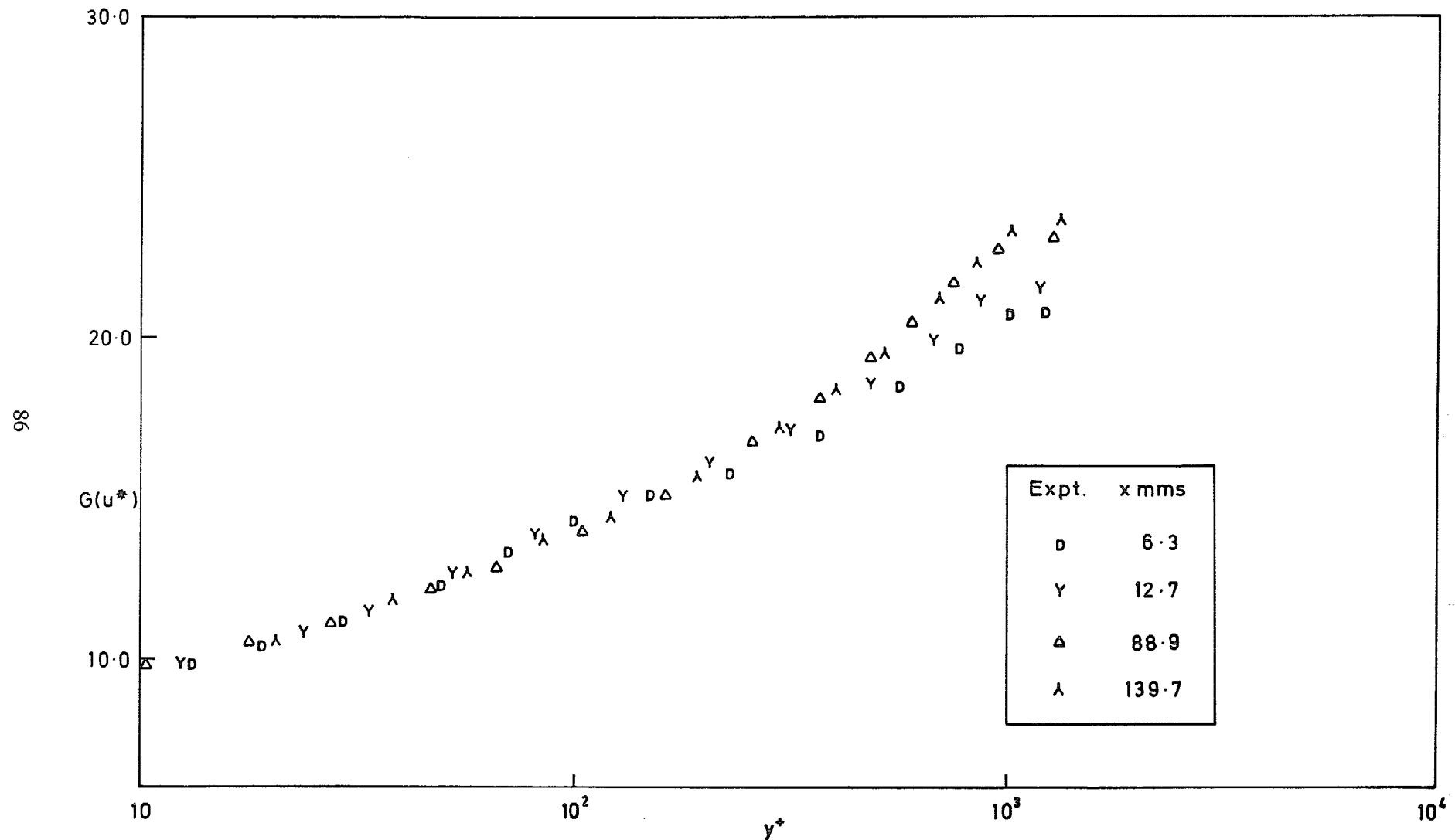


FIG. 39. $G(u^*)$ vs $\log(yU_r/\nu_w)$ ($M = 3.6$; $F = 0.00164$).

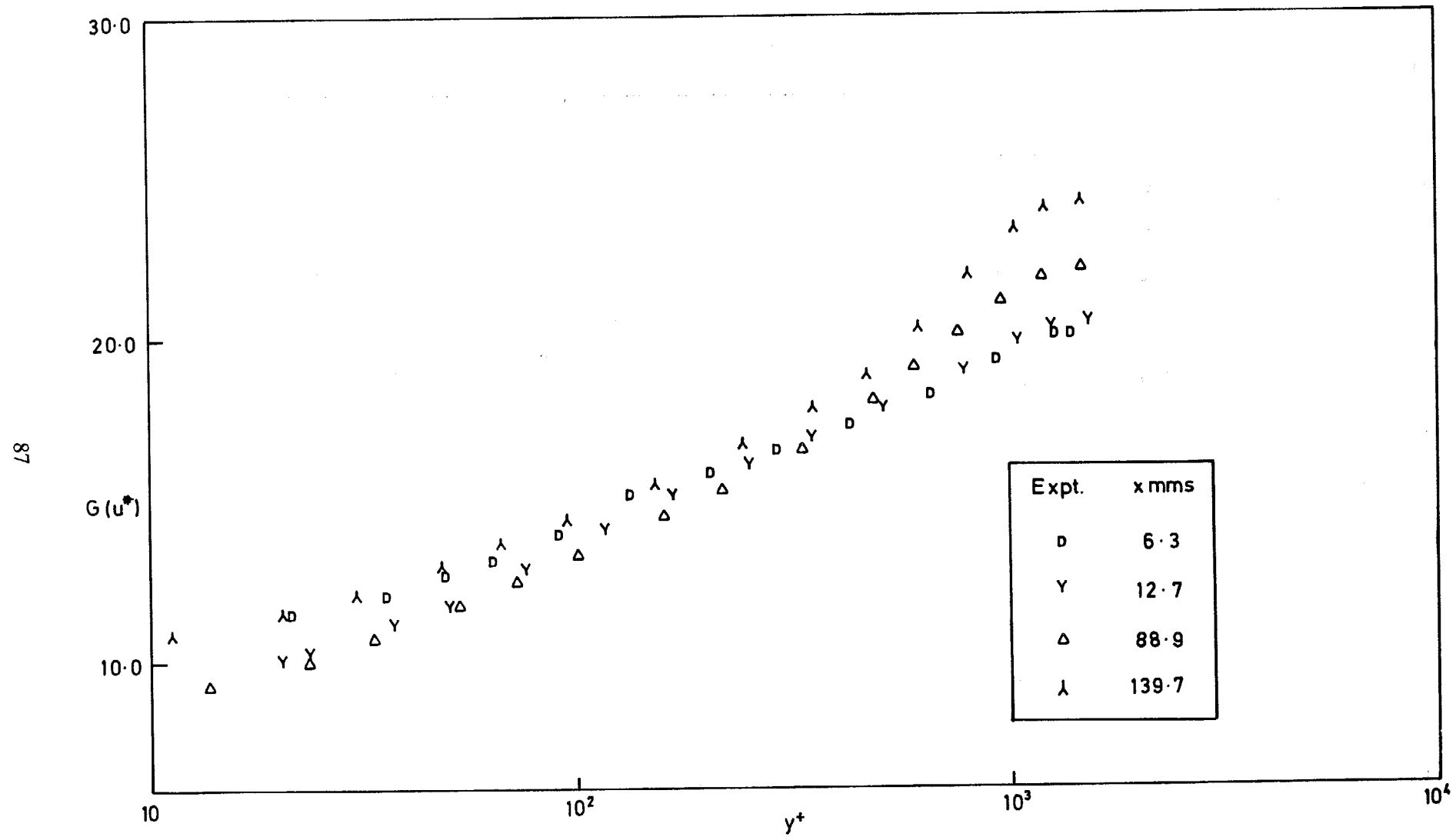


FIG. 40. $G(u^*)$ vs $\log(yU_r/\nu_w)$ ($M = 1.8; F = 0.00446$).

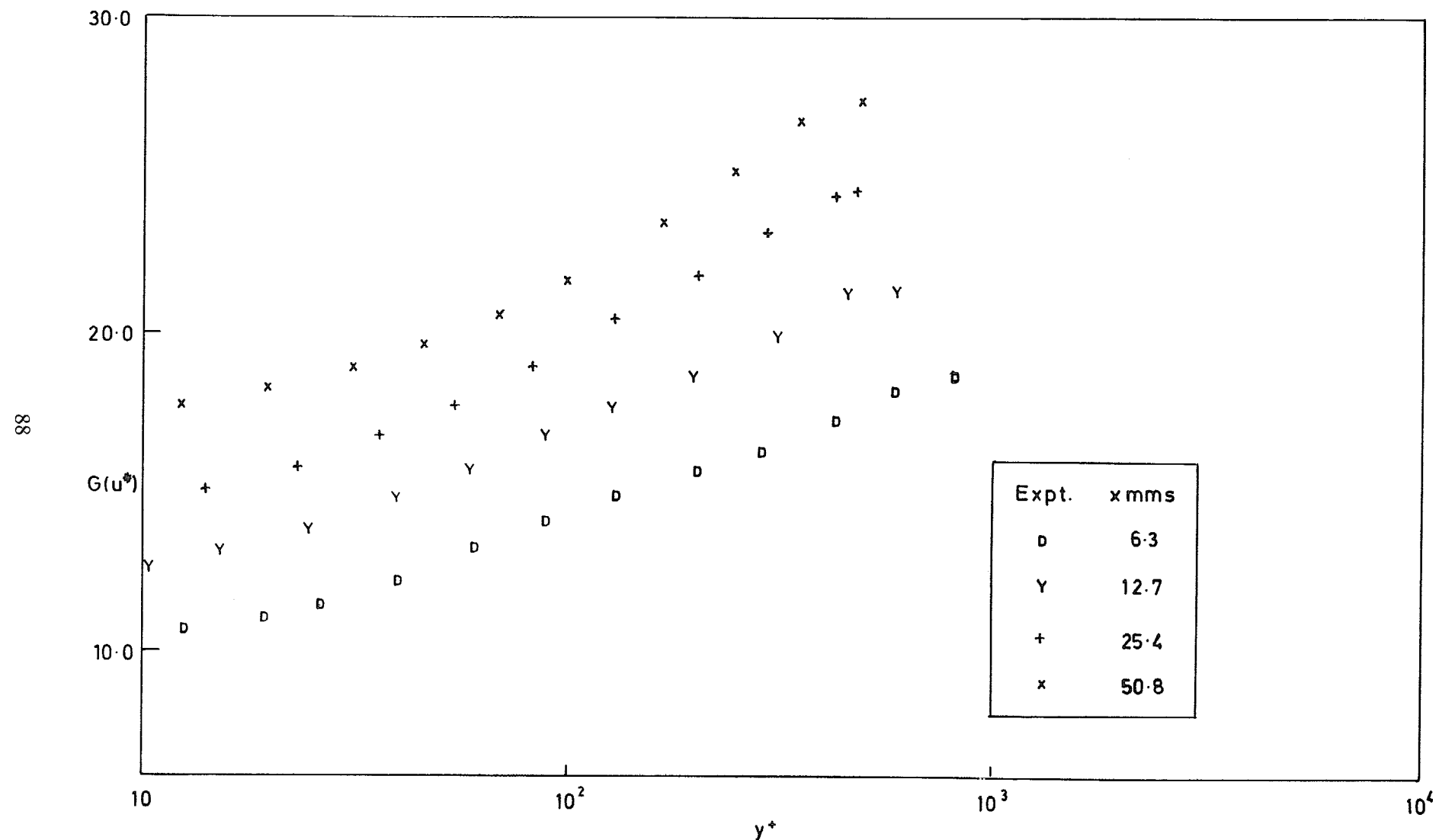


FIG. 41. $G(u^*)$ vs $\log(yU_r/\nu_w)$ ($M = 3.6; F = 0.00421$).

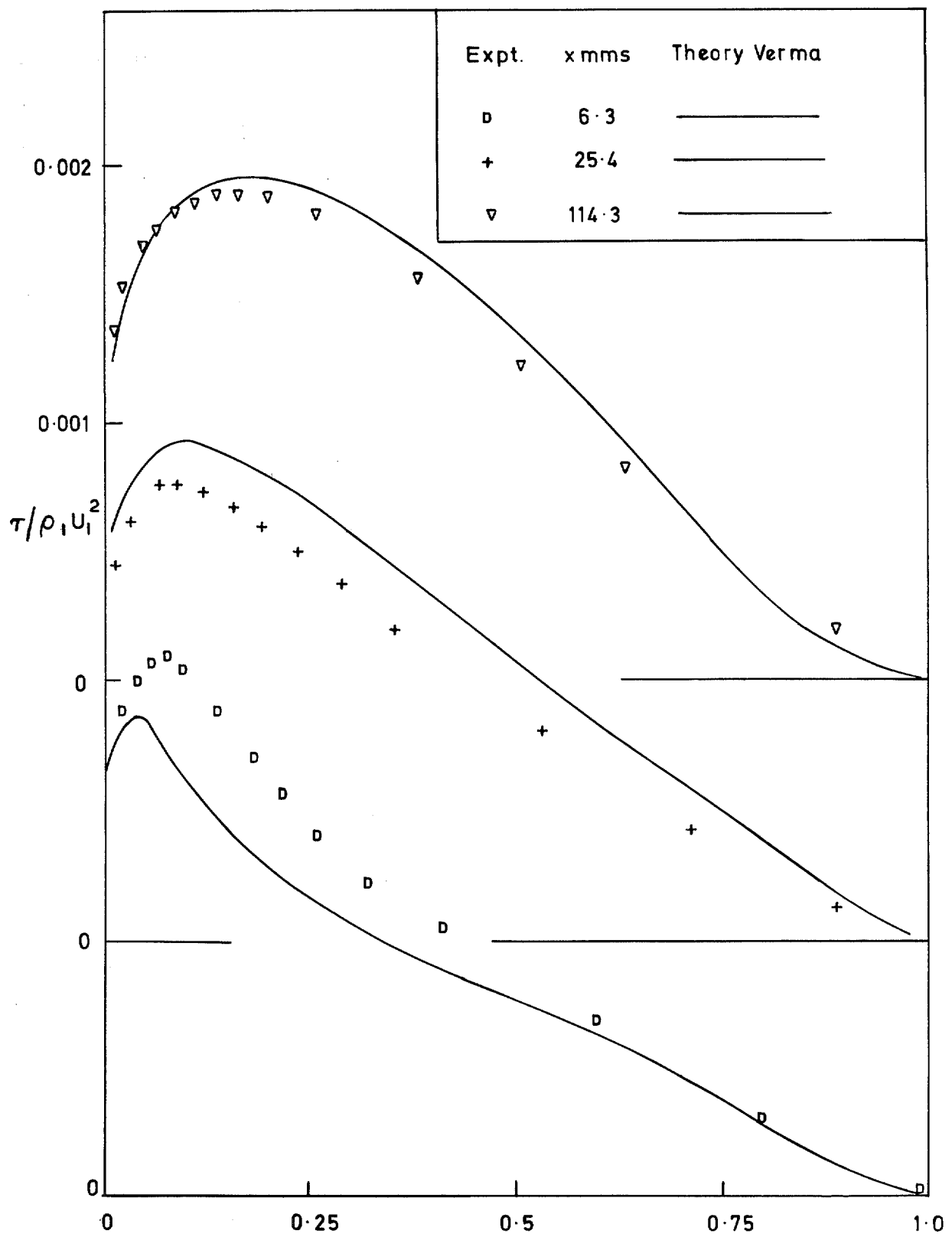


FIG. 42. Shear stress profiles ($M = 1.8; F = 0.00311$).

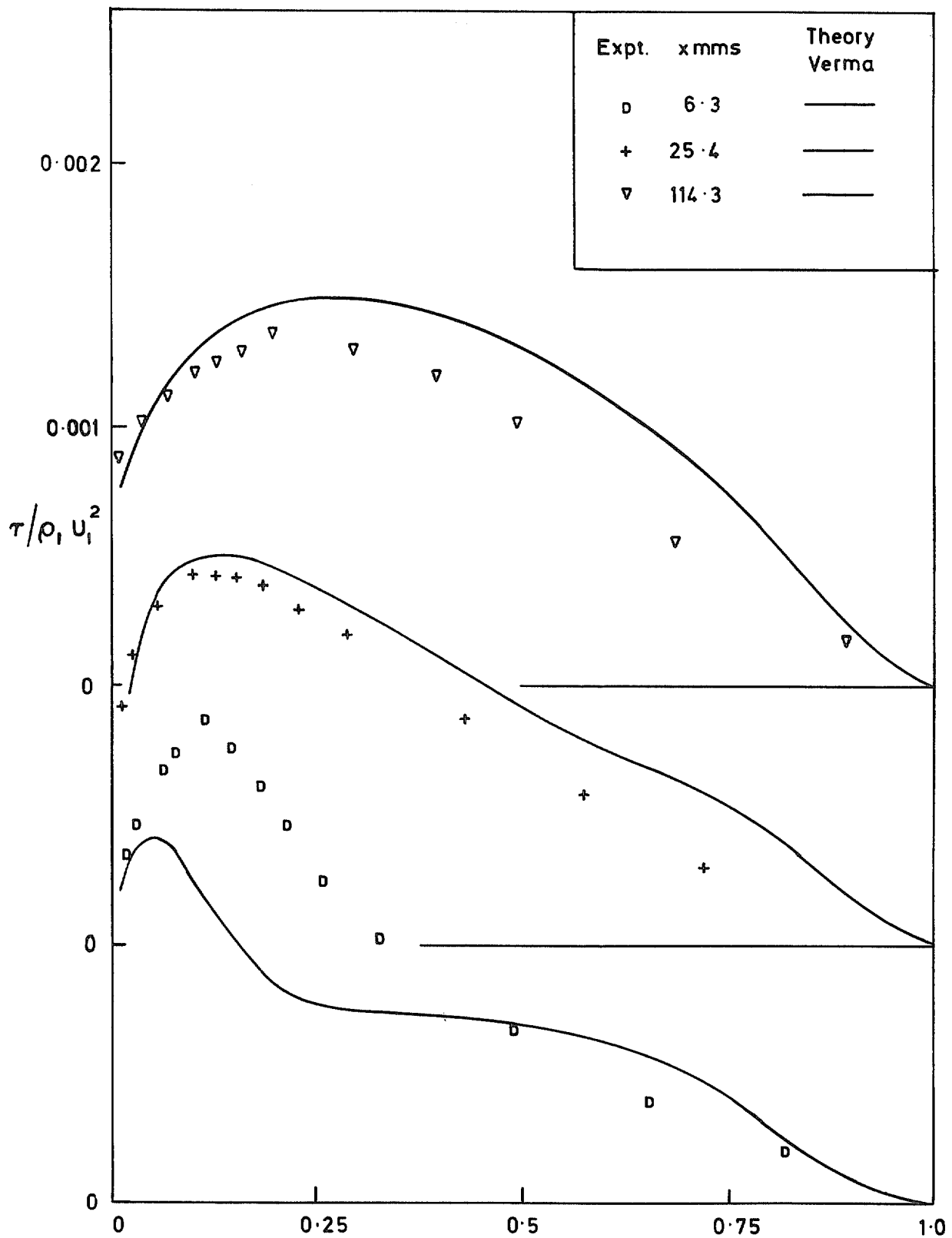


FIG. 43. Shear stress profiles ($M = 3.6$; $F = 0.00294$).

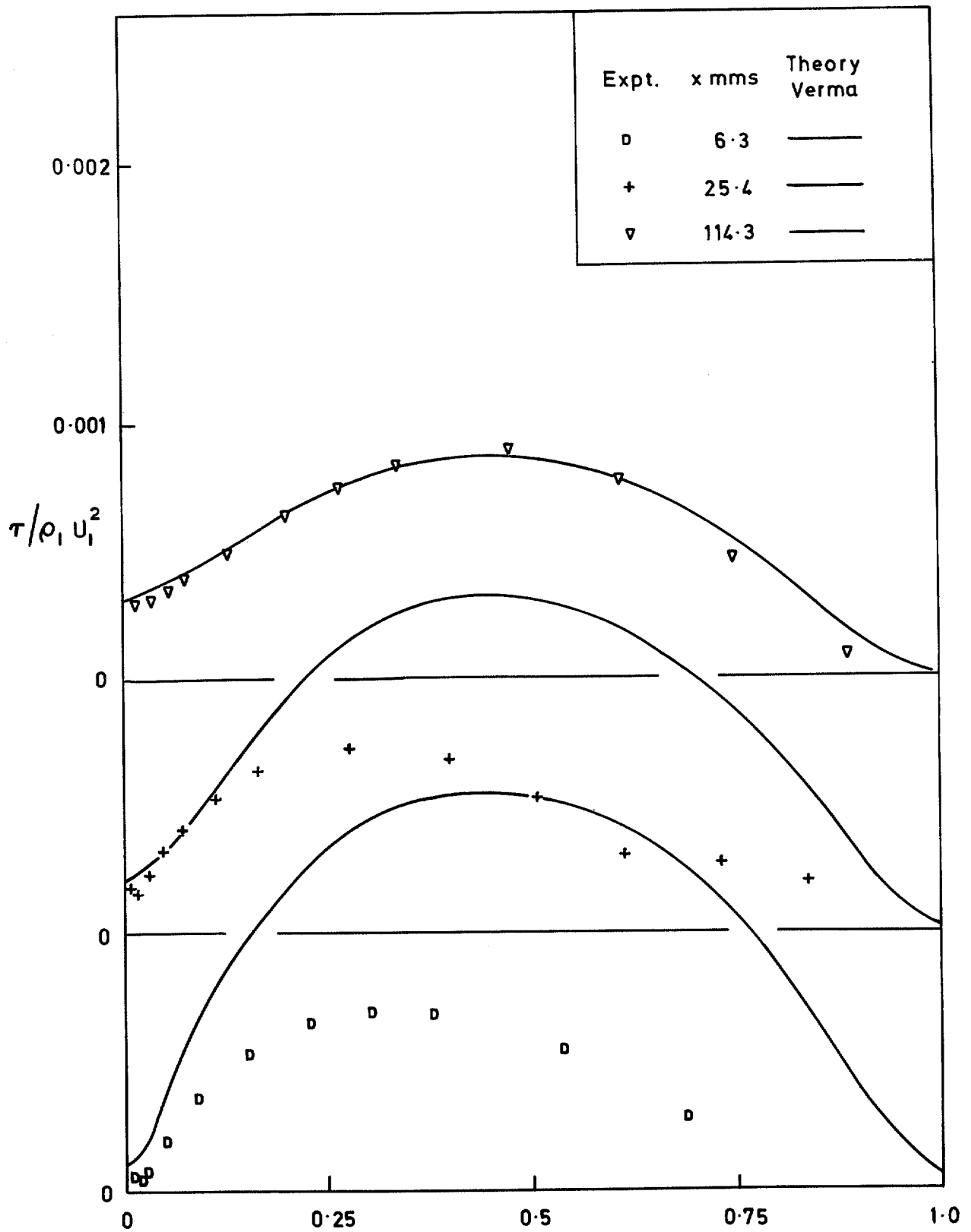


FIG. 44. Shear stress profiles ($M = 3.6; F = 0.00294$ porous-solid).

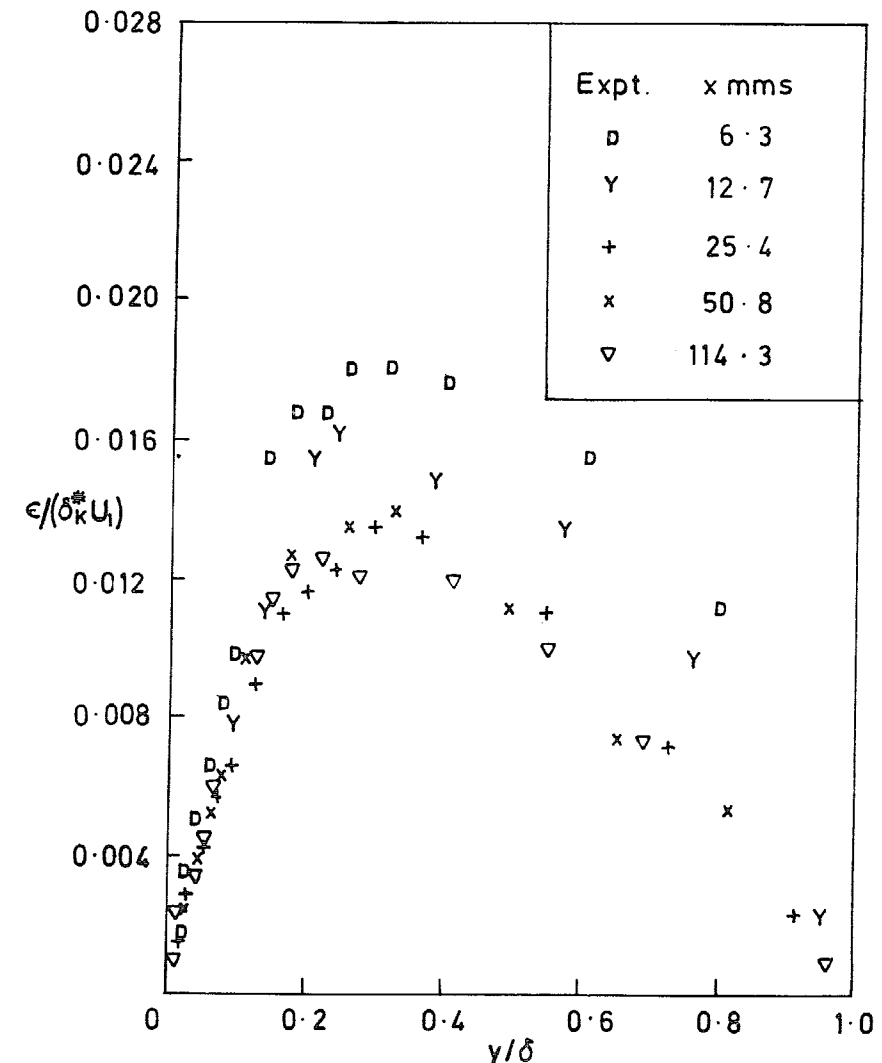
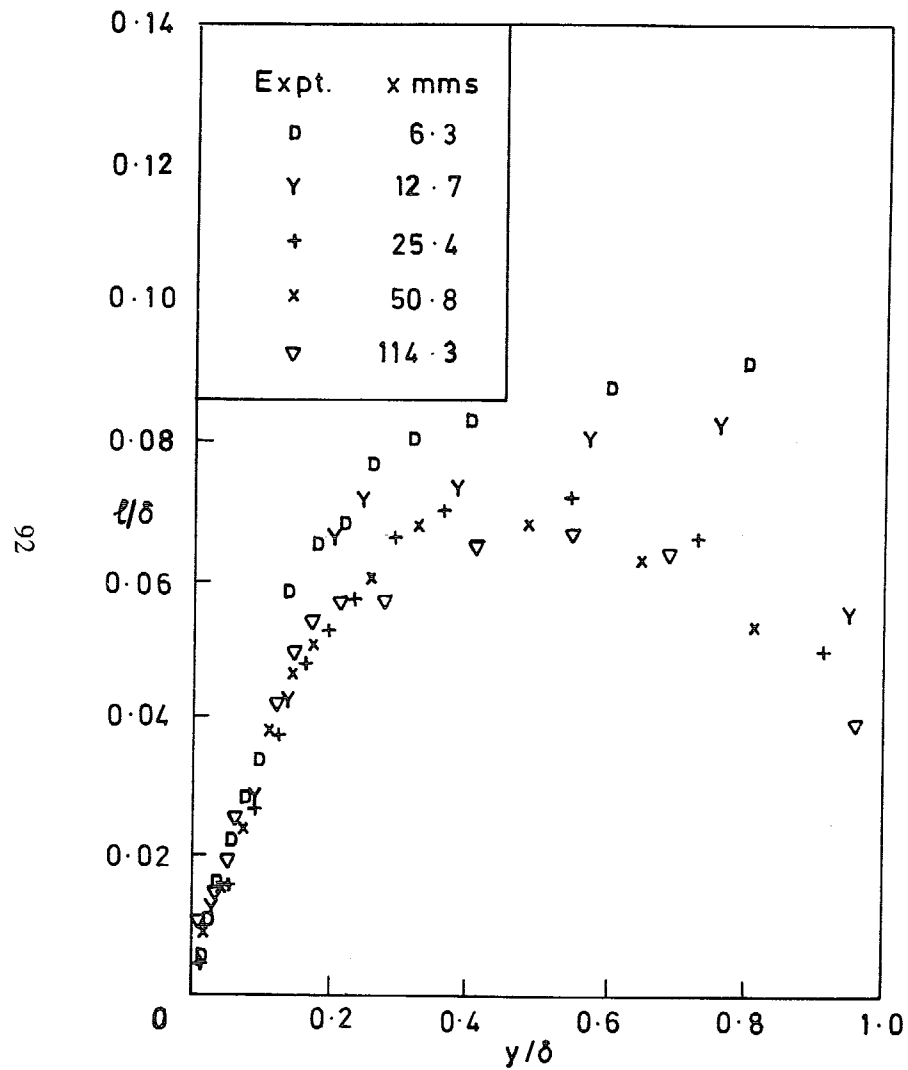


FIG. 45. Mixing length and eddy viscosity distributions ($M = 1.8$; $F = 0.00174$).

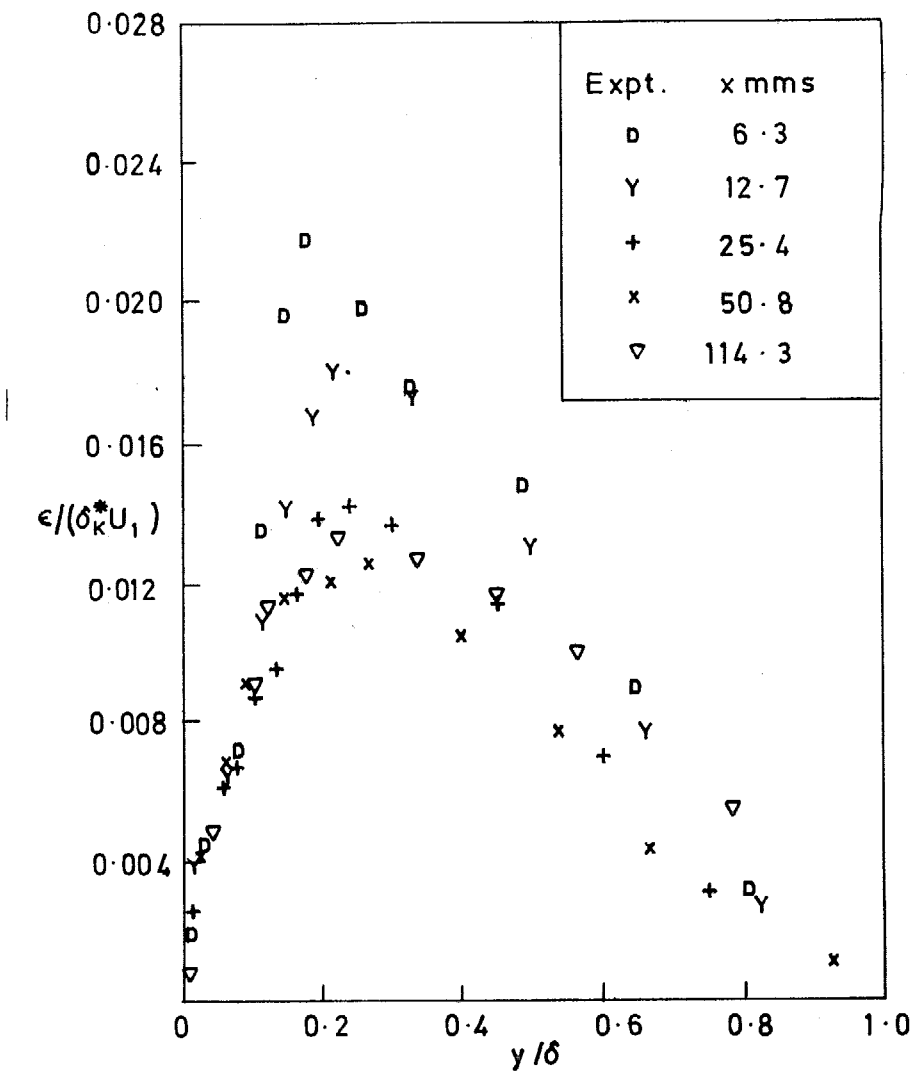
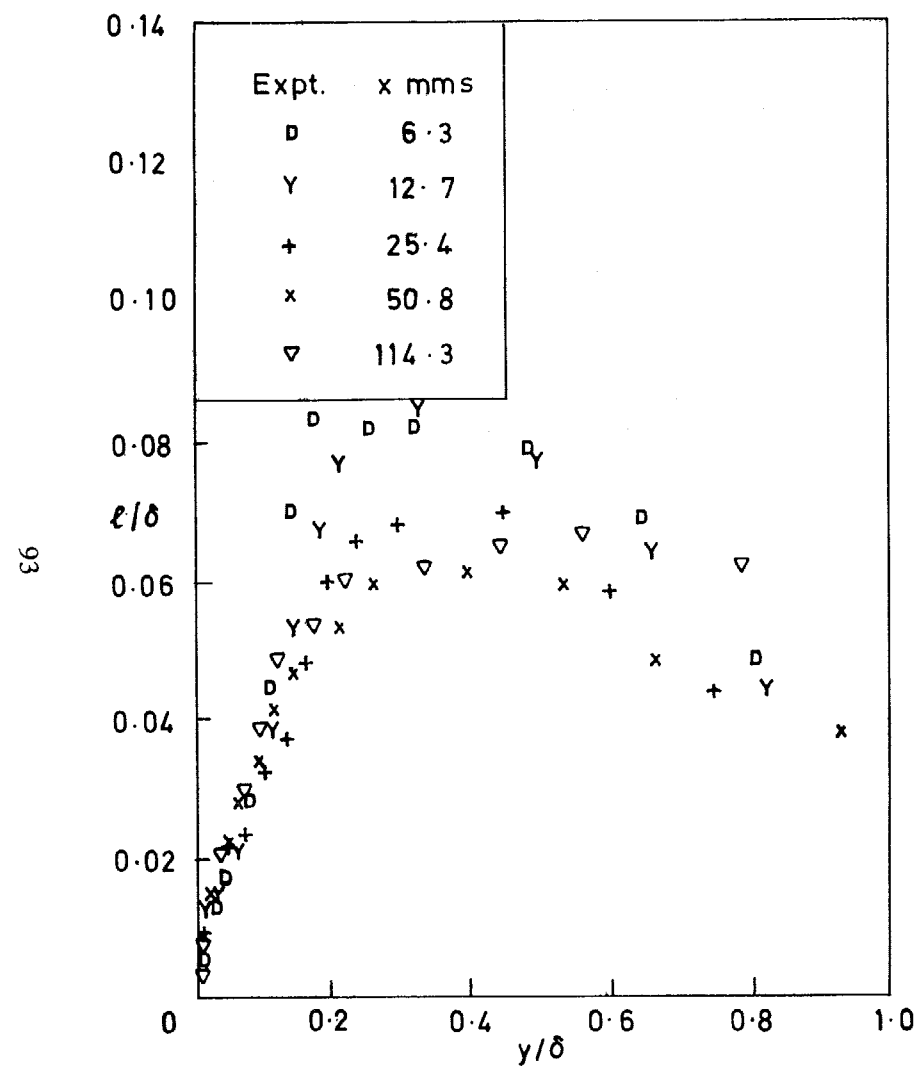


FIG. 46. Mixing length and eddy viscosity distributions ($M = 3.6; F = 0.00164$).

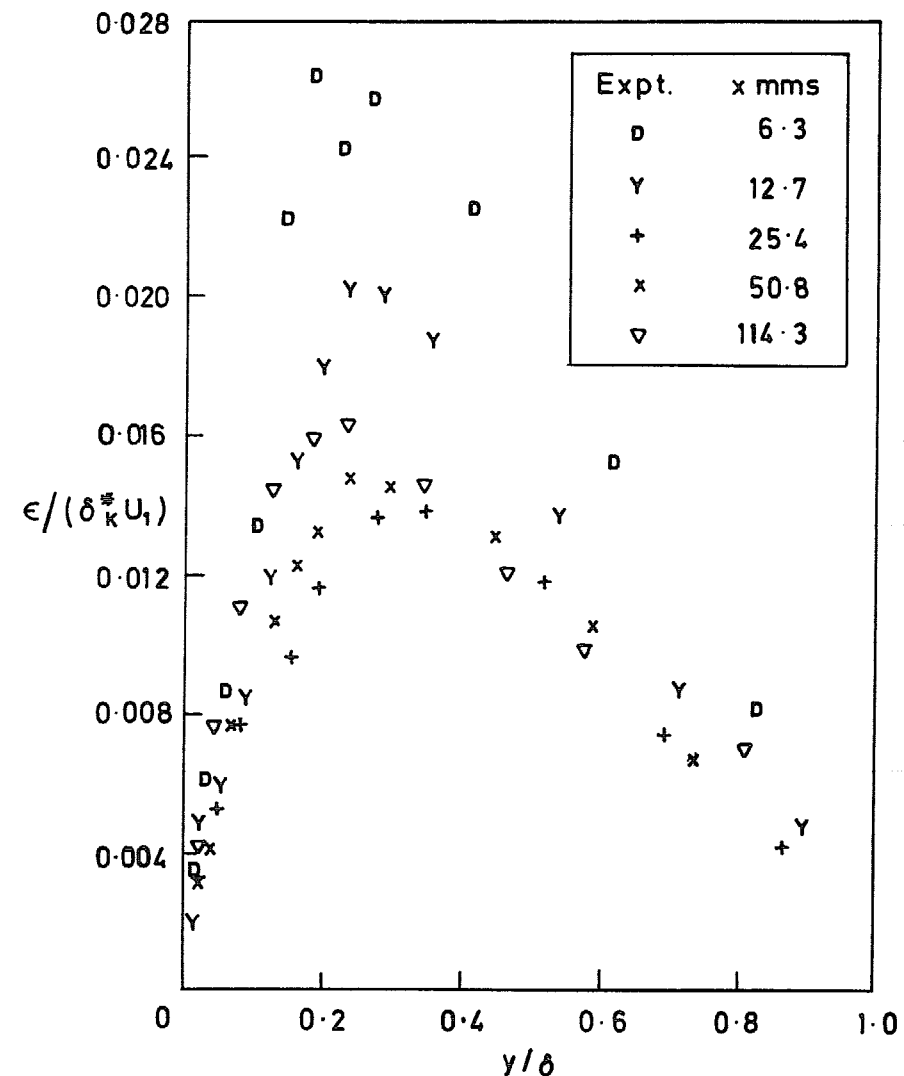
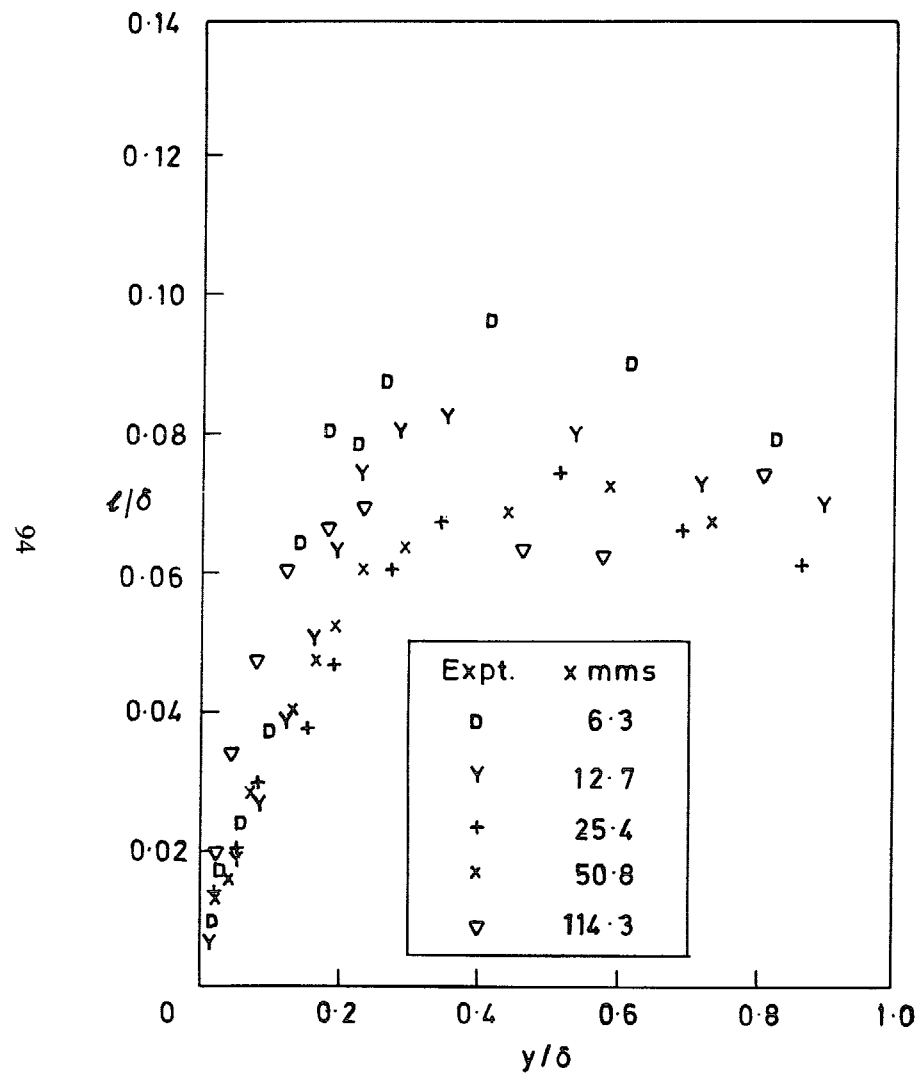


FIG. 47. Mixing length and eddy viscosity distributions ($M = 1.8$; $F = 0.00446$).

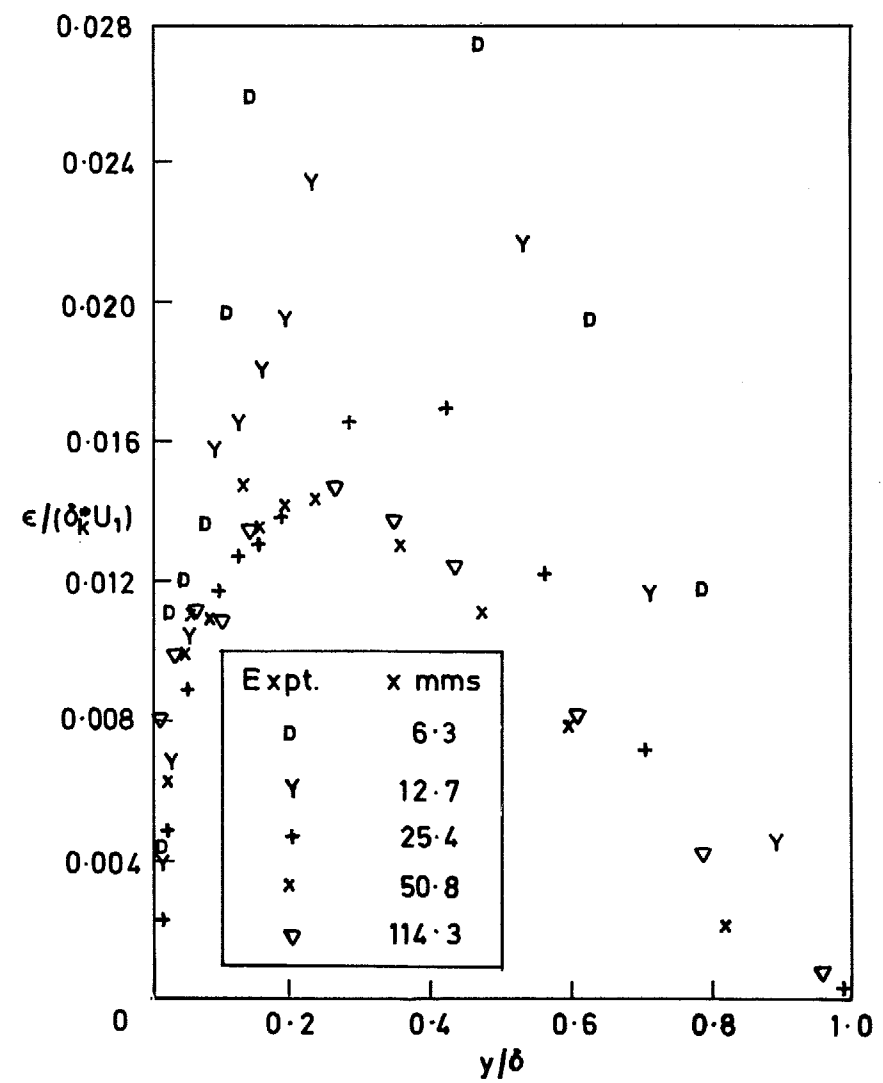
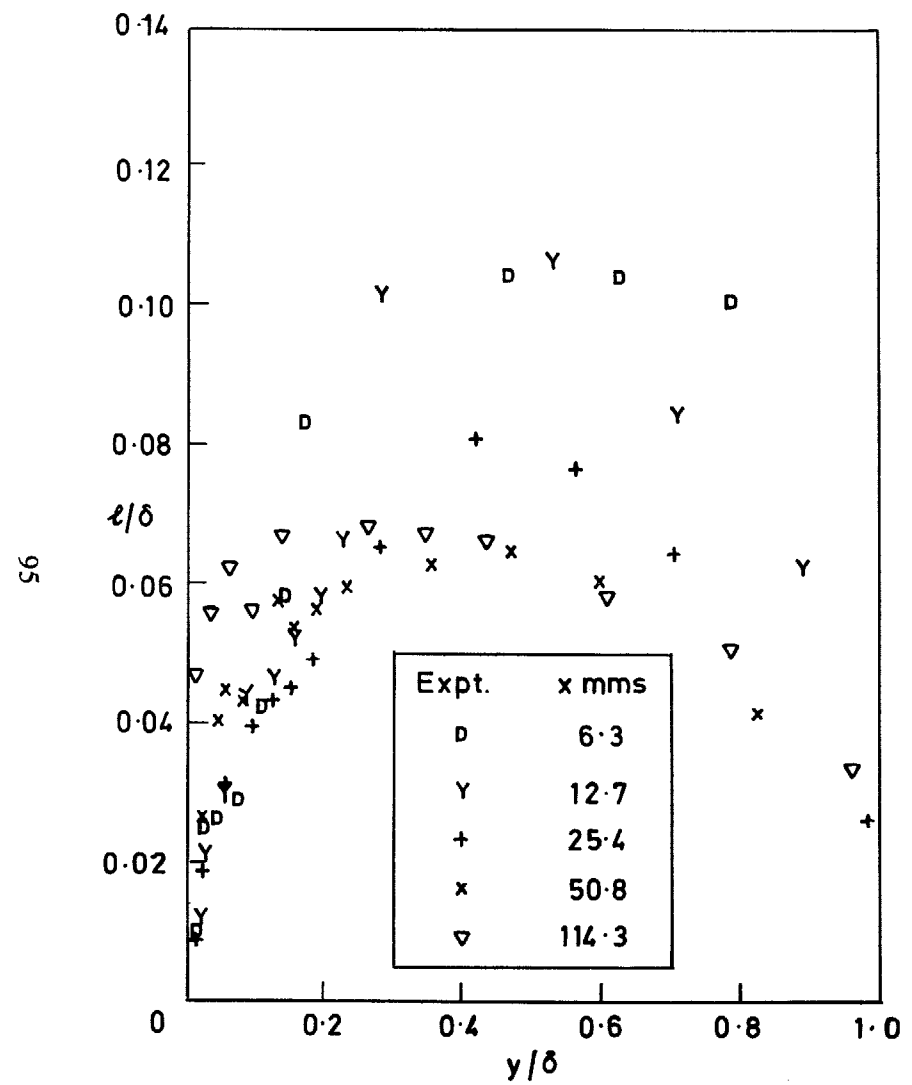


FIG. 48. Mixing length and eddy viscosity distributions ($M = 3.6$; $F = 0.00421$).

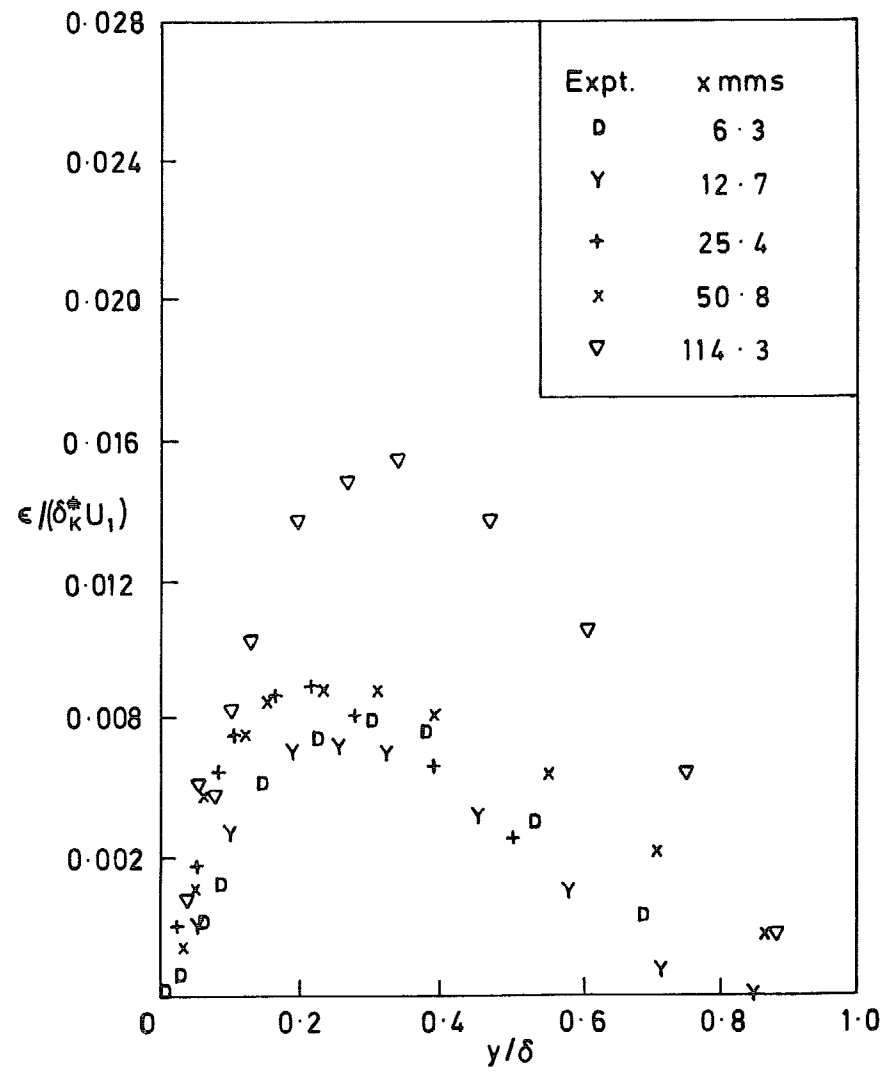
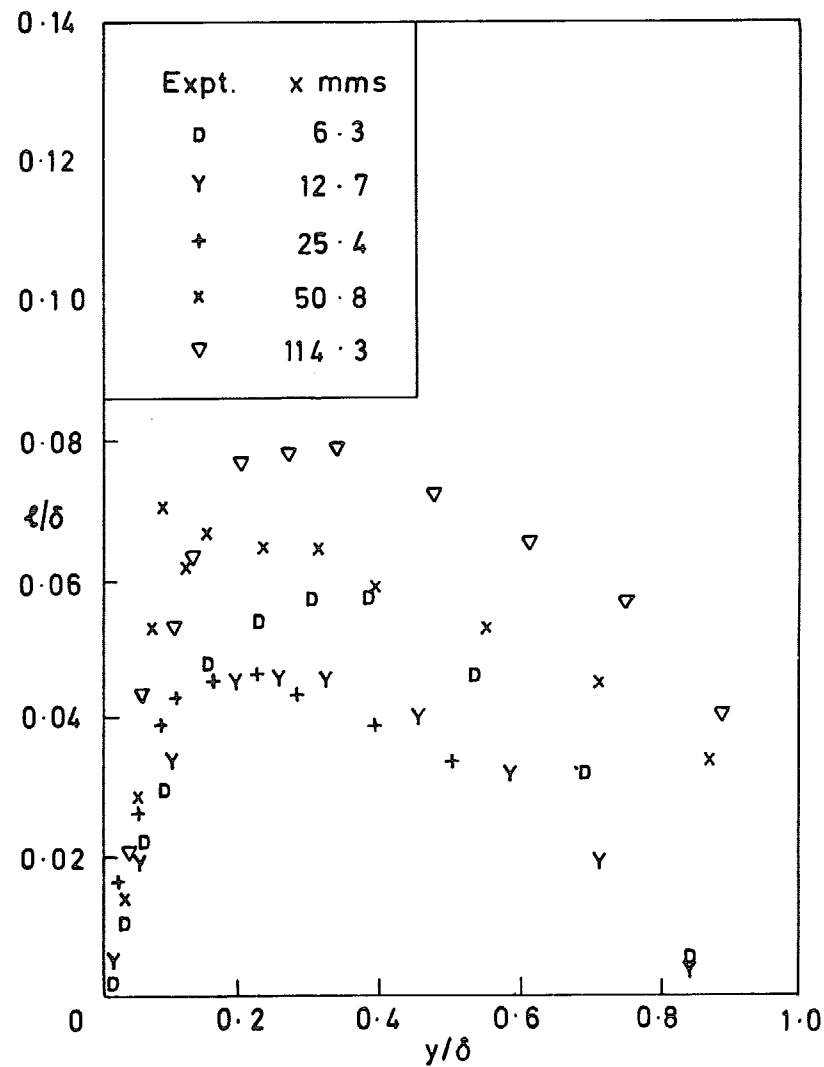


FIG. 49. Mixing length and eddy viscosity distributions ($M = 3.6$; $F = 0.00294$ porous-solid).

R. & M. No. 3780

© Crown copyright 1977

HER MAJESTY'S STATIONERY OFFICE

Government Bookshops

49 High Holborn, London WC1V 6HB
13a Castle Street, Edinburgh EH2 3AR
41 The Hayes, Cardiff CF1 1JW
Brazennose Street, Manchester M60 8AS
Southey House, Wine Street, Bristol BS1 2BQ
258 Broad Street, Birmingham B1 2HE
80 Chichester Street, Belfast BT1 4JY

*Government publications are also available
through booksellers*

R. & M. No. 3780
ISBN 0 11 470925 4*